NONDESTRUCTIVE CHARACTERIZATION OF BEARING STEELS BY MAGNETIC BARKHAUSEN NOISE TECHNIQUE

A MASTER'S THESIS

in

Metallurgical and Materials Engineering

Atılım University

by

Ebru ARSLAN

JUNE 2017

NONDESTRUCTIVE CHARACTERIZATION OF BEARING STEELS BY MAGNETIC BARKHAUSEN NOISE TECHNIQUE

A THESIS SUBMITTED TO

THE GRADUATE SCHOOL OF NATURAL AND APPLIED SCIENCES

OF

ATILIM UNIVERSITY

BY

EBRU ARSLAN

IN PARTIAL FULFILLMENT OF THE REQUIREMENTS FOR THE
DEGREE OF

MASTER OF SCIENCE

IN

THE DEPARTMENT OF METALLURGICAL AND MATERIALS
ENGINEERING

JUNE 2017

Approval of the Graduate School of Natural and Applied Sciences, Atılım University.

Prof. Dr. Ali KARA

Director

I certify that this thesis satisfies all the requirements as a thesis for the degree of Master of Science.

Prof. Dr. Naci SEVİNÇ

Head of Department

This is to certify that we have read the thesis "Nondestructive Characterization of Bearing Steels by Magnetic Barkhausen Noise Technique" submitted by "Ebru ARSLAN" and that in our opinion it is fully adequate, in scope and quality, as a thesis for the degree of Master of Science.

Asst. Prof Dr. Caner ŞİMŞİR
Co-Supervisor

Asst. Prof Dr. Kemal DAVUT
Supervisor

Examining Committee Members

Asst. Prof Dr. Kemal DAVUT

Prof. Dr. Naci SEVİNÇ

Prof. Dr. C. Hakan GÜR

Date: 22.06.2017

I declare and guarantee that all data, knowledge and information in this document has been obtained, processed and presented in accordance with academic rules and ethical conduct. Based on these rules and conduct, I have fully cited and referenced all material and results that are not original to this work.

Name, Last name: Ebru ARSLAN

Signature:

ABSTRACT

NONDESTRUCTIVE CHARACTERIZATION OF BEARING STEELS BY MAGNETIC BARKHAUSEN NOISE TECHNIQUE

Arslan, Ebru

M.Sc., Metallurgical and Materials Engineering Department

Supervisor: Asst. Prof. Dr. Kemal Davut

Co-Supervisor: Asst. Prof. Dr. Caner Şimşir

June 2017, 106 pages

One of the most popular type of bearing steels is 100Cr6. The strength, toughness, hardness, fatigue life, wear resistance of it can be improved by heat treatment applications which also changes the microstructure. For controlling the microstructure, traditional metallographic and XRD- based methods, that involve taking representative specimens from lots, are used. Magnetic Barkhausen noise (MBN) technique may provide an alternative nondestructive, fast and practical measurement method to those traditional techniques. This study aims at investigating the possibility of nondestructive characterization of microstructure of heat treated 100Cr6 bearing steels by using the MBN technique. For that purpose, 100Cr6 steel specimens were heat treated in a quenching dilatometer under different austenitization conditions and then quenched to room temperature and to -130°C, in order to generate variations in their microstructures. After heat treatment applications, microstructural properties of the specimens including the fraction and distribution of carbides, amount of retained austenite and also hardness were determined by metallographic and XRD analysis. Moreover, MBN measurements were performed and then the results were correlated to the microstructural parameters. MBN signals correlate with the microstructure variations in the 100Cr6 steel samples via simple linear relations; however, the prediction bands were quite wide and the MBN technique was not sufficiently sensitive, for direct characterization of hardness, retained austenite and carbide fraction of the specimens that were quenched to room temperature. In order to characterize these interdependent microstructural parameters via MBN technique, non-linear relations based on carbide dissolution kinetics are needed. On the other hand, the MBN measurement results of the sub-zero treated specimens showed that;

elimination of retained austenite significantly improved the goodness of fit of on those linear relations. Although coefficient of determinations of both carbide fractions and hardness were acceptable, it can be improved by developing a newer non-linear model. Nevertheless, all of the results were promising for the future applications of MBN technique on nondestructive characterization of microstructure variations in 100Cr6 steels.

Keywords: Magnetic Barkhausen Noise, microstructure, retained austenite, austenitization, hardness, 100Cr6 bearing steels

ÖZ

RULMAN ÇELİKLERİNİN MANYETİK BARKHAUSEN GÜRÜLTÜSÜ YÖNTEMİ İLE TAHRİBATSIZ KARAKTERİZASYONU

Arslan, Ebru

Yüksek Lisans, Metalurji ve Malzeme Mühendisliği Bölümü

Tez Yöneticisi: Yrd. Doç. Dr. Kemal Davut

Ortak Tez Yöneticisi: Yrd. Doç. Dr. Caner Şimşir

Haziran 2017, 106 sayfa

100Cr6 çelikleri rulman yapımında yaygın olarak kullanılırlar. Isıl işlem uygulamaları ile değişen iç yapısal özelliklerine bağlı olarak; yüksek gerilimlere karşı dayanımı, yorulma ömrü, tokluğu, sertliği, aşınma direnci gibi özellikleri geliştirilebililir. Bu iç yapısal özelliklerin muayenesi, geleneksel metalografik ve XRD tekniklerinin bir arada kullanılmasıyla yapılabilir. Ancak bu yöntemler numune hazırlama gereksinimi bulunan yöntemlerdir. Bu sebepten; tahribatsız ve hızlı ölçüm alınmasını sağlayan Manyetik Barkhausen gürültüsü (MBN) tekniği, bu geleneksel karakterizasyon yöntemlerine alternatif olarak değerlendirilmiştir. Bu çalışmanın amacı 100Cr6 çeliklerinin MBN yöntemiyle tahribatsız muayene edilebilirliğinin araştırılmasıdır. Bu bağlamda, 100Cr6 çelik numuneler, içerisinde farklı içyapısal özelliklerin oluşturulabilmesi adına farklı sıcaklıklarda östenitlenip oda sıcaklığına ve -130°C'ye hızlı soğutulmuştur. Bu işlemlerin ardından numunelerin sertliği, karbür miktarları, dağılımları, kalıntı östenit miktarları, metalografik ve XRD ölçüm yöntemleriyle belirlenmiştir. Ayrıca, her bir numune MBN yöntemi ile de muayene edilmiştir. Son olarak, elde edilen içyapı sonuçlarıyla MBN sonuçları arasındaki bağlantılar incelenmiştir. MBN tekniğinin, kurulan lineer korelasyonlar kapsamında oda sıcaklığına hızlı soğutulan 100Cr6 çelik numunelerin iç yapısal özellikleriyle korele edilebilir olduğu gözlenmiştir; ancak tahmin aralıklarının oldukça geniş olması sebebiyle, bu numunelerin iç yapısında oluşan sertlik, kalıntı östenit ve karbür miktarların doğrudan belirlenebilmesi için yeterince hassas olmadığı sonucuna varılmıştır. Birbirlerine bağlı olarak değişen bu özelliklerin MBN ile karakterize edilebilmesi; karbür çözünme kinetiğine bağlı olarak, tüm bu değişkenlerin hem kendi aralarında hem de MBN sinyalleri üzerindeki eş zamanlı etkileri arasında lineer olmayan bir ilişki kurulması ile mümkün olabileceği düşünülmektedir. Bunun haricinde, sıfır altı ısıl işlemine tabi tutulan numunelerde, kalıntı östenitin tamamen yok edilmesi, MBN sinyalleri üzerindeki kalıntı östenit etkisini tamamen ortadan kaldırılmıştır. Bu sebepten hem sertlik ve hem de kardür oranları için kurulan lineer korelasyonlarda belirgin bir iyileşme görülmüştür. Bu korelastonların R^2 değerleri kabul edilebilir düzeyde olmasına rağmen tüm iç yapısal değişkenlerin MBN sinyalleri üzerindeki eş zamanlı etkisi göz önünde bulundurularak lineer olmayan modeller kurulmasıyla iyileştirilebilinir. Bu doğrultuda, MBN tekniğininin, 100Cr6 çeliğinin iç yapısal karakterizasyonu konusunda, gelecekte yapılacak daha detaylı ve kapsamlı çalışmalar ile geliştirilebilir olduğu düşünülmektedir.

Anahtar Kelimeler: Manyetik Barkhausen Gürültüsü, iç yapı, kalıntı östenit, östenitleme, sertlik, 100Cr6 rulman çeliği

To my Family...

ACKNOWLEDGEMENT

I would like to express my sincere gratitude to my supervisor Asst. Prof. Dr. Kemal DAVUT for his guidance, encouragement, and support throughout my entire postgraduate program. I also would like to express my special appreciations and thanks to my co-supervisor Asst. Prof. Dr. Caner ŞİMŞİR for sharing his own simulations' results and his knowledge which are related to this study, and his precious help, support, and guidance.

I would like to express my deepest gratitude to Asst. Prof. Dr. Volkan KILIÇLI from Gazi University for his kind help, patience, encouragement, support, and guidance during my undergraduate and postgraduate programs.

I would like to express my sincere appreciations to ORS Bearings Inc., specifically for providing the raw materials and also for preparing the specimens for the dilatometer tests. I also would like to express my gratitude to Metal Forming Center of Excellence for their kind help and technical support. I also would like to express my thanks to Ozan Müştak, Yahya TUNÇ, Yasin DEMİRKOL for their technical support.

I would like to express my deepest appreciations and thanks to my sister Elif Dilara ŞEKER, my mother Hülya ÇAKIR, and my grandparents Emine ÇAKIR and İsmail ÇAKIR for their love without any expectations, precious faith in me, patience, guidance, and their encouragements throughout my life. I also would like to express my special gratitude to my parents-in-law Rufiye CENKCİ and Ömer Kerim CENKCİ, and my sister-in-law Figen CENKCİ YURTALAN for their kind support and encouragement since we met.

I owe my precious fiancé Bahri CENKCİ great debt of gratitude for his priceless support, patience, love and inspiration.

Special thanks to H. Hava IŞIK, Sinan AKBULUT, Büşra GÖKSU, Seçil YILDIZ, Bahadır Burak GÖKÇE, Zeynep ÖZTÜRK, and Hüseyin HIZLI for their valuable friendships, kind support and patience during our friendships.

Finally, I also would like to acknowledge Onatus Company and Thermo-Calc Gmbh for their permission to use DICTRA and ThermoCalc softwares, which were mainly

used by Asst. Prof. Dr. Caner ŞİMŞİR to analyze the austenitization of the present bearing steel.

Last but not least, I am grateful to the examining committee members Prof. Naci SEVİNÇ, and Prof. Hakan GÜR for their valuable comments on this thesis. Moreover, the stimulating discussions of Dr.–Ing. Hamdullah MERDANE from ORS Bearings Inc. and Dr. Halim MEÇO from FNSS Systems Co. Inc. before and during the thesis defense is gratefully acknowledged.

TABLE OF CONTENTS

LIST OF TABLES

LIST OF FIGURES

LIST OF ABBREVIATIONS

Abbreviations

A_1	A_1 temperature
A_3	A_3 temperature
A_{c1}	A_{c1} temperature
A_{c3}	A_{c3} temperature
A_{cm}	A_{cm} temperature
AGS	Austenite grain size
ASTM	American Society for Testing and Materials
Avg.	Average
B_s	Bainite start temperature
BCC	Body Centered Cubic
BCT	Body Centered Tetragonal
CCT	Continuous Cooling Transformation
$d_{carbides}$	Carbide diameter
DIN	German Institute of Standardization
DP	Dual Phase
EN	European Standard
FCC	Face Centered Cubic
FEG	Field Emission Gun
LVDT	Linear Variable Differential Transformer
MBN	Magnetic Barkhausen Noise
M_f	Martensite finish temperature
M_s	Martensite start temperature
PSD	Position Sensitive Detector
RMS	Root mean square
RT	Room temperature
SEM	Scanning Electron Microscope
SI	Sensitivity index
TTA	Time-Temperature- Austenitization
TTT	Time-Temperature- Transformation
T_γ	Austenitization temperature

t_γ	Austenitization time
VI	Validity index
wt.	weight
XRD	X-Ray Diffractometer

LIST OF SYMBOLS

γ	Austenite
°C	Celsius centigrade
K	Kelvin
M	Magnetization
H_0	Applied magnetic field
χ	Magnetic susceptibility
χ_0	Relative susceptibility
μ_0	Permeability
μ_r	Relative permeability
B	Magnetic induction
J	Magnetic polarization
H	Magnetic field
H_c	Coercive field
m_s	Magnetic saturation
M_r	Magnetic remanence
f	frequency
σ	Electrical conductivity
δ	Penetration depth of magnetic field
N	Newton
MHz	Millihertz
kHz	Kilohertz
V	Voltage
HV	Vickers Hardness
R^2	Coefficient of determination
min	Minute
s	Second
mm	Millimeter

CHAPTER 1

INTRODUCTION

Ball bearings are used almost in all applications which require rotational movement. Therefore, they are widely used in a diverse set of industries, including automotive, aircraft, aerospace, electronic appliances, energy etc. In those industries and applications there is a high demand to support the rotationally moving components and to carry the applied load without failing by utilizing the reduction of contact area between the rotating components [1].

Properties such as hardness, toughness, fatigue strength and wear resistance needed to be primarily concerned in terms of working conditions of ball bearings. Therefore, material selection of a bearing is important to provide the desired properties such as essential mechanical properties (i.e. strength, fatigue resistance and durability), high hardenability, machinability and good dimensional stability. Typical high carbon steels which contain approximately 1 wt. % of carbon and 1.5 wt. % of chromium provide these material requirements and hence 100Cr6, SAE 52100, En31, SUJ-2 alloy steels can be used as raw materials of bearings. All of these materials are referred to as bearing steels; and 100Cr6 steel is one of the most commonly referred type.

Mechanical properties of the materials directly depend on their microstructures, which can be altered via heat treatment procedures. Heat treatment procedures can alter the microstructure by changing the grain size of the material, amount of phases, carbides and other precipitates per unit area, their size and distributions; all of which influence the hardness [2]. Due to this fact, proper heat treatment applications provide great improvement of the 100Cr6 steel’s properties to satisfy the system requirements. For instance, quenching process provides an apparent increase of the hardness where spheroidization process increases the toughness by decreasing the hardness of the bearing steel. Another example is homogenization process which provides elimination of micro segregations and stress relief in the material [3]. In order to characterize the microstructure various method such as metallographic examinations, microscopic characterizations, XRD based measurements etc. were employed.

Metallographic examinations allow characterization of macro and micro structure of the materials. It generally aims at revealing the micro-constituents in the material structure via microscopic examinations. Metallographic preparation method varies with the type of the material and the aim of the examination. Therefore, selecting the proper preparation method has significant importance on the results. Due to this fact, there are some requirements of this technique such as selection of the location of specimen and its size, proper cutting, mounting, grinding and polishing techniques, correct etching conditions (i.e. etchant solution, time, temperature, agitation etc.) and also selecting the proper microscopic system to reveal the microstructure of materials [4]. Another technique is X-Ray Diffraction (XRD) which allows the determination of volume percentage of retained austenite by comparing the intensity of face centered (i.e. austenite) and body centered (i.e. ferrite) crystallographic phases. This technique has also some requirements (i.e. sample preparation, X-Ray equipment and data analysis methods) with respect to the material and case [5].

Material characterization has major importance on the industrial applications for assurance of desired conditions to avoid the failure of the work piece or the system. However, the requirements of both characterization techniques cause loss of time which is also vital for the industry. Therefore, there is an increasing demand of new characterization techniques which provide quick measurements and reliable results.

Magnetic Barkhausen noise (MBN) technique is a good alternative to traditional metallographic and XRD based characterization methods. It is sensitive to microstructural properties of the materials and also provides fast and nondestructive evaluation of ferromagnetic materials. The basic principle of MBN technique is to measure the discontinuous flux changes in the material by applying an external magnetic field. Irreversible process of magnetization causes the nucleation, annihilation and growth of domains, also affects their motions and rotations. MBN response of the material is sensitive to these domain configurations which are influenced by microstructural properties such as grain boundaries, dislocations, precipitates, phases and their distribution, hardness, and residual stress state. In other words, the microstructural features affect the dynamic behavior of domains and their displacement between these pinning obstacles which cause sudden flux jumps in the material. These sudden flux jumps cause the formation of MBN signals and they are detected by a pick-up coil which is placed near to the material surface [6]–[9].

1.2. Aim of the Study

As it was emphasized in the previous chapter, bearing steels have major importance in several industrial sectors. Obviously, each of these emerging sectors has growing need of fast and nondestructive characterization of their components. Magnetic Barkhausen noise (MBN) technique is a good alternative measurement technique for non-destructive characterization of ferromagnetic materials due to its sensitivity of microstructural variations in the materials. The major advantages of this technique can be listed as:

- ✓ Non-destructive
- ✓ Extremely fast (compared to the traditional methods)
- ✓ Reliable (especially for the case of comparison of the same materials)
- ✓ Compatible for automation.
- ✓ Allows 100% inspection.

Considering these advantages, various studies have been published on nondestructive characterization of 100Cr6 steel by MBN technique. Most of those researches were about post-processing of MBN signals, evaluation of residual stress state, and nondestructive detection of grinding burn in case hardened 100Cr6 steels. However, almost nothing has been reported on the nondestructive characterization of microstructure of heat treated 100Cr6 steels by the MBN technique.

Thus, this study aims at closing this gap by investigating the MBN response of heat treated 100Cr6 steels. Applications of different austenitization conditions (different combinations of time and temperature) to the specimens produced variations in carbide fraction and distribution, amount of retained austenite and hardness of the matrix in the microstructure. As it was widely known, MBN signals are sensitive to each of these microstructural variants. These variants are interdependent properties of the microstructure, and there are both linear and non-linear relations between the microstructural properties and the MBN response of the materials. The present study aims at studying those relations and correlations in order to investigate the applicability of MBN technique to characterize the microstructural variations of 100Cr6 bearing steels.

Within the scope, the following Chapter 2 “Theory and Literature Survey” will give detailed information about properties and microstructure of 100Cr6 steels, their heat treatment procedures, and also about the theory and basic principles of the MBN technique. Moreover, brief review of related researches in the literature will be given in this chapter. It will be followed by Chapter 3 “Process Description” which will give details about experimental works of this present. In this context, details of applied heat treatment programs, destructive and non-destructive microstructural characterization techniques will be given in the 3rd Chapter. Then, all of the results of each experimental work and their relations will be discussed in Chapter 4 “Results and Discussions”. Finally, it will be concluded in the 5th Chapter “Outlook and Conclusion”.

CHAPTER 2

THEORY AND LITERATURE SURVEY

2.1. General Properties of DIN-EN 100Cr6 Alloy Steel

Bearings are commonly made from DIN-EN 100Cr6 alloy steel which is also referred to “bearing steel”. Chemical composition range of 100Cr6 steel is given in Table 2.1.

Table 2.1 Chemical composition range of DIN-EN 100Cr6 alloy steel (in wt.%) [10]

C	Mn	Si	Cr	Ni	Mo	Cu	S	P
0.90-1.05	0.25-0.45	0.15-0.35	1.40-1.65	≤0.30	-	≤0.30	≤0.025	0.03

Microstructural properties such as the type of phases, precipitates, micro-constituents and their amounts, sizes, distributions, grain size values and, hardness and also residual stress state directly influence the bearing life. Therefore, material properties can be enhanced by utilizing the correct heat treatment procedure which in turn will improve the mechanical properties of the bearings [11].

The forming, heat treatment, microstructure as well as the performance of 100Cr6 steel has been investigated over two centuries [12]. Depending on the common usage area of 100Cr6 alloy steel, there are many investigations and studies can be reached in the literature. According to subject of this study, following subsections will summarize the investigations and the studies about heat treatment and microstructural properties of 100Cr6 alloy steels.

2.1.1. Heat Treatment of DIN-EN 100Cr6 Alloy Steel

Heat treatment is the procedure that is applied for providing improvement of material performance in the system by enhancing the material properties. It involves mainly thermal and sometimes; chemical and mechanical processes to obtain desired structures and hence the desired properties. Therefore, relationship between the material structure and the property has to be well understood in order to provide successful heat treatment applications. Proper design and application of heat treatment procedures provide optimum adjustment of amounts, compositions and distributions of micro-constituents and phases. Modification of microstructures will alter the mechanical, chemical and physical properties of the materials [13], [14].

In order to design correct heat treatment procedures, it is necessary to know the CCT and TTT, TTA diagrams, and hardenability of the materials. Hardenability of steels can be understood by some experimental techniques (i.e. Jominy end quench test) and by estimation of hardenability curves by modeling the cooling conditions mathematically due to the grain size and chemical information. Besides, different phase fields and their critical temperature-time boundaries can be determined from the Time-Transformation-Austenitization (TTA) diagram of SAE 52100 steel (Figure 2.1). As it is clearly seen in the figure, carbides remains up to A_{cm} [15].

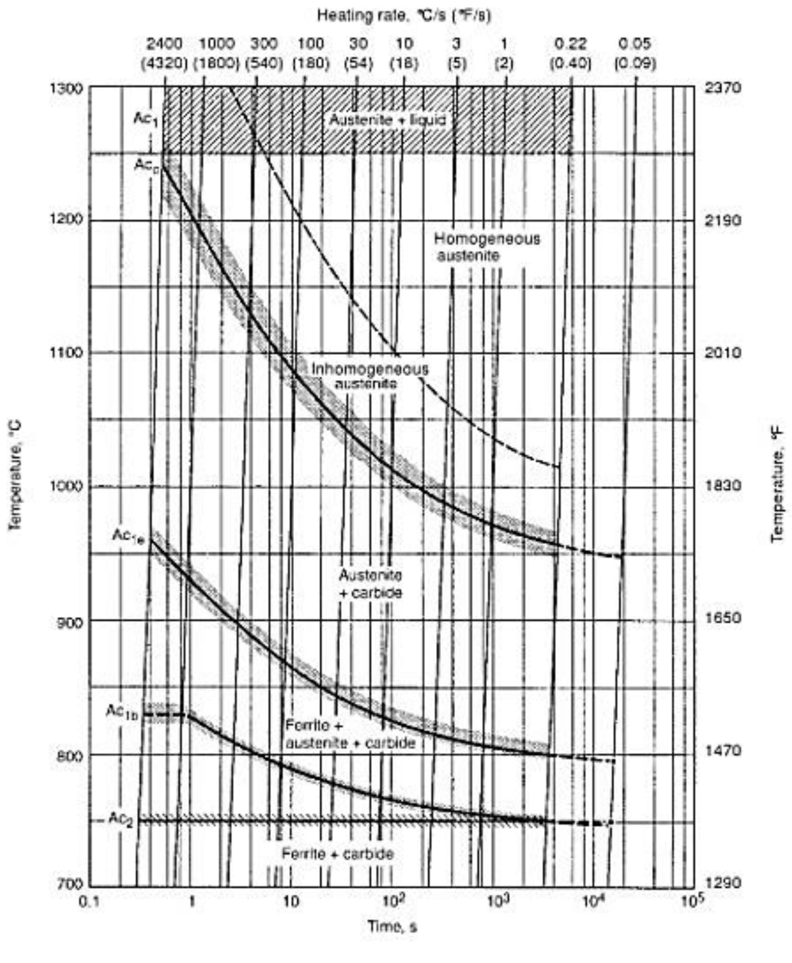

Figure 2. 1 TTA diagram of SAE 52100 steel [15]

In addition, isothermal transformation diagrams of steels enable the well understanding of austenite transformation and formation of constituents. Figure 2.2 represents the TTT diagram of SAE 52100 steel which austenitized at 843 °C and had grains sized as 9. And also it was ferrous based and contains 1.02% of carbon, 0.36% of manganese, 0.20% of nickel, 1.41% of chromium. As can be seen in the TTT diagram of SAE 52100 steel, austenite transformation given as a function of time and temperature in this figure and it also shows the microstructural response of the steel for any cooling conditions from the austenitization temperature.

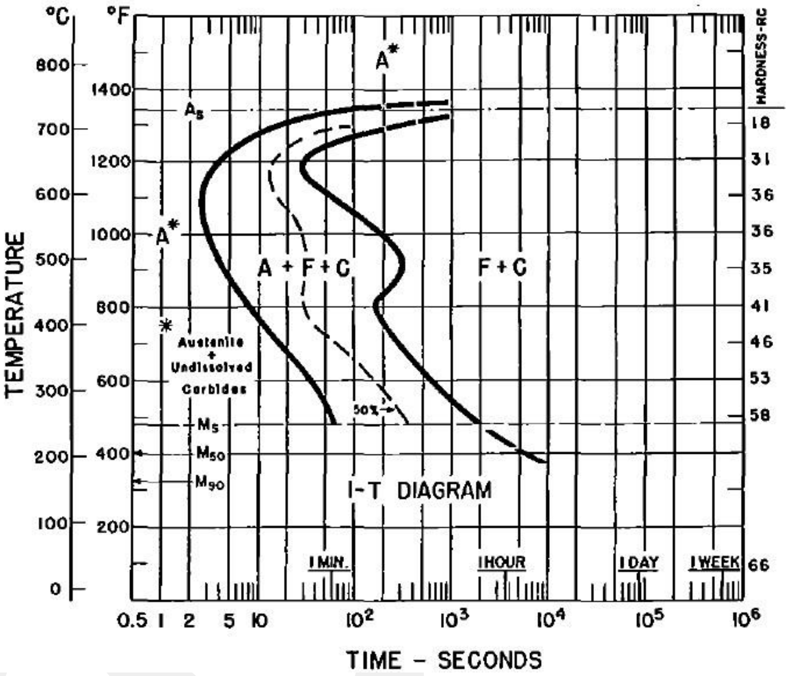

Figure 2. 2 TTT diagram of SAE 52100 steel alloy (Fe-1.02%C-0.36Mn-0.20%Ni-1.41%Cr, austenitized at 843°C, ASTM grain Size:9) [16]

Except few steels, increasing the amount of alloying elements and austenite grain size delay the isothermal transformation and these cooling curves slide to right side of the diagram. Therefore, generally hardenability of steels is improved by increasing the amount of alloying elements and austenite grain size due to this behavior of isothermal transformation [16], [17]. Moreover, amount of alloying elements and austenite grain size also affect martensite start (M_s) temperature of steels.

Due to the importance of phase transformation on the material properties, prediction of critical temperatures is vital to utilize new designs for compositions of alloying elements or parameters of heat treatment procedures. Therefore, many researches have been made of prediction of critical temperatures based on compositions of substitutional alloying elements and austenite grain size (AGS). Trzaska have studied on calculation of Ac_1, Ac_3, M_s and B_s temperatures of steel as a function of its chemical composition. The multiple regression method have been used for modeling of these critical temperatures and it has been found that this method was useful for calculating the determination of the correlation ratio of the variables of the model [18]. Beside, Peet have made an investigation about M_s prediction as a function of alloying compositions. A hybrid model was developed by combining multiple linear regression methods with thermodynamic models and Neural networks [19]. Wang et al. have examined the influence of chemical composition of steel on M_s temperature by using thermodynamic data and artificial neural network model. The results of this study show that most of the elements affect the M_s temperature in similar manner. Since the degree of influence strongly depend on the interactions of alloying elements, no linear relation was found [20].

Several studies have also been reported about grain size influence on prediction of M_s temperature. Garcia Junceda et al have studied about M_s temperature dependence on AGS. They considered different austenitization temperatures and different soaking times. The results showed that as soaking time and austenitization temperature increases individually both M_s temperature and AGS increased. In addition, the results of their study support that very fine AGS strongly affect the M_s because they observed that slight variations of very fine AGS caused great changes in M_s temperature values [21].

Jae Lee et al. have considered AGS influence for both composition dependent and independent cases. It has been resulted as high temperature austenitization procedures and compositions of alloying elements such as C and Mn influence the AGS. Moreover, M_s temperature was lowered by both enrichment of alloying elements and refinement of AGS. Moreover, finer AGS values caused reduction of M_s temperature even for the same chemical compositions [22]. Similarly, Seok Yang et al. have developed a model in order to estimate the variations of M_s temperature based on AGS [23].

Epp et al. have investigated the results of in situ X-ray diffraction (XRD) analysis and computer simulation of SAE 100Cr6 steel for different austenitization temperatures.

Carbide contents and lattice parameter of austenite have been measured by XRD experiments and the results have been compared with the computer simulation models. The results showed that, carbide content decreased asymptotically with increase of soaking temperature, since driving force decreased with reduction of carbide content. In addition, lattice parameter of austenite increased with occupation of carbides in the interstitial site of the lattice of austenite with carbides dissolution. This behavior also followed an asymptotic trend because the reduction of driving force due to the decrease of carbide dissolution rate during austenitization. This study supported the fact that, austenite phase quickly saturated by carbide dissolution, and the dissolution stops as long as no driving force presented [24].

A typical heat treatment procedure of 100Cr6 steel includes austenitization at between 830°C and 850°C, followed by quenching for martensitic transformation, and then tempering at between 100°C and 200°C. Varying the parameters of heat treatment procedure causes generation of different type of phases. Since all of those phases (martensite (~64HRC), bainite (~34 HRC), pearlite (~29HRC), and austenite (~17HRC)) indicates different properties, the selected heat treatment parameters directly influence the final properties of the materials.

Generally, 100Cr6 bearing steel is available in annealed, spheroidized, quenched, and tempered condition for industrial applications. Following subsections will give brief information about the heat treatments that brings the steel to those mentioned conditions..

2.1.1.1. Spheroidization

Austenite phase starts to form in the microstructure of steel, when the temperature reaches A_1 point of the steel. A_1 is the critical temperature to provide rapid carbide solubility.

Hypoeutectoid steels contain austenite and ferrite phases between A_1 and A_3 temperatures, and moreover, above A_3 temperature the microstructure of the steels becomes fully austenitic. However, to obtain this fully austenitic structure, it is necessary to provide sufficient soaking time and temperature. Otherwise, undissolved carbides will persist in the structure. For this reason, austenitic structure will be inhomogeneous.

The intercritical range for hypereutectoid steels such as 100Cr6 is between A_1 and A_{cm}. Also, the sufficient temperature and time conditions affect austenitic transformation and carbide dissolution in the same manner of hypoeutectoid steels.

Homogeneity of microstructure is critical considering the improvement of annealed structures. The influence of austenitization temperature is as follows:

- ✓ Higher austenitization temperature provides more homogeneous structures because of the occurrence of lamellar carbides.
- ✓ Lower austenitization temperature provides less homogeneous austenitic structure because of the occurrence of spheroidal carbides.

In terms of utilization of carbide dissolution; machinability and uniform response of hardenability of hypereutectoid steels such as 100Cr6 can be strongly improved by spheroidization treatment [17].

Further heat treatment procedures can be applied to spheroidized steel to obtain martensitic or bainitic transformations in the microstructure of 100Cr6 steel. It is well known that carbon and chromium contents have crucial effect on spheroidization kinetics; which can be summarized as:

- ✓ Increase of carbon content cause an increase on nucleation sites amount which provides spheroidization treatment.
- ✓ Chromium content decreases inter lamellar spaces between pearlite.

As it is expected, spheroidization has an important influence on bainitic and pearlitic transformation of austenite phase in 100Cr6 steel. Dissolution kinetics can be altered by adjusting soaking time and temperature in spheroidization treatment.

Therefore, in this study; 100Cr6 steel in a spheroidized condition was used as a raw material to prepare specimens and further heat treatment procedures were performed to obtain variations in the structure of the specimens [25].

2.1.1.2. Austenitization and Quenching

Both austenitization and quenching conditions have great influence on desired properties of the final material. Temperature and time are the main parameters for austenitization process where cooling rate has vital importance on quenching process.

Basic definition of quenching is rapid cooling of parts from their austenitization temperatures which are typically between 815 ^{o}C to 870 ^{o}C for steels. Conditions of quenching process directly affect the final types or amounts of the existing phases, presence of carbides in the structure or grain boundaries. For example, most steels subjected to different type of quenching procedures to obtain controlled amount of martensite. Therefore, parameters of quenching procedure strongly influence hardening properties of the material. Parameters such as selection of quenchant, cooling rate, specimen section and thickness are needed to be considered to apply proper type of quenching treatment which is crucial for obtaining desired structures [17].

The dependence of final properties of materials on austenitization time and temperature will be given in the subsections which are related to microstructural properties of 100Cr6 steels.

2.1.1.3. Sub-zero Treatment

Sub-zero treatment is also called as “cryogenic treatment” and it covers;

- ✓ Cooling the material between -50^{o}C and -270^{o}C which is absolute zero
- ✓ Holding at sub-zero temperature during sufficient time to obtain structural changes in the material
- ✓ Raising the temperature to room temperature
- ✓ Further tempering processes (optional)

This process is important especially for the high carbon steels which contain more than % 0.83 carbon. Final martensitic structure depends on the range of M_s and M_f temperatures of the steel rather than a stable temperature value. Therefore, final type of martensite can be controlled by adjusting the cooling conditions. Moreover, as it is considered on the previous chapters M_s and M_f range depends on the carbon amount of the material. Due to this fact of martensitic transformation, M_f point reduces to sub-zero temperatures for the steels which contains % 0.7 carbon in the structure. Therefore, sub-zero process is necessary to obtain complete martensitic transformation of austenite phase. The main purpose of this process is to provide fully martensitic transformation of retained austenite for hypereutectoid steels such as 100Cr6 [26].

Although, the type of sub-zero treatment influences the fracture toughness; and it generally causes a decrease of this property when compared to room temperature quenched steel specimens. In addition, amount of retained austenite decreases where hardness, amount of secondary carbides increase and carbide size refines. All of those changes improve wear resistance [27], [28].

2.1.1.4. Tempering

Tempering of steels is the process that includes reheating of the steels to a temperature below the critical point in order to improve the toughness and ductility, and it may also causes a raise of matrix grain size. Generally, hardened steels are subjected to tempering treatment in order to provide desired mechanical properties and to relieve residual stresses which were obtained after quenching [17].

Transition carbides have been reported to precipitate from supersaturated martensite of quenched bearing steel during the tempering treatment at 160°C. This carbide precipitation causes a relief of quenching stresses, which in turn improves the strength of the material [11].

2.1.2. Microstructure of DIN-EN 100Cr6 Alloy Steel

The heat treatment applications directly influence the microstructural properties of the materials, as emphasized at the previous section. Generally, steels are heated to austenitization temperature and hold at that temperature for sufficient time, then cooled down at different cooling rates or treated isothermally to obtain desired phases in the structure. After combinations of these thermal applications, the final microstructure of the steel can be composed of martensite, bainite, retained austenite and carbides.

There are many studies reported in the literature about these phase transformations of 100Cr6 steel, and this chapter will cover the microstructural variations, and so the improvements of material properties with respect to applied heat treatment procedures.

2.1.2.1. Martensitic and Bainitic Transformations

Perez et al. have studied prediction of dimensional changes with utilization of a quantitative analysis and predictions with the experimental results. Within the aim of their study, they have investigated microstructural development of martensitic 100Cr6 steel during tempering; and the prediction of dimensional changes which were obtained as a result of; (i) ε carbides precipitation, (ii) retained austenite decomposition, (iii) cementite precipitation, (iv) recovery of the dislocations, (v) coarsening of the martensite structures. They have performed two types of heat treatment, one with and the other without sub-zero process. As it is expected, the specimen which have subjected to the sub-zero treatment consisted of lower amount of retained austenite. Moreover, the results have showed a good agreement was found between measured and predicted dimensional changes [29].

Chakraborty et al. have investigated development of microstructural refinement of bainite and martensite in 100Cr6 steel. Therefore, they have considered two different cases; (i) the specimens which were subjected to prior cold deformation at different degrees were austempered at the same conditions, (ii) the specimens which were not subjected to any cold deformation were austempered at the same temperature but different time conditions. The result of this study showed that, as austempering time increased bainite and carbide fractions were increased whereas amounts of martensite and retained austenite were decreased. Besides, as the cold deformation degree was increased, bainite fraction was reduced and retained austenite amount was increased. Another result of this study showed that, bainitic refinement can be obtained by cold deformation process. This refinement improved the impact strength with increasing hardness and also improved tensile strength via utilizing duplex martensite, bainite structures [30], [31].

Amey et al. have examined influence of heat treatment conditions on the degree of distortion with respect to phase transformation of 100Cr6 steel. Different type of heat treatment procedures were performed on the specimens and individual martensitic, bainitic and superbainitic structures were obtained in each of the specimens. They have reported that, cooling rate has the major influence on dimensional changes. Cooling rate decreased by changing the cooling medium from water and oil to salt bath. The highest cooling rate was reached by water quenching, whereas slower cooling rate was utilized by oil quenching, both of which resulted in martensitic transformation.

Besides, even slower cooling rate was provided by salt bath quenching. Decreasing of cooling rate caused reduction of dimensional changes. Therefore, they have emphasized that, bainitic transformation can be utilized in order to avoid dimensional change during heat treatment [32].

2.1.2.2. Retained Austenite

Luzginova et al. have studied on development of thermal stability of retained austenite during bainitic isothermal transformation in 100Cr6 steel. They have reported that, retained austenite decomposition temperature depends on the soaking time for bainitic transformation. In addition, the thermal stability of retained austenite increased with chromium content by cementite dissolution. Also, volume fraction of retained austenite increased with increasing carbon content of austenite [33].

Püttgen et al. have investigated microstructural properties of 100Cr6 steel after semi-solid treatments. They have reported that, the microstructure of 100Cr6 steel consisted of martensite and great amount of retained austenite after semi-solid treatment and following rapid cooling process. The result of their study showed that, semi-solid treatment provided approximately the same hardness values but decreased the toughness compared to conventionally hardened steel. In addition, occurrence of MnS inclusions caused intergranular fraction of the quenched materials [34].

2.1.2.3. Carbides

Stickels have made an investigation about service life of through hardened 100Cr6 steel by treating the materials with carbide refinement process. Due to this reason Stickles have considered three cases; (i) fully carbide dissolution, (ii) isothermal transformation of austenite to pearlite or bainite, (iii) commonly used austenitization, quenching and following tempering treatments. The results have showed that, extension of soaking time caused coarsening of ultrafine carbides. Generally, ultrafine carbides increase the hardness. In addition, it was found that the specimens which contained ultrafine carbides also contained higher amount of retained austenite based on quick carbon saturation of austenite structure [35].

2.1.3. Residual Stress

Residual stresses are usually obtained in the structure after both thermal and mechanical processes. Since they cause reduction of fatigue life of component, they are undesirable in the structure. Especially tensile residual stresses can easily cause a failure, whereas the compressive stresses on the surface of the work piece improve the load bearing capacity at surface contact areas. Thus, existence of compressive stresses in the structure is beneficial for the fatigue life of a component [11]. Since it is vital for the performance and life of a component, the residual stresses has been studied vastly. A brief review of the related studies about 100Cr6 steels is given below:

Rivero et al. have published a study about residual stress deviations in 100Cr6 steel due to phase transformation in the microstructure. The comparison of the magnitude of residual stresses in the rolling direction to those in the opposite direction to rolling direction showed that dominant mechanism for generation of compressive residual stress was martensitic transformation of austenite rather than plastic deformation or strain hardening. Based on the result of this study it was recommended to provide martensitic transformation of austenite for enhancing the performance and extending the life of bearings [36].

Stickels et al. have made a research on influence of heat treatment on controlling the residual stress values in 100Cr6 steel. They have found that carburizing treatment can also be utilized to generate compressive stresses on the surface of the steel. Carbide fraction increased in the surface layer due to the carbon addition during austenitization, and so surface of the bearing reached higher hardness values than the interior regions. By considering the results of rolling contact fatigue test, it has been reported that the carburizing treatment increased the bearing life [37].

Apart from those mentioned here, there are many other studies in the literature about heat treatment applications, microstructural variations and residual stresses of 100Cr6 bearing steel. Within the scope of this study, which is basically non-destructive evaluation of microstructural variations in 100Cr6 steel specimens, only the fundamental principles have been included. After considering those referred studies in the literature, different heat treatment processes were utilized to obtain microstructural variations in the 100Cr6 steel specimens. The details of those heat treatments will be given in the 3rd chapter.

The following subsection will cover detailed information about Magnetic Barkhausen noise technique and its applications based on microstructural features of ferromagnetic materials.

2.2. Theory of Magnetic Barkhausen Noise Technique

Ferromagnetic materials consist of great number of magnetic regions which are called as “domains”. Inherently, magnetic fields of these domains randomly oriented as a result of energy minimization. These random orientations provide magnetization cancellation of domains, and thus the total magnetization reveals as zero. When an alternating magnetic field subjected to a ferromagnetic material, these magnetic domains will align parallel to applied field. Motion of domain walls due to this external field will cause abrupt flux jumps which are called as Magnetic Barkhausen noise (MBN) [38].

Following subsections will cover fundamental information about principles of magnetization and magnetic behavior of materials for better understanding of Magnetic Barkhausen noise generation in the structures of materials.

2.2.1. Background of Magnetic Barkhausen Noise

Magnetic Barkhausen noise technique is related to domain wall motion in the ferromagnetic materials. Due to the applied field response of domain walls, a noise signal is detected by MBN measurement system. Therefore, in order to understand Barkhausen noise phenomenon, it is needed to be clarified the properties of magnetic materials and related domain walls motion due to the applied field. For this reason following subsections will cover information about magnetic materials, domain behavior with respect to applied magnetic field and MBN measurement system.

2.2.1.1. Fundamentals of Magnetic Materials

Materials can be classified as magnetic and non-magnetic with respect to their response to applied magnetic field. Therefore, the materials that are respond to an applied magnetic field, called as magnetic materials. This property of a material can be characterized by magnetic susceptibility which is directly related to both magnetization (M) (A/m) and intensity of applied magnetic field (H_0) (A/m). Magnetic susceptibility (χ) (Wb/Am) is quantified as following equation;

$$\chi = M/H_0 \tag{2.1}$$

Magnetic susceptibility is a tensor, because it may be different for individual crystallographic directions of single crystals. For the materials that are magnetically isotropic, magnetization and applied magnetic field are parallel to each other, and for this case magnetic susceptibility is scalar.

Permeability (μ_0) (Wb/Am) is relevant to susceptibility (χ). And moreover, for the case of linear magnetization (M) and applied magnetic field (H_0), and for magnetically isotropic materials, permeability (μ_0) can be measured by following equation;

$$B = \mu_0 . H \tag{2.2}$$

B (Wb/m^2) is magnetic induction.

Due to the inherent relation of μ_0 and χ, dimensionless in other words scalar value of susceptibility which is called as relative susceptibility (χ_0) can be quantified as a unit of permeability (μ_0):

$$\chi_0 = \chi/\mu_0 \tag{2.3}$$

Relative susceptibility is the quantity of magnetism level of the material. If this value is 10^{-5} weak magnetization occurs, whereas the value of 10^6 provides to generation of strong magnetization. Relative susceptibility is influenced by applied magnetic field. Thus, for some conditions; if there is a non-linear relation between magnetization and applied magnetic field the χ_0 is negative. Due to this fact, behavior of relative susceptibility influences the magnetism and its type. Therefore classification of magnetic materials can be done by considering permeability and susceptibility [38], [39].

2.2.1.1.1. Magnetic Properties of Materials

Magnetic materials can be classified as diamagnetic, paramagnetic, antiferromagnetic, and ferromagnetic and ferrimagnetic with respect to their response of applied magnetic field.

✓ *Diamagnetism*

The relative susceptibility (χ_0) of diamagnetic materials is negative and very weak. It is approximately between -10^{-6} and -10^{-2}. In other words, diamagnetic materials have no inherent magnetic moment. Applied external magnetic field generates the weak and negative magnetic moment in the diamagnetic material.

✓ *Paramagnetism*

Paramagnetic materials have positive and weak relative susceptibility (χ_0) which is approximately between 10^{-6} and 10^{0}. Magnetic alignment of atoms in paramagnetic materials is random as it is visualized in the Figure 2.3-a. These random alignments do not provide cancellation of all magnetic moment. Therefore, it has net magnetization.

When magnetic field applied to a paramagnetic material, complete magnetic moment alignment of atoms is generated. Therefore, great amount of magnetic moment occurs in the material. Temperature dependence of paramagnetism explained by Curie Law which shows that thermal agitation raises by increase of temperature which causes reduction of relative susceptibility. This relative susceptibility reduction is based on more difficult atomic moment alignment due to adverse influence of thermal agitation on magnetic alignment.

✓ *Antiferromagnetism*

Antiferromagnetic materials contain two magnetic sub-lattices which individually consist of parallel magnetic moment. Due to the equal magnitude but opposite orientation of these sub-lattices as shown in Figure 2.3-b, complete cancellation of magnetization is provided. Therefore, the magnetic moment is zero in antiferromagnetic materials.

✓ *Ferrimagnetism*

Ferrimagnetic materials also contains two oppositely oriented magnetic sub-lattices, but their magnitudes are not equal to each other as it is represented in Figure 2.3-c. Therefore, complete cancellation cannot be provided, and so ferrimagnets has net magnetic moment. Moreover, a ferrimagnetic material transforms to paramagnetic material at and above its Néel temperature.

- ✓ *Ferromagnetism*

The relative susceptibility of a ferromagnetic material is approximately between the range of 10 to 10^7, which means that great amount of magnetization occurs due to the parallel alignment of atomic magnetic moments by application of external magnetic field. The atomic magnetic alignment is as represented in Figure 2.3-d [38], [39].

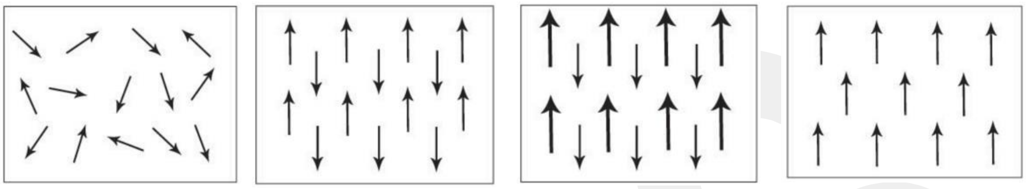

(a) (b) (c) (d)

Figure 2. 3 Representative magnetic moment alignment fo (a) Paramagnetic, (b) Antiferromagnetic, (c) Ferrimagnetic, and (d) Ferromagnetic materials [40].

Ferromagnetic materials consist of microscopic magnetic domains and application of magnetic field causes the generation of irreversible and nonlinear magnetization behavior of these magnetic domains. This behavior of ferromagnets can be explained by J-H, B-H or M-H curves, where J represents magnetic polarization, B is the magnetic flux density, M is the magnetization and H represents magnetic field. Detailed explanation of ferromagnetic hysteresis loop and dynamic behavior of domains will be given in following subsection for better understanding of this inherent characteristic of ferromagnetic material [41]–[44].

2.2.1.1.2. Magnetic Domain Behavior and Ferromagnetic Hysteresis

As a result of energy minimization, atomic magnetic moments have a tendency for parallel alignment in ferromagnetic materials. This kind of alignment provides an increase on magnetostatic energy based on the generation of great external field which is schematically represented in Figure 2.4-a. Due to this tendency, various magnetic domains are generated in a ferromagnet and each magnetic domain has own magnetic moment. In addition, since antiparallel magnetization occurs in the domains that separated by a domain wall, magnetostatic energy is reduced [38]. This antiparallel alignment is schematically illustrated in the Figure 2.4-b for better understanding.

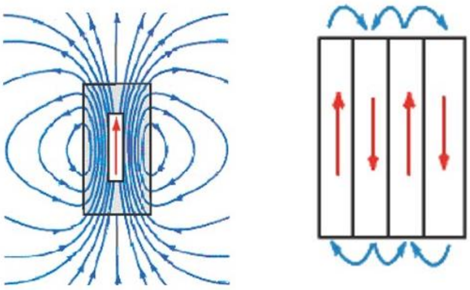

(a) (b)

Figure 2. 4 (a) atomic magnetic moment alignment (b) antiparallel magnetization of domaions [45]

In the case of magnetization direction sharply transits from one to another, very high exchange energy will be generated to keep the configuration of domains in equilibrium state. However, these sharp transitions are avoided by formation of a domain wall of a certain width which provides encompassment of the stepwise variation of atomic magnetic moments orientation. Due to this fundamental behavior which is shown in Figure 2.5, exchange energy is reduced, since the transition is smoother and aligned opposite direction to magnetization of domain [38].

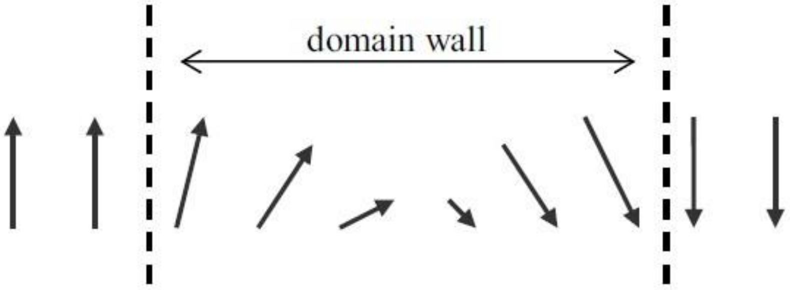

Figure 2. 5 Magnetic domain wall comprise atomic magnetic moment of stepwise variation of orientation [38]

Domain walls are classified as Bloch wall and Néel wall. Bloch wall is where the rotation of atomic magnetic moment occurs outside of the plane; and Néel wall is where atomic magnetic moment remains in plane during rotation. These rotations of atomic magnetic moments are schematically illustrated in Figure 2.6. Domain walls which separate the different oriented domains classified as 180^o, 90^o for iron, since the alignment tendency of domain magnetization through favored crystallographic axes.

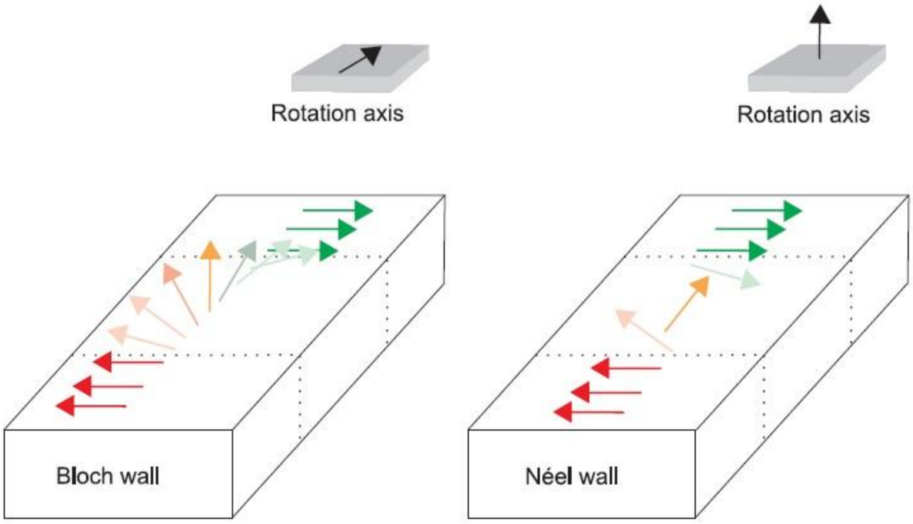

Figure 2. 6 Atomic magnetic moment rotations for Néel and Bloch walls [46]

Occurrence of remanence and coercivity caused by magnetic domain walls, and so the domains. They also cause the formation of ferromagnetic hysteresis [38]. When magnetic field applied to a ferromagnet, existing ferromagnetic order in the magnetic domain changed in spontaneous order. These variations in domains due to applied field are schematically represented on hysteresis loop of ferromagnetic materials in Figure 2.7. And also the critical values of M and H are specified below:

- Origin:	unmagnetized state	**-** H_c:	coercive field that sign of M changes
- m_s :	saturated state	**-** M_r:	remanent state in zero field

As can be seen from the Figure 2.7; both magnetization and magnetic field are zero on the origin which is the un-magnetized state. Magnetization immediately appears even application of slight magnetic field. Non-linear increase will occur if the magnetization initiates from the zero point of magnetic field. Further, increase of applied magnetic field cause occurrence of greater amount of magnetization in the structure which will also cause the elimination of individual magnetizations of domains by creating spontaneous magnetization in the direction of applied magnetic field at m_s point of magnetization. Due to this magnetic alignment of domains, m_s point is also known as the saturation of magnetization. M_r is the remanent state which is the value of magnetization that remains in the structure after removing the magnetic field. H_c is the necessary reverse magnetic field to reach zero state of magnetization. The sign of magnetization will change with further increase of this reverse magnetic field, and it will also reach a saturation with respect to parallel alignment magnetization of domains to applied field [39].

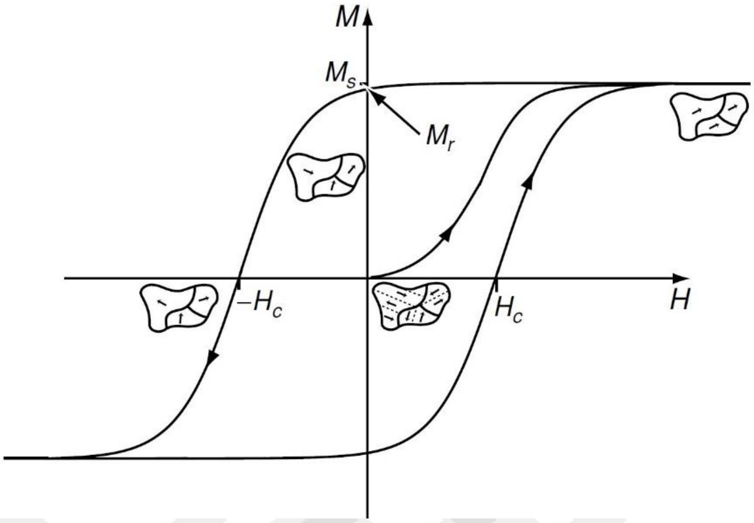

Figure 2. 7 Ferromagnetic hysteresis loop [39]

Moreover, ferromagnetic hysteresis loop show the properties of nucleation, domain wall displacement and coherent rotation. For better understanding of this behavior, it is illustrated in Figure 2.8. Reversible wall motion is observed in between the points 1 to 2 which is the part of hysteresis that represents initial magnetization state. In this initial state domain walls are pinned by pining sites but return to their initial configurations when magnetic field is removed. Therefore, reversible domain wall motion occurs in this state of magnetization. On the part of the curve between the points 2 to 3, irreversible Barkhausen jumps starts to form with irregular domain wall motion. This gradually eliminates the individual magnetic moment alignment of domains with further increase of magnetic field by raising the volume of domains that oriented in the direction of applied field. In addition, between the points3 to 4 individually magnetized domains coherently rotate through the direction of applied magnetic field. Besides, in this state irreversible domain wall is observed and it is known as saturation of magnetization. Irreversible domain nucleation starts in between points 5 to 6 and magnetization is reduced to zero, which is the point of coercive field (H_c). A ferromagnetic material cannot reach to initial state if it is not heated to above Curie temperature and cooled in zero field [39].

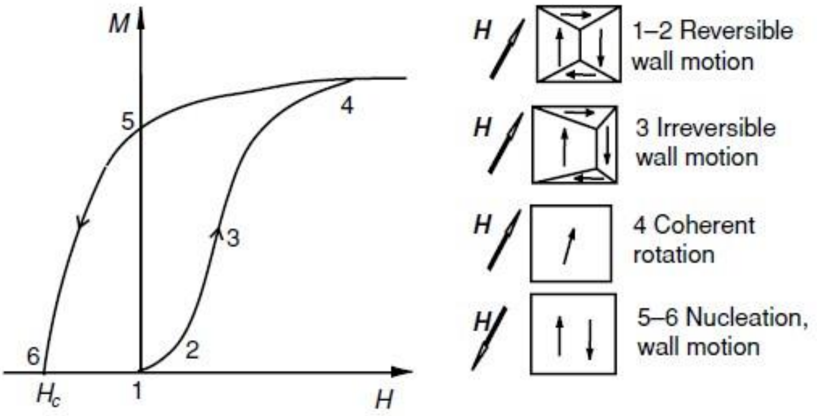

Figure 2. 8 Representative behavior of domain wall motion on ferromagnetic hysteresis. [39]

As explained above, applied magnetic field strength or stress state affect the magnetic domain configurations with respect to domain wall displacement.

Enhancing the technological applications of Magnetic Barkhausen noise (MBN), the magnetic domain response to applied magnetic field or stress can be detected. This detection is especially based on obstruction of domain walls by pining sites in the magnetic microstructure [38]. Detailed information about MBN technique will be given in following subsection.

2.2.1.2. Principles of Magnetic Barkhausen Noise Technique

As it is mentioned in the previous subsection, ferromagnetic hysteresis cycle consist of random discontinuous motions of magnetic domain walls with respect to their response to applied magnetic field. These discontinuous motion of domain walls cause the formation of Magnetic Barkhausen noise which is detected as sudden irreversible flux changes. As it is schematically illustrated in Figure 2.9 (a), these irreversible flux changes are mainly observed in the steepest sections of ferromagnetic hysteresis.

Magnetic moment of domains orient nearly parallel to the direction of applied magnetic field, due to their tendency to alignment through external field. Domain walls will move between neighbor domains and the ferromagnetic materials will be magnetized with increase in volume of these magnetically aligned domains.

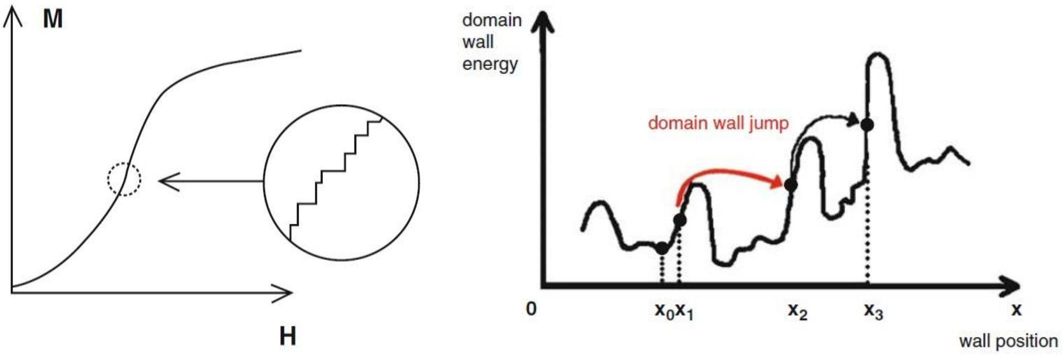

(a) (b)

Figure 2. 9 (a) Irreversible discontinuous flux changes represented in M-H curve (b) Irreversible domain wall displacement [38].

As illustrated in Figure 2.9-a, domain wall displacement through the pinning sites cause generation of sudden irreversible flux changes by influence of applied alternating magnetic field. Since domain walls obstruct by a number of pinning sites, they may lose some energy during their displacement. Therefore, they may not restore to their initial configurations after removing the external field. Schematic observation of this behavior is given in Figure 2.9-b. As it is seen in the figure, x_0 is assumed as the initial position of domain wall. As soon as it encountered with a pinning site, its energy will increase to jump over the obstacle. Although domain wall pass over the obstacle, it will not return to its initial energy level. Therefore, MBN also can be defined as irreversible jumps of domain walls occurred by passing over these pinning obstacles such as dislocations, inclusions, grain boundaries, precipitates, inhomogeneous micro-constituents, and other imperfections. Due to this fact, all irregularities in the structure of a ferromagnet retards domain wall motion, thus it is the reason of irregular and discontinuous varieties in magnetization [38].

2.2.1.2.1. Magnetic Barkhausen Noise Equipment

Due to inherent magnetic behavior of Barkhausen noise, it can be detected by the system that is able to sense magnetic flux variations in the materials. Figure 2.10-a illustrates the basic configuration of a typical MBN system. This system has a core that magnetized by alternating current to induce a magnetization in the test material. As a result of this applied current, magnetic domain wall motion occurs in the magnetized area of specimen and causes the formation of voltage pulses in the pick-up coil which is closely located to surface of the material. These detected voltage pulses represent the Barkhausen noise signals which are illustrated in Figure 2.10-b [47].

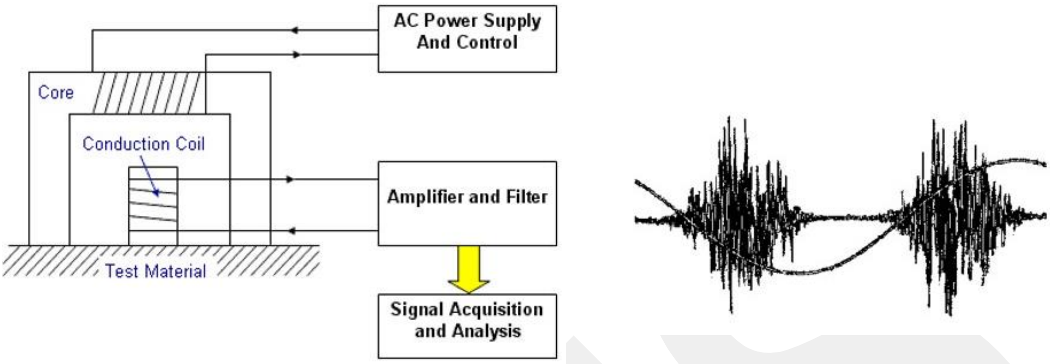

(a) (b)

Figure 2. 10 (a) Schematic representation of MBN system, (b) Representative MBN signal profile [47]

2.2.1.2.2. Magnetic Barkhausen Noise Parameters

Regardless of inhomogeneity in the microstructure, acquired magnetic field affects the detected MBN signals. Since their influence on power of magnetizing produced in the coils, magnetizing frequency and voltage are important parameters. For example, application of lower magnetizing voltage may cause the formation of weaker MBN signals that cannot be distinguished from the background noise. Although increasing the magnetizing voltage value will raise the signal intensity, further increase of magnetizing voltage beyond the saturation will cause a reduction of the sensitivity of the measurement. In addition, frequency variations affect the magnetic field penetration which also affects the result of the MBN measurements. The penetration depth can be calculated as follows:

$$\delta = \frac{1}{\sqrt{f\pi\mu_0\mu_r\sigma}} \tag{2.4}$$

δ : Penetration depth of magnetic field (mm)

f : Frequency (Hz)

μ_0 : magnetic permeability of vacuum (H/mm)

σ : Electrical conductivity (S/m)

μ_r : relative permeability (H/mm)

For example, while high frequency values reveal the MBN response of the thin layer of a surface, low frequency values increase the penetration depth, so reveal the MBN response of deeper distance from the surface. Therefore, these parameters have to be optimized to improve the sensitivity and accuracy of detected MBN signals [48]–[50].

By taking into account of this parameter on detected MBN profile characteristics, in the present study, a parameter optimization work have been done to specify the good combinations of magnetizing voltage and frequency to obtain proper MBN profiles, and so the results. Details of this optimization work will be given in 4th Chapter.

In order to analyze detected MBN signals which is obtained by series of voltage pulses and bursts as shown in Figure 2.11, different properties of MBN profiles are examined such as root mean square (RMS) value of voltage, peak height, peak position and peak width of the signal.

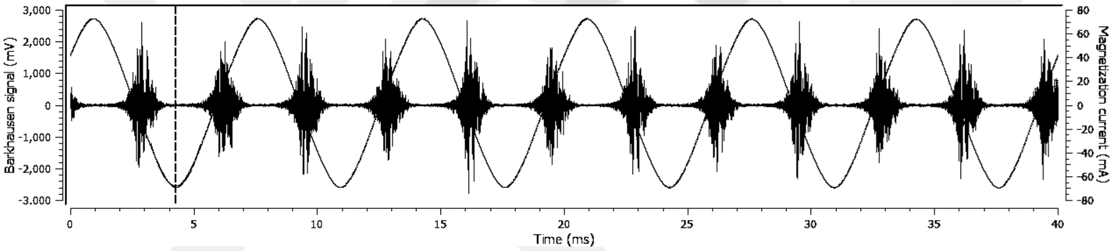

Figure 2. 11 Typical profile of Magnetic Barkhausen noise signal

Although all the properties of MBN profiles reflect the MBN response in the same manner, RMS value is the property which is mostly used to characterize MBN profiles due to its stability for each inspection cycle. It is calculated as following equation:

$$RMS\ (mv) = \sqrt{\frac{1}{n}\sum_{i=0}^{n-1} x_i^2} \tag{2.4}$$

Commercial MBN systems provide RMS value measurement of voltage signal over one full cycle and displays its numeric value instantly.

The MBN signals (RMS, peak height, peak position, peak width) are sensitive to deformational changes, residual stress state and microstructural features such as phases in the structure, grain boundaries, precipitates, inclusions and other imperfections. The relations between MBN response and microstructural features will be discussed in following subsection for better understanding of MBN phenomena.

2.2.2. Application of Magnetic Barkhausen Noise Measurement

Barkhausen noise technique is an alternative non-destructive inspection technique which still needs to be improved. Since it is a very promising for non-destructive evaluation, many studies have been done to understand the inherent characteristics of this technique. The following subsection will cover the literature review of MBN technique.

2.2.2.1. Influence of MBN Parameters

Blaow and Shaw have investigated MBN profile variations by changing the applied magnetic field strength and number of coil winding that affect the coil sensitivity. They have used case carburized steels as for this purpose and found that weak level of excitation field cause the formation of two peaks in equal height. Moreover, they have also found, with increase of excitation field, heights of both peaks increased but not equally. When certain excitation level have exceeded, saturation of magnetization is reached and no increased have observed in MBN intensity. In addition, they have investigate the coil sensitivity effect and have reported that, increasing the number of coil winding caused an increase on peak height of weak level excitation field [48].

2.2.2.2. Phase Fraction Influence on MBN Response

Moorthy et al. have used the MBN technique to evaluate the microstructural variations with respect to grain size, retained austenite, ferrite fractions, and also the related hardness of the structure. They have found a decrease of MBN response due to the increase of hardness with respect to increase of dislocation density. Also it is emphasized that, MBN response depend on inclusions, carbide precipitates and grain boundaries. They have reported that although strong influence of these microstructural variations on MBN response, individual effects of each property (i.e. inclusion, carbide precipitates, and grain boundary) cannot be distinguished from each other, unless some exclusive conditions is provided [51].

Davut and Gür have studied on microstructural characterization of spheroidized steel by MBN technique. Their study was concluded as the pearlitic structures gave lower MBN response, since cementite lamellae obstruct the domain wall motion. Increase of spheroidization level caused an increase of the distance between the cementite particles which cause a reduction of surface area of pinning sites. Thus, Barkhausen noise activity raises [52].

Neyra Astudillo et al. have studied on correlation between RMS value of MBN response and martensitic transformation that induced by plastic deformation of steel specimen. They have reported that, MBN technique has enabled to specify the initial point of martensitic transformation and also the estimation of fraction of formed martensite as a function of strain [53].

Kaplan et al. have investigated the possibility of non-destructive characterization of DP steels by MBN technique. They have characterized microstructures and hardness of their specimens both conventional destructive technique and MBN inspection technique. The results of this study showed that, there was a considerable correlation between volume fraction of martensite phase and MBN response of the specimens. A reduction of MBN response of ferrite has observed with increase of percentage of martensite phase. They have concluded their study as; MBN response have reduced due to the formation of finer martensite and increase of martensite percentage that cause higher dislocation density in the structure which obstructs nucleation and motion of domains [54].

Kahrobaee and Kashefi have used MBN technique to provide non-destructive evaluation of retained austenite fraction. They have found that, saturation magnetization level and permeability of the specimens were reduced where coercivity raised with increase in the amount of retained austenite. On the other hand, it is reported that, maximum amplitude of MBN signal raised with increase of retained austenite fraction. They have emphasized that, MBN technique was found a useful non-destructive technique on retained austenite characterization of D2 tool steel specimens, due to the matching of the retained austenite evaluation results of MBN technique and XRD technique [55].

2.2.2.3. Carbide Fraction Influence on MBN Response

Gatelier-Rothea et al. have investigated the carbide type, size, distribution and density influence on MBN by comparing MBN response of pure and carbon - iron binary alloyed specimens. The results of this study showed that, MBN response has been affected by the presence of carbides and they have influenced magnetic field dispersion which raise the amount of domain wall jumps and so, increased the RMS amplitude of detected MBN signals. However, coarsening of cementite precipitates have caused a reduction of RMS value [56].

2.2.2.4. Hardness Influence on MBN Response

Luo et al. have studied about utilizing the MBN technique for non-destructive hardness measurements. They have performed both hardness and MBN measurement and then compared the results. Finally, a good correlation was found between hardness and MBN response. Moreover, they have studied on improvement of sensitivity and accuracy of MBN measurement with analyzing the frequency domain which was utilized to eliminating the signals that are independent to the hardness of the specimens. Besides, they have reported that elimination of independent signals improved the accuracy of MBN measurement [57].

Santa-aho et al. have studied MBN applicability on characterization of case depth of hardened steels. They have reported that, besides, hardness, compositional and also the microstructural gradients such as residual stress had an influence on MBN response. However, they have concluded their study as reliable case depth estimation could have been done till depth of 1 mm via MBN measurement. They have also reported that, examination of magnetizing voltage sweeps made possible to measure the compositional gradients for deeper case depth values [58].

Franco et al. have investigated the possibility of hardness and microstructural characterization on the steel samples that were subjected to Jominy test. They have examined the hardness and microstructures of the specimens with both destructive techniques and MBN measurements. Comparison of the results of the study have showed that, there was a linear correlation between hardness and MBN response of the specimens and formation of different microstructures due to the different cooling rate also influenced the detected MBN signals as; increase of MBN response have been observed by changing the microstructures from martensitic structure to the coarser structure that consist of ferrite, cementite and bainite [59].

2.2.2.5. Grain Size Influence on MBN Response

Ktena et al. have been investigated the applicability of MBN measurement on microstructural characterization. Due to the aim of their study, MBN measurement have been performed on differently grain sized specimens and it was found that MBN response decreased with increasing in grain size [60].

Chukwuchekwa et al. have been done a research on grain size and orientation variations effect on MBN signal. They have reported that, increase of grain size enabled of easier domain wall displacement and therefore, greater MBN signal has been detected from the specimens with a larger grain size. Also, disorientations of grains caused restraining of MBN signal level [61].

Anglada-Rivera et al. have researched that applied tensile stress and grain size influence on detected MBN signal. They have reported that, applied stress caused an increase of amplitude of MBN signal up to a maximum point, after that maximum point exceeded further increase of tensile stress caused decrease of MBN signal amplitude. They have also been examined the characteristics of obtained hysteresis loop by varying the grain size in stressed specimens. Finally, it is concluded that increase of grain size resulted a decrease on maximum MBN signal amplitude which was explained by enhancement of easier domain wall motion with coarsening of the grains in the structure [62].

2.3. Magnetic Barkhausen Noise Applications on EN 100Cr6 Alloy Steel

Many studies are available in the literature about characterization of 100Cr6 steel which is the selected as experimental specimen of present study. Therefore, this subsection will cover the review of these studies about correlation between different properties of 100Cr6 steel and MBN profile and signals.

Since high frequency methods cause the formation of Barkhausen noise which consists of the noise signals that cannot be attributed to relative domain wall motion with respect to pinning obstacles in the structure. Therefore, Blažek et al. have made an investigation on 100Cr6 steel specimens for distinguishing the pure MBN signal from the raw noise signal. They have concluded their study as; during MBN measurements at high frequency levels the detected raw noise signal mainly consists of redundant noise signals which were formed by thermal and vibration effect on the sensor. However, at low frequencies these thermal and vibration effects were very little, and so it was negligible. Therefore, they have emphasized the importance of post-processing or filtering the raw noise signal of MBN measurements to provide a proper and meaningful noise signal [63].

Desvaux et al. have researched the MBN measurement capability on evaluation of residual stress state on the surface of the bearing. Due to the aim of their study, they have measured residual stresses by using both XRD and MBN measurement systems, and then compared the results to insure the reliability of MBN technique on surface residual stress estimation. The results showed that, MBN response have reduced with increasing the magnitude of tensile residual stresses, and a constriction of the amplitude of the signal have been observed for the case of increasing compression stresses. Moreover, meaningful accordance was found between the surface residual stress results of XRD and MBN techniques [64].

Mičietová et al. have studied non-destructive characterization of ground 100Cr6 steels by MBN technique. The specimens were classified due to surface preparation method with respect to selected worn grinding wheel. They have observed that damage level of the specimen surface strongly depends on the initial hardness of the bearings. This fact has caused a thermal softening on hard materials, whereas rehardening on soft materials with respect to white layer formation on the surface. The results also showed that although MBN signals can be correlated with the microstructure of the surface of the specimen, stronger relation was found between the hardness and MBN. Barkhausen signal amplitude was reduced with rehardening process where it was increased with thermal softening of the surfaces [65].

Neslušan et al. have made a research on possibility of non-destructive characterization of grinding burn in case-hardened bearing steels by MBN technique. The results showed that there is a positive correlation between residual stress and the MBN response of the case-hardened layer of the surface. MBN response raised with increase of residual stress. Moreover, in contrast to case-hardened layer MBN response of inner region was higher due to its larger amount of carbide fraction. Besides, it was observed that reduction of lattice parameter, which measured via XRD method, caused higher

MBN signals. In addition, increase in volume fraction of retained austenite resulted a reduction in detected MBN signal [66].

Although, many studies have been reported on the non-destructive characterization of 100Cr6 steel by Barkhausen noise technique, there is almost no study on correlating MBN measurements with microstructural changes in heat treated 100Cr6 steels. Therefore, this study aims at closing this gap by investigating relations between the MBN response and the microstructural features that are generated by heat treatment procedure. In this study, experimental works have been arranged in order to analyze these relations. Following chapter will cover the details of experimental works, and the results of these works will be given in 4th Chapter.

CHAPTER 3

PROCESS DESCRIPTION

This work aims at investigating the possibility of nondestructive characterization of 100Cr6 alloy steel's microstructure by Magnetic Barkhausen noise technique. Therefore, all arrangements were done to obtain variations in the microstructure and then to characterize them. Regarding to this motivation, experimental work of this study covers;

(i) dilatometric analysis of quenching and subzero treatments applied after austenitization at various temperatures for a range of durations; which produced variations in the microstructures of the specimens,
(ii) metallographic investigations to determine the carbide fractions and distributions,
(iii) hardness measurements to determine matrix hardness,
(iv) XRD measurements to determine retained austenite fraction,
(v) MBN measurements to investigate the micro-magnetic response of the specimens.

Detailed information about each experimental procedure will be given in following subsections.

3.1. Heat Treatment of 100Cr6 Steel Specimens

In this present work, Bähr-Thermoanalysis GmbH DIL-805 A/D quenching dilatometer was used to apply heat treatment procedures which were selected by considering the following two related purposes:

(i) Formation of microstructural variations in 100Cr6 steel specimens,

(ii) Estimation of M_s and M_f temperatures of the specimens with respect to their heat treatment conditions

Therefore, two different dilatometric analyses were performed to the specimens:

(i) Quenching dilatometry
(ii) Sub-zero dilatometry

In addition, all the heat treatment applications were performed under vacuum to avoid formation of an oxidation layer on the specimen surface. This was critical for following MBN and XRD measurements.

Following subsections will cover more detailed information about the dilatometer system and experimental programs that used in this present study.

3.1.1. Quenching Dilatometry and Test Conditions

Dilatometer is a system that measures dimensional changes of a material as a function of both time and temperature. Thus, collected data provides to determine the start and the end point of phase transformations on the thermal curve with respect to relative change in length or diameter.

Quenching applications of a dilatometer cover;

- ✓ Inductive heating of the specimen under air, inert gas or vacuum to specified temperature,
- ✓ Holding the specimen at that temperature to provide isothermal transformation,
- ✓ Cooling the specimen with gas or water at linear or exponential cooling rates

DIL-805 A/D Baehr-Thermoanalysis GmbH can perform experiments in a temperature range between -150°C to 1300°C and it is capable to apply maximum 4000 K/s of heating rate and 2500 K/s of cooling rate. Water cooled copper coil is used as an inductive heat generator to heat the specimens. Water, air, He, Ar, or N_2 can be used for quenching to cool the specimens at desired cooling rates. Moreover, displacement transducer (LVDT) is used to measure the longitudinal dimension change in specimens during transformation. Relative dimension changes can be occur during isothermal holding and/or quenching due to phase transformation. Time-temperature-transformation (TTT) and continuous-cooling-transformation (CCT) diagrams and so the critical temperatures of transformations can be determine by examination of these thermal curves [67].

For industrial applications, austenitization temperatures of 100Cr6 steels were between 840°C and 860°C. Thus, three different austenitization temperatures were selected around this range, which includes T_γ values below and above of the industrial range. So, in this present study, specimens were heated to 800°C, 850°C and 900°C at a heating rate of 100°C/s and hold at those temperatures for different time ranges under 10^{-4} mbar vacuum. After austenitization, all the specimens were quenched to room temperature (RT) at a cooling rate of 200°C/s by He gas. For better understanding, each set of heat treatment procedure was indicated in the Table 3.1. In addition, time and temperature diagrams of the specimens that were quenched to RT were given in the Figure 3.1. Since the phase transformation rates directly depend on the austenitization conditions, heat treatment applications were performed under different combinations of austenitization time and temperature. Where transformations rates were relatively slower at austenitization temperatures of 800°C and 850°C, faster transformations occurred at 900°C of austenitization temperature. Therefore, shorter time ranges selected for the samples austenitized at 900°C.

Table 3. 1 Temperature & time program for each set of heat treatment procedure

Austenitization temperature	***Austenitization time (minute)***								
800°C	0.17	2.5	5	10	30	60	120		
850°C	0.17	2.5	5	10	30	60	90	120	
900°C	0.17	0.5	1	2	4	8	16	30	60

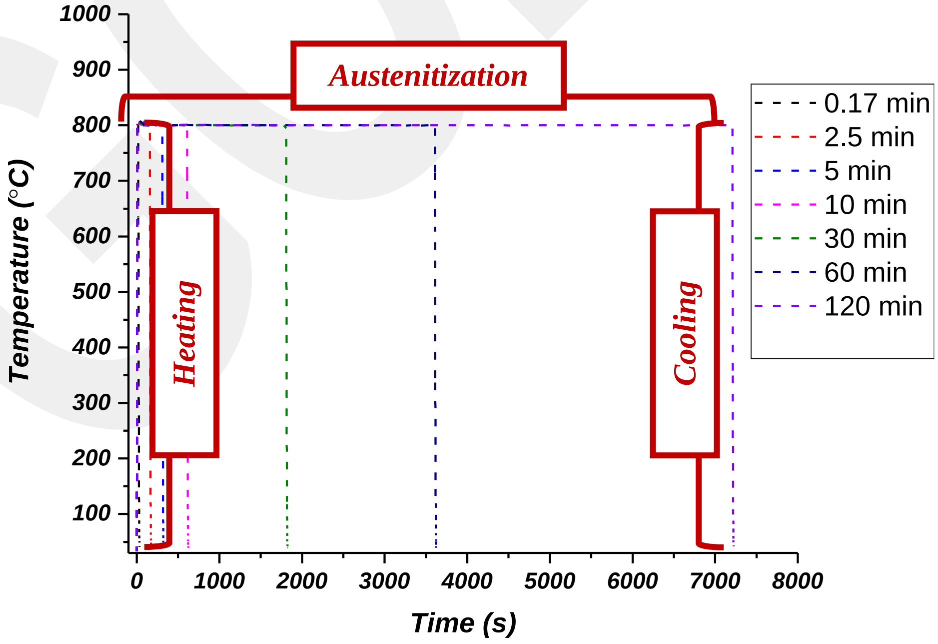

Figure 3. 1 Representative temperature and time diagram of the specimens that were austenitized at 800°C, then quenched to RT

3.1.2. Subzero Dilatometry and Test Conditions

Subzero dilatometry enables measuring the transformation strains below room temperature. As it is known, martensitic transformation of austenite in 100Cr6 steel finishes below the temperature of 0°C. Therefore, subzero treatment was necessary to estimate martensite finish (M_f) temperature and to provide fully martensitic transformation.

In this present work, specimens were heated to 800°C, 850°C and 900°C at a heating rate of 100°C/s and austenitized between 10 seconds to 120 minutes, and then cooled to approximately -130°C with liquid nitrogen at a cooling rate of 200°C/s. The austenitization time and temperature combinations were indicated in Table 3.2. Moreover, representative time and temperature diagrams of 800°C, 850°C and 900°C for 30 minutes of austenitization were given in Figure 3.2.

Table 3. 2 Temperature & time program for each set of sub-zero treatment procedure

Austenitization temperature	*Austenitization time (minute)*								
800°C	0.17	2.5	10	30	60	120			
850°C	0.17	2.5	10	30	60	90	120		
900°C	0.17	0.5	1	2	4	8	16	30	60

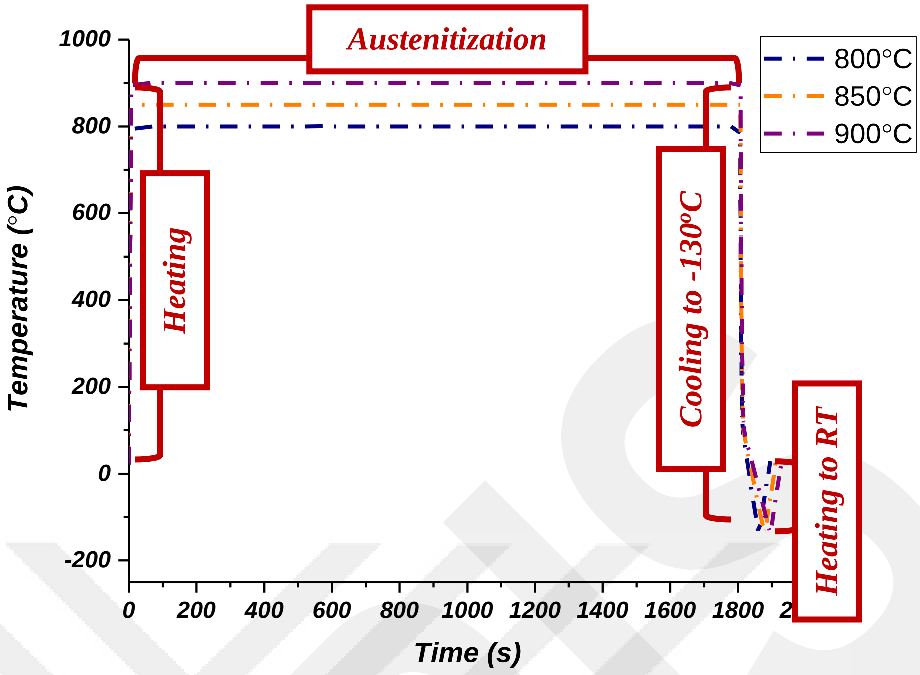

Figure 3. 2 Representative temperature and time diagram of sub-zero treatment procedures for 30 minutes of austenitization at (a)800°C, (b)850°C, and (c) 900°C, then quenched to -130°C

After these subzero treatments, in order to estimate M_f temperatures, transformation strains for each set of experiment were specified by examination of collected length in change data as a function of time and temperature.

3.2. Specimen Preparation

Specimens were produced from the same cylindrical 100Cr6 billet by application of the same machining and grinding processes in order to eliminate (if not bring to a negligible level) the influence of specimen preparation on the results. Two different types of specimens, listed below, were produced for each dilatometer mode;

(i) Solid specimens for quenching mode (Figure 3.3.a)
(ii) Hollow specimens for subzero mode (Figure 3.3.b)

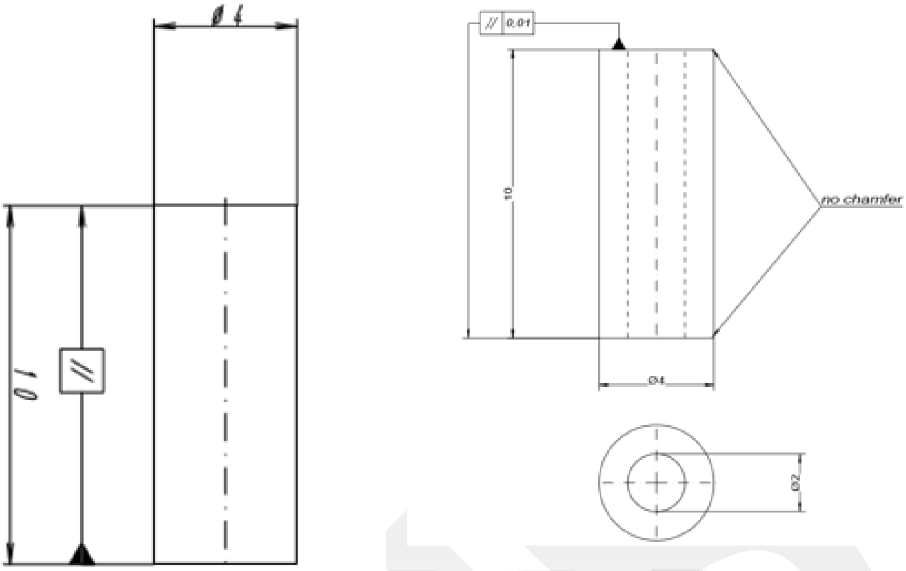

(a) (b)

Figure 3. 3 Technical drawing of (a) solid specimens for quenching mode, (b) hollow specimens for subzero mode

Besides, elemental analyses were performed by Bruker Q4 Tasman optical emission spectroscopy which provides identification and quantification of alloy elements in the base material. Measured elemental composition of raw 100Cr6 billet was given in following Table 3.3.

Table 3. 3 Chemical composition of as received 100Cr6 (wt. %)

C	Si	Mn	P	S	Cr	Mo	Ni	Cu	Al	V	Fe
0.995 ± 0.006	0.262 ± 0.006	0.294 ± 0.002	0.0079 ± 0.0003	<0.150	1.395 ± 0.006	0.016 ± 0.0007	0.041 ± 0.0007	0.096 ± 0.0009	0.015 ± 0.0005	<0.0050	based

3.3. Microstructural Characterization

After heat treatment procedures, all the specimens were subjected to metallographic preparation according to ASTM E03 [4]. Each specimen was prepared by following the steps that listed below;

(i) All the specimens were mounted into a bakalite resin via mounting press.

(ii) Then grounded with 320-500 grit of SiC papers and followed by polishing steps with 9 µm, 3 µm, 1 µm of diamond paste and final polishing with colloidal silica solution respectively.

(iii) After surface preparation, all the specimens etched with picral (2%) solution in order to reveal the microstructure of the heat treated specimens.

ZEISS Merlin scanning electron microscope (SEM) with field emission gun (FEG) was used to examine the microstructural properties of the specimens.

All the images were taken at an acceleration voltage of 15 kV by collecting the signals via back-scattered electron detector. Analytical working distance was between 6 and 8.5 mm. For each specimen 10 images from randomly selected positions were taken at 5000x magnification. Then, all the images were analyzed by Image J software in order to determine the accurate carbide fractions and distributions of all the specimens [68].

3.4. Hardness Measurements

Zwick ZHV 10 micro hardness device was used to measure macro and micro Vickers hardness values of the specimens. 4.903 N of load was applied for taking macro hardness and 0.4903 N of load was applied for taking micro hardness measurements at a test speed of 25mm/min. Minimum 5 indentations were made at randomly selected locations on each specimen.

3.5. X-Ray Diffraction Measurements

Heat treated 100Cr6 specimens contain retained austenite in their microstructures after quenching to room temperature. GE-Seifert X-Ray diffractometer was used to measure the retained austenite fractions of the specimens in accordance the ASTM E975-13 [5]. For a typical XRD measurement, the interaction volume extends 5 to 10 microns below the surface.

X-Rays were generated by chromium tube operating at 40 kV and 40 mA, and transmitted to specimen surface through 3 mm collimator. Position sensitive detector (PSD) was used to detect the diffracted X-Rays from the surface of the specimen from a range of 60° to 172° two theta angles. The intensities of the peaks at 79° and 129° and two theta angles which gives reflections from {200} and {220} family of planes were used to determine the volume fraction of austenite (FCC-iron). For determining ferrite (BCC-iron) the peaks at 106° and 157° two theta angles giving reflections from {200} and {211}family of planes were used.

3.6. Magnetic Barkhausen Noise Measurements

Magnetic Barkhausen noise measurements were performed by using a commercial system Stresstech Rollscan 300 and raw signal data was analyzed by the MicroScan 600 software. Sinusoidal cyclic magnetic field was subjected via ferrite core C-coil. Then, generated noise signals were collected by a general purpose sensor (S1-18-13-01) at a sampling rate of 2.5 MHz. Collected raw MBN signals were filtered with wide band pass filter between 50-1000 kHz.

The penetration depth of MBN measurement can be in between 10 and 1000 microns, which can be controlled by varying magnetizing frequency. Their relation was given in equation 2.4. Thus, in order to characterize the influence of MBN parameters (frequency and voltage) on applied magnetic field, magnetizing voltage was varied between 1 and 16 V in steps of 1 V and magnetizing frequency was varied between 50 and 1000 Hz in steps of 50 Hz. According to this set of varying measurement parameters, each specimen was subjected totally 320 MBN measurements.

The results and of all experimental work and discussions will be given in the 4th Chapter.

CHAPTER 4

RESULTS AND DISCUSSIONS

In this part, all of the results will be given under three main subsections:

(i) First; martensite start and finish temperature determinations of heat treated 100Cr6 steel specimens were given under the title: *Dilatometric Analysis*

(ii) Secondly; microstructural properties that were characterized by metallographic and microscopic techniques, image processing, hardness and XRD measurements were given under the title: *Microstructural Characterization*

(iii) Finally; correlations of microstructural properties with MBN measurements were discussed under the title: *Magnetic Barkhausen Noise Measurements.*

4.1. Dilatometric Analysis

Austenite starts to transform to martensite at M_s temperature. Thus, it is the highest temperature for martensitic transformation. Besides, M_f is defined as the lowest temperature that austenite transforms to martensite. These critical temperatures are directly depend on the chemical composition and thermal history of the material i.e. initial thermal conditions, austenitization temperature (T_γ), austenitization time (t_γ), heating and cooling rate [69].

Continuous cooling transformation (CCT) diagrams were constructed via JMatPro software with respect to T_γ of 800°C, 850°C and 900°C and given in Figures 4.1-4.2 and 4.3 respectively. Initial compositional input was selected same as present experimental material; also critical time and temperature influence on M_s temperatures were compared at the same cooling rate for different austenitization temperature values. It was clearly observed from the CCT diagrams; as T_γ decreases, M_s temperature increases and martensitic transformation starts in shorter time range which was defined as elapsed time for cooling from T_γ to a temperature below M_s.

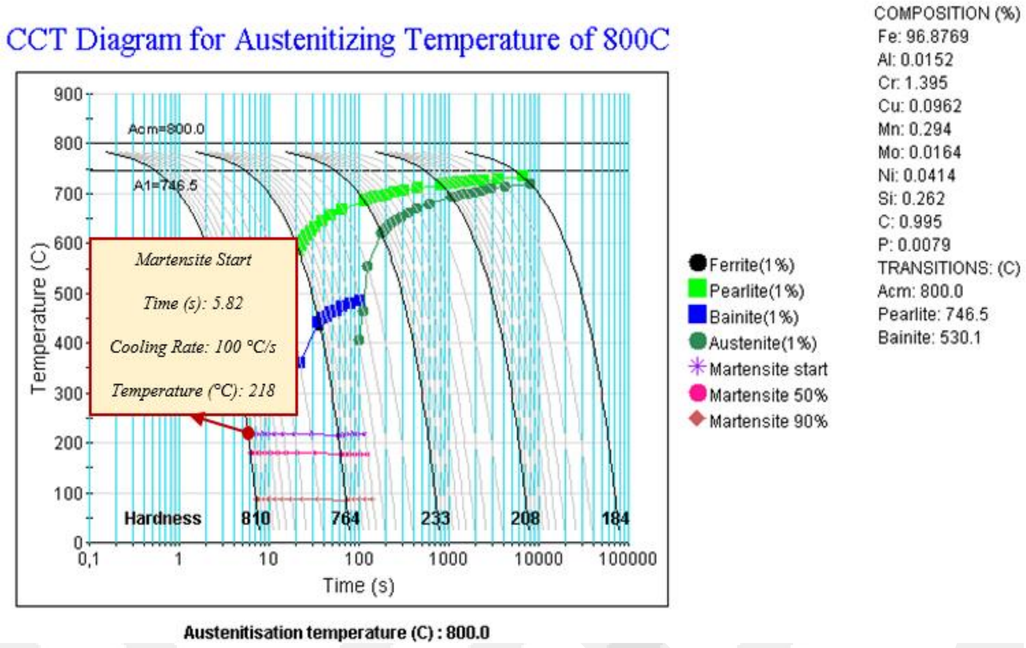

Figure 4. 1 CCT diagram for austenitization temperature of 800°C

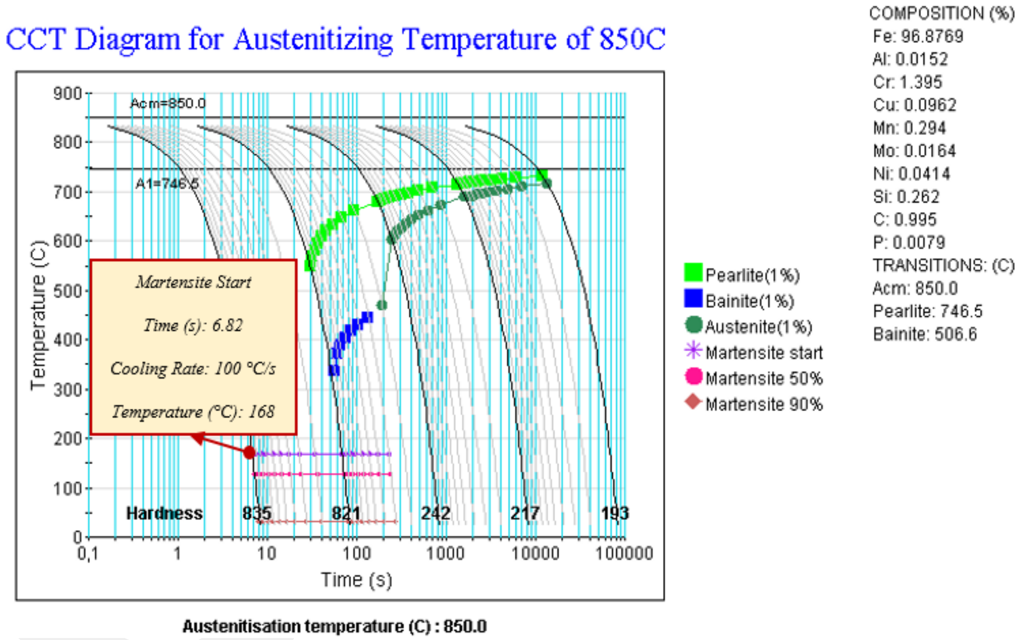

Figure 4. 2 CCT diagram for austenitization temperature of 850°C

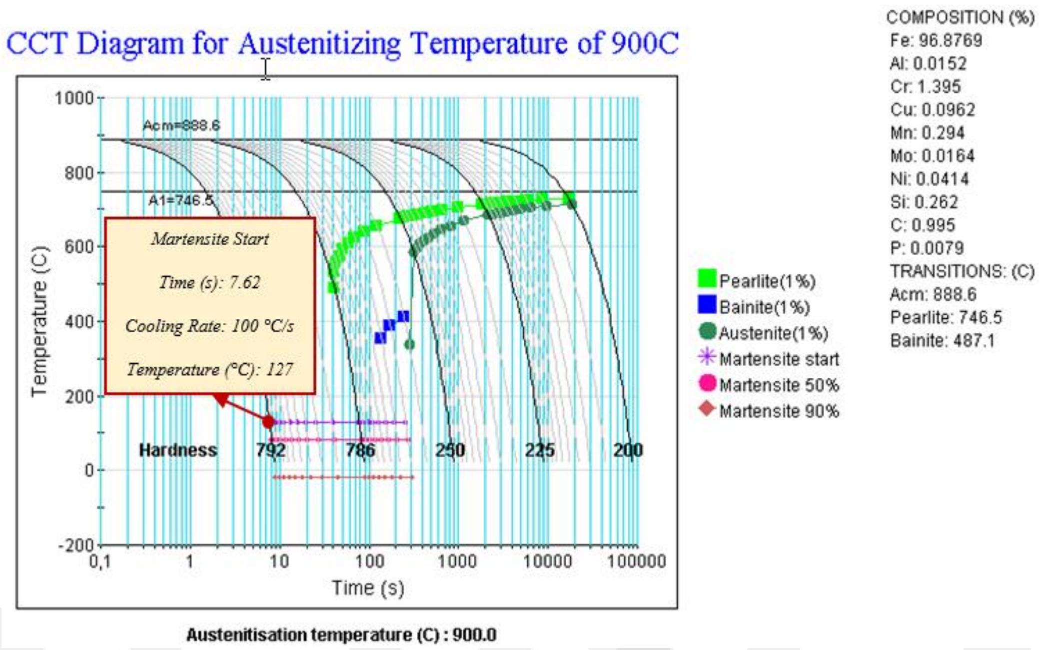

Figure 4. 3 CCT diagram for austenitization temperature of 900°C

This behavior of M_s change may be caused by more than one interdependent reasons;

i. Increase of T_γ cause a significant increase of carbide dissolution in FCC lattice structure of austenite. C and Cr fractions in austenite phase with respect to both T_γ and t_γ were given individually in Appendix A. These plots were reconstructed by using the data which were obtained via Thermo-Calc Software. Obviously, more carbide will be dissolved in austenite at higher T_γ values and for longer durations.

ii. Since carbon stabilizes the austenite, increase of dissolved carbides in austenite lattice structure will cause a retardation of martensitic transformation. Moreover, Cr enrichment also caused a reduction of necessary cooling rate for martensitic transformation based on its effect on hardening depth.

iii. Finally, this retardation will cause a reduction of M_s temperature for higher T_γ values. This was also observed in the phase transformation diagrams which were given in Figure 4.4. They were constructed as a function of volume% of austenite and martensite phases via JMatPro software with respect to T_γ of 800°C, 850°C and 900°C at a cooling rate of 200°C/s. It was clearly seen in these theoretical diagrams, M_s temperature lower with increasing austenitization temperature. Beside, cooling from T_γ to room temperature was not sufficient to complete martensitic transformation. Therefore, subzero treatments were performed to determine the M_f temperatures of the specimens for each set of experiment.

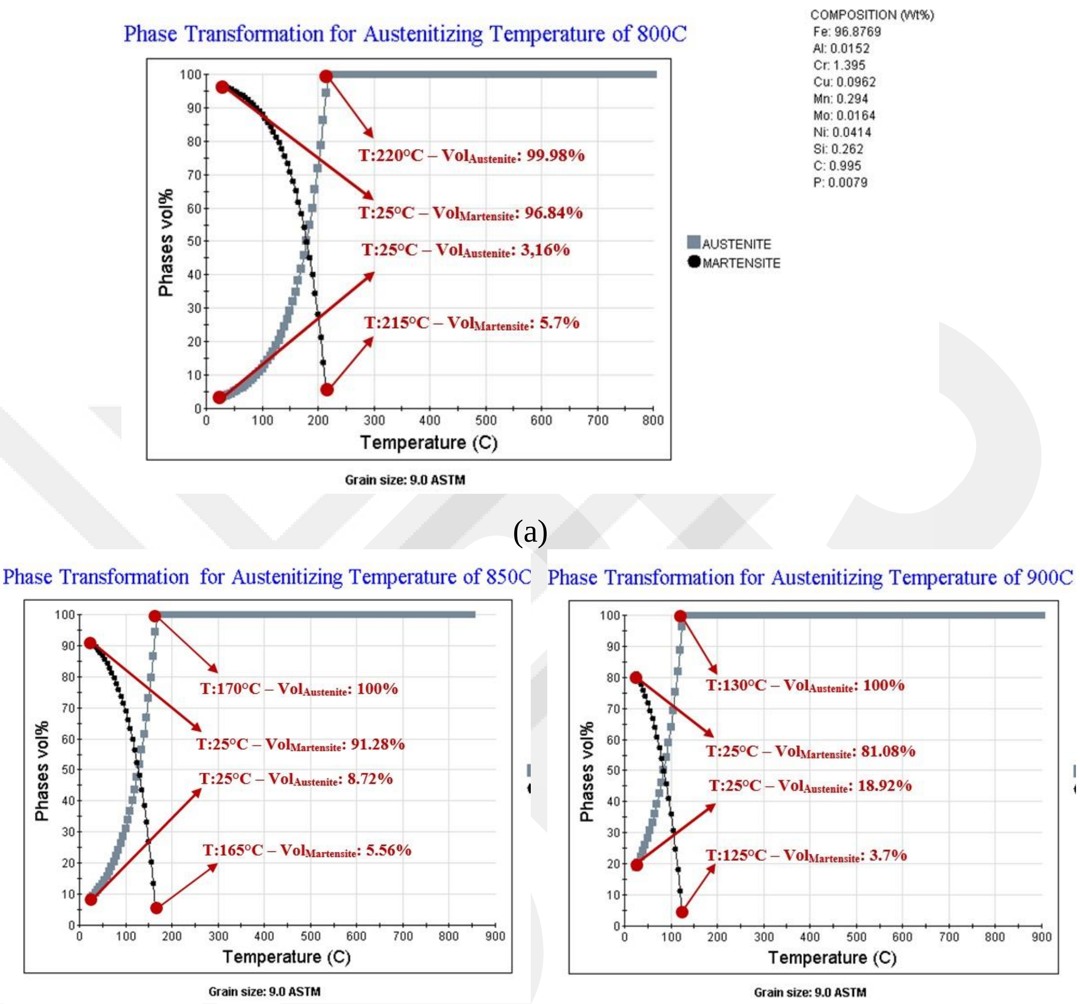

(a)

(b) (c)

Figure 4. 4 Phase transformation of 100Cr6 steel that austenitized at (a) 800°C, (b) 850°C, and (c) 900°C

As it is well known, BCC ferrite transforms to FCC austenite at T_γ and this transformation is completed after holding at this temperature for sufficiently long soaking time. During austenitization, carbides which are present in the prior microstructure start to dissolve in FCC lattice structure of austenite. After quenching, these dissolved carbides cause a dimension change due to transformation of FCC austenite to BCT martensite with rapid cooling of the material. So, this is basically caused by martensitic transformation of austenite by distortion of lattice structure.

Therefore, M_s temperature can be estimated by determining the temperature that sudden dimension change is observed.

Linear expansion variation (as a function of phase transformation) with respect to temperature change during cooling from T_γ was illustrated in the diagrams that were given in Figure 4.5. They were constructed via JMatPro software with respect to T_γ of 800°C, 850°C and 900°C at a cooling rate of 200°C/s. Based on these diagrams, it was obvious that maximum dimension change observed as soon as austenite starts to transform to martensite. Besides, immediately, sharp linear expansion changes occur in the structure. The linear expansion data read from the diagrams showed that, austenite starts to transform to martensite at approximately -1% of relative dimension change. In addition, after beginning of martensitic transformation, linear expansion became smaller for further cooling steps.

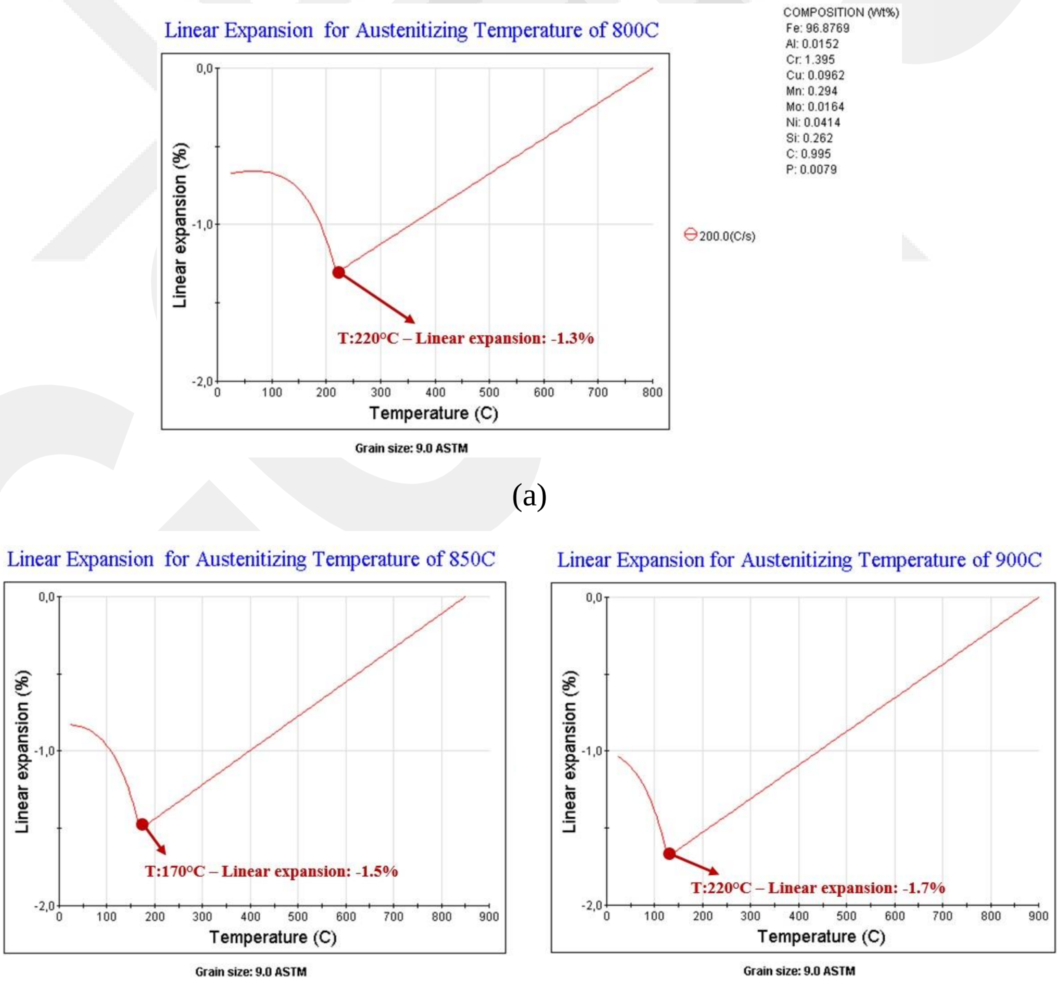

(a)

(b) (c)

Figure 4. 5 Linear expansion change of 100Cr6 Steel during cooling from 800°C to RT at a 200°C/s of cooling rate

In this present work, initial conditions including chemical composition, heating and cooling rates, and other test conditions were the same but the austenitization time and temperature were varied. Raw change in length data which was collected during dilatometric analysis was used to estimate M_s and M_f temperatures for each test condition. In addition, all of these results were compared with inferences which were made from previous theoretical diagrams (Figure 4.1, 4.2, 4.3, 4.4, 4.5 and Appendix A).

Experimental cooling curves were drawn with respect to austenitization temperatures of 800°C, 850°C and 900°C and illustrated in Figures 4.6-a, b, and c respectively. Based on the diagrams in Figure 4.5, temperatures where relative change in length was approximately -1% was specified as M_s temperatures and these calculated M_s temperature values were given in Table 4.1 for each individual set of experiment.

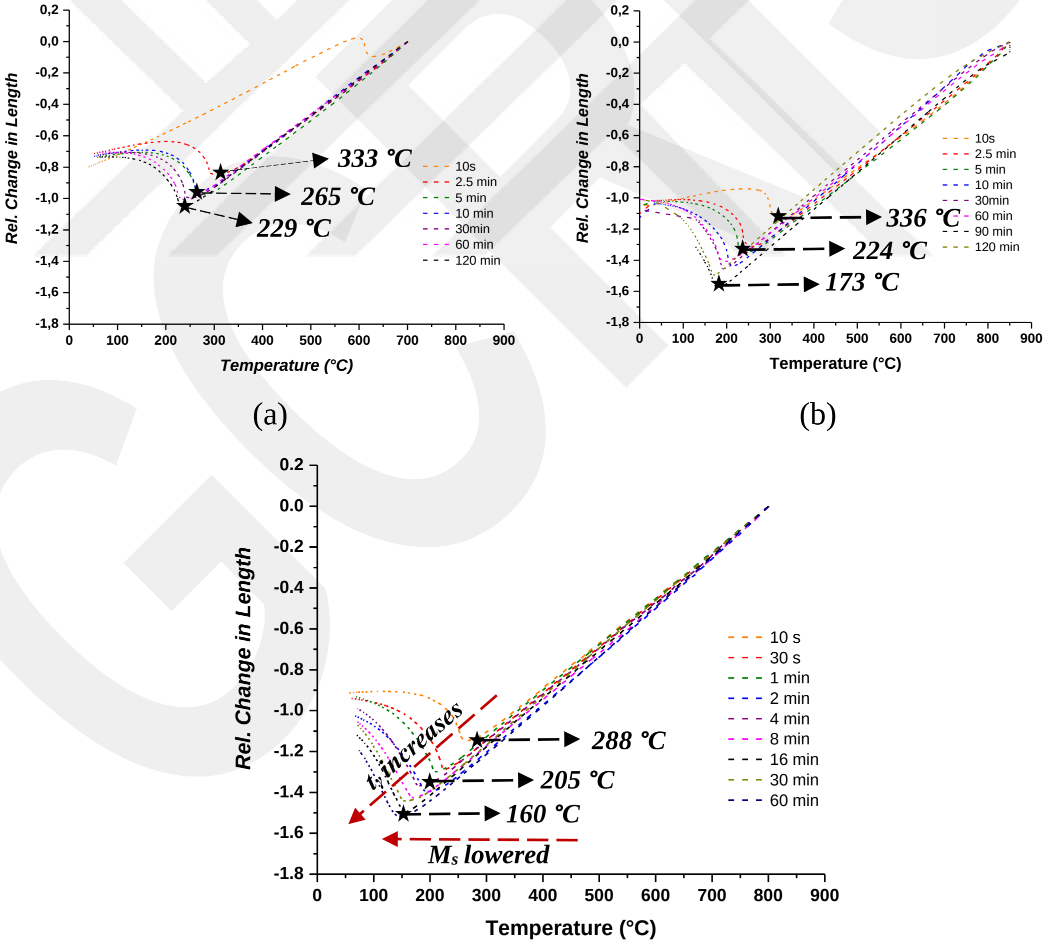

(a) (b)

(c)

Figure 4. 6 Dilatometric cooling curves for specimens that were austenitized at (a) 800°C (b) 850°C (c) 900°C then cooled to room temperature

As it was seen in the Figures 4.6-a, b, c; cooling curves, shift to lower M_s temperature values, if T_γ was kept constant and t_γ was increased. Moreover, relative change in length values became larger with increasing austenitization time due to the increase of dissolved C and Cr amount in the FCC structure. This behavior of M_s temperature change with respect to t_γ was observed due to similar interdependent reasons of T_γ influence on M_s change:

i. Although T_γ is constant, raise of t_γ will cause an increase of carbide dissolution in FCC lattice structure of austenite. This time dependence of C and Cr dissolution in FCC austenite were also represented in Appendix A.
ii. Since austenite was stabilized by increase of C amount in FCC structure, delayed martensitic transformation of austenite occurred in the specimens.
iii. Consequently, M_s temperature decreased for longer t_γ values due to the delayed martensitic transformation of austenite.

Since the martensitic transformation of austenite delayed, its transformation will be completed for longer time ranges. Thus, M_f temperature also lowered for higher t_γ and T_γ values. Calculated M_s (Table 4.1) and M_f (Table 4.2) temperature values were plotted with respect to austenitization conditions for better understanding of both time and temperature dependence of critical temperatures. These comparisons of M_s and M_f temperatures were given in Figure 4.7 a, and b respectively. As it was clearly observed in these figures, similar trends were followed for each set of experiment. Both of these critical temperatures decreased for two different conditions due to the reasons that were explained above;

i. Increasing austenitization temperature while austenitization time kept constant
ii. Increasing austenitization time while austenitization temperature kept constant

Table 4. 1 M_s temperatures of each set determimed from dilatometric analysis

T_γ (°C)	***800***	***t_γ (min)***	***0.17***	***2.5***	***5***	***10***	***30***	***60***	***120***		
		M_s (°C)	-	333	287	265	255	233	229		
	850	***t_γ (min)***	***0.17***	***2.5***	***5***	***10***	***30***	***60***	***90***	***120***	
		M_s (°C)	336	279	268	224	201	194	187	173	
	900	***t_γ (min)***	***0.17***	***0.5***	***1***	***2***	***4***	***8***	***16***	***30***	***60***
		M_s (°C)	288	238	230	220	205	191	170	162	160

Table 4. 2 M_f temperatures of each set determined from dilatometric analysis

T_γ (°C)	800	t_γ (min)	0.17	2.5	10	30	60	120			
		M_f (°C)	-	184	124	-31	-79	-103			
	850	t_γ (min)	0.17	2.5	10	30	60	90	120		
		M_f (°C)	199	33	-73	-82	-104	-116	-111		
	900	t_γ(min)	0.17	0.5	1	2	4	8	16	30	60
		M_f (°C)	152	101	45	-32	-54	-62	-70	-88	-116

As it was seen from the curves of M_s and M_f temperature variations in Figure 4.7; a sharp decrease was observed for shorter austenitization time values while it became smoother for longer austenitization durations. This asymptotic trend of curves might be explained by considering faster carbide dissolution occurred in FCC austenite structure at early stages of austenitization due to higher driving force. Since these critical temperature variations directly influenced by this fact of carbide dissolution, sharp changes observed at very early stage of austenitization and it became smoother for longer duration of austenitization.

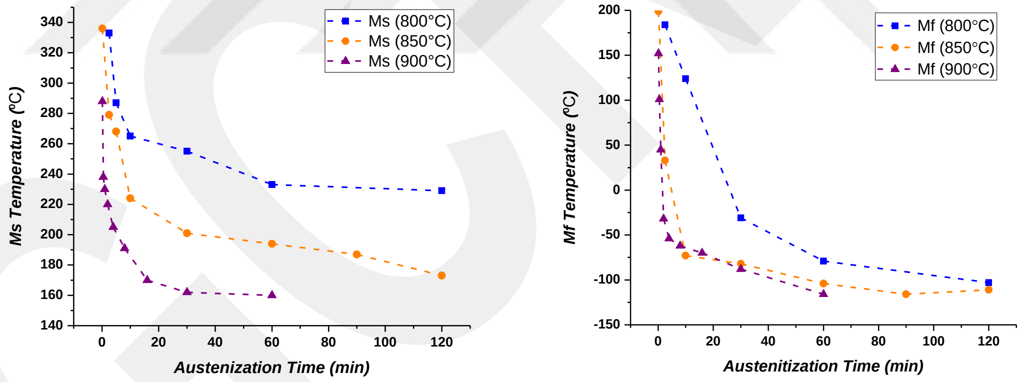

(a) (b)

Figure 4. 7 Comparison of (a) M_s temperatures (b) M_f temperatures

In addition, it was also seen from the experimental cooling curves (Figure 4.6-a, b, c) martensitic transformation obtained for each heat treatment condition except 10 second of austenitization at 800°C. Since this combination of T_γ and t_γ was not sufficient for austenitization, martensitic transformation was not able to occur due to absence of austenite in the structure.

In addition to all of these experimental works, M_s temperatures were also calculated using eight different empirical formulas (Table 4.3) all of which were developed for low alloy medium carbon steels. The empirical formulas allow estimating the Ms temperature as a function of chemical composition. Due to chemical composition requirement of these formulas, C and Cr fractions for each experimental conditions were taken from the simulation results of C, Cr dissolution (Appendix A), and compared with experimental results (Figure 4.8).

As can be seen from the Figure 4.8 (a), (b) and (c) predicted M_s values did not perfectly match with the experimental ones, especially for the shorter austenitization time. This behavior can be explained as:

(i) C and Cr dissolution simulations have been performed by assuming that only C and Cr were present in the material. Therefore, the specified values of C and Cr from this graph might not present exact condition since other elements present in 100Cr6 steel (given in Table 3.3) has been neglected.

(ii) All of the empirical formulas used to estimate Ms, assume that, all of the elements dissolve in the microstructure. The specimens that were austenitized at 900°C longer than 8 minutes, and the specimens that were austenitized at 850°C longer than 30 minutes might be close to this situation.. Thus, some of the predicted M_s values which were calculated by using the formulas of 2, 4, 7, and 8 in Table 4.3 were close to the experimental values. The greatest difference between the calculated and the experimental Ms values was detected in the samples austenitized for shorter durations. This can be explained by heterogeneous distribution of carbon, specifically at the exterior side of carbides. This heterogeneity might also cause occurrence of more than one M_s temperatures.

(iii) Besides, all the possible interactions between elements were not considered in these empirical formulations. For some formulations (4 and 6), only the interaction between C and Cr were considered and the rest was neglected.

Consequently, all of these considerations might clarify the reason of observation of high variations between the predicted and calculated M_s temperature values.

Table 4. 3 Emprical formulas for M_s prediction [70], [71]

1 ●	M_s (K)=772-300C-33.3Mn-11.1Si-22.2Cr-16.7Ni-21.2Mo
2 ▲	M_s (K)=812-423C-30.4Mn-12.1Cr-17.7Ni-7.5Mo
3 ▼	M_s (K)=811-361C-38.9Mn-38.9Cr-19.4Ni-27.8Mo
4 ◆	M_s (K)=785-453C-16.9Ni-15Cr-9.5Mo+217C^2-71.5CMn-67.6CCr
5 ◀	M_s (°C)=521-353C-22Si-24.3Mn-7.7Cu-17.3Ni-17.7Cr-25.8Mo
6 ▶	M_s (°C)=512-453C-16.9Ni-15Cr-9.5Mo+217C^2-71.5CMn-67.6CCr
7 ⬢	M_s (°C)=834.2-473.9C-33Mn-16.7Cr-17.7Ni-7.5Mo
8 ★	M_s (°C)=561-453C-33Mn-17Cr-17Ni-21Mo

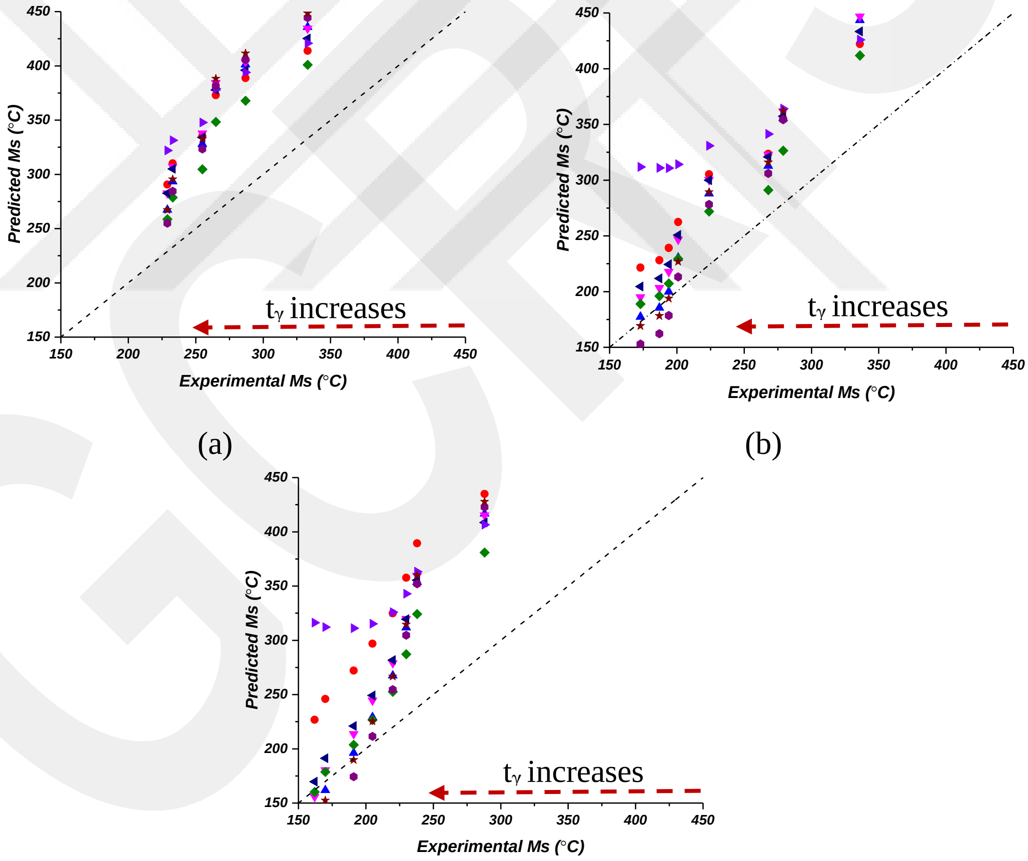

(a)

(b)

(c)

Figure 4. 8 Comparison of predicted and experimental M_s values for austenitization temperature of (a) 800°C, (b) 850°C and (c) 900°C. The symbols were indicated in the Table 4.3, next to related emprical formulation.

4.2. Microstructural Characterization

Carbide dissolution was the main mechanism of influence of austenitization temperature and time on microstructural variations. Since the carbides present in the initial microstructure dissolved during austenitization, they caused significant changes in the final microstructure of the specimens. For better understanding of final microstructural variations, initial microstructural properties of raw material were characterized. The results showed that; approximately 15% (14.5±0.87 area %) of spheroidized carbides were present in ferrite matrix. Besides, the hardness was measured as 200±8 HV and approximately 3% of retained austenite was detected in the structure of the raw material. Initial microstructure of spheroidized 100Cr6 steel specimens was shown in Figure 4.9 which was composed of dispersed spheroidal carbides in a ferrite matrix.

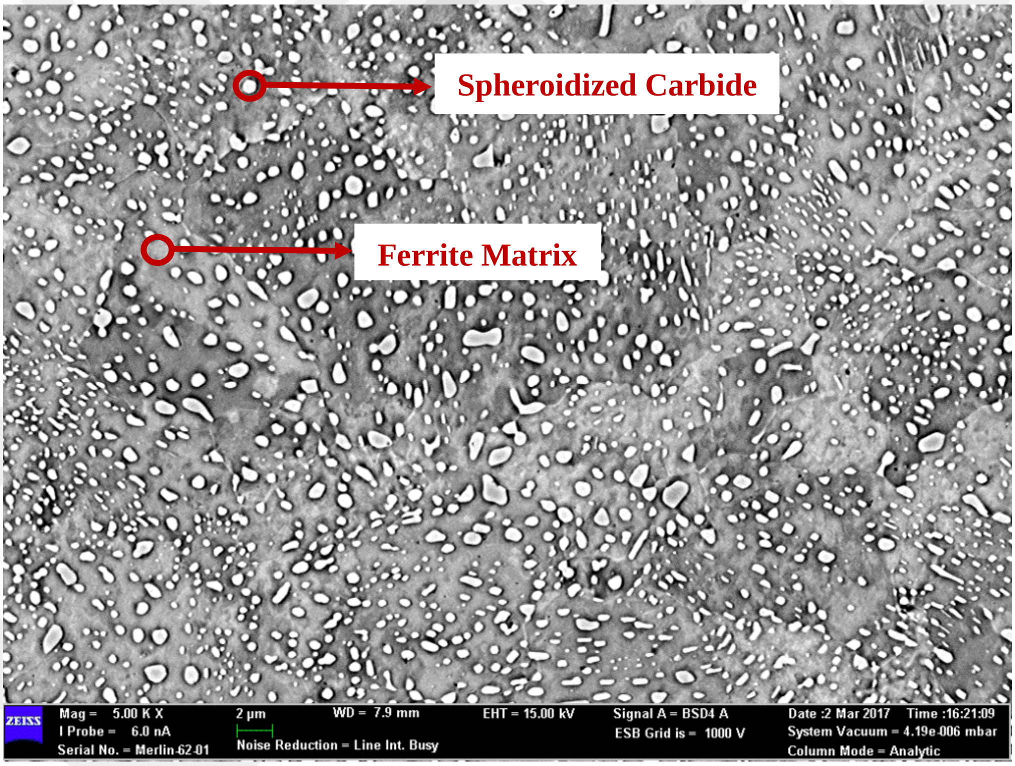

Figure 4. 9 BSD micrograph of as received 100Cr6 steel specimen showing the spheroidized condition at 5000x

Since all the specimens were extracted from the same raw material, identical specimens were subjected to heat treatment procedures at different austenitization conditions. Therefore, carbide dissolution behavior was investigated with respect to variations of austenitization time and/or temperature values. Considering the simulation results of the carbide dissolution and phase transformation of EN 100Cr6 steel (Figure 4.10) of the study which had been by Epp et al, ferrite starts to transform austenite and carbides starts to dissolve above 730°C, and then the amount of both carbides and ferrite decrease while austenite increases [24].

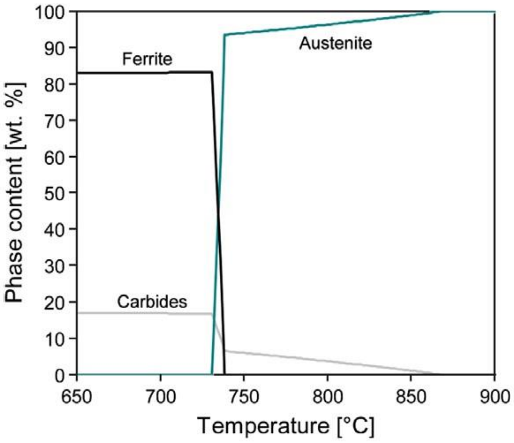

Figure 4. 10 Carbide dissolution and phase transformation of EN 100Cr6 steel [24]

In this study, similar transformational changes and carbide dissolution behavior was observed. As it was represented in Figure 3.1, heat treatment procedures covered three main processes; (i) heating, (ii) austenitization, and (iii) quenching. In order to understand the related microstructural changes all of these three steps individually considered.

(i) Raw material's microstructure that consists of 14.5% of carbide in ferrite matrix started to change above A_1 temperature of 100Cr6 steel. At that temperature, ferrite started to transform to austenite and carbides started to dissolve in austenite structure.

(ii) During austenitization, the fraction of austenite increases whereas carbides dissolve and their fraction decrease as austenitization temperature and/or time increases. C and Cr dissolution behavior in austenite were given Appendix A as a function of T_γ and t_γ. These theoretical curves were constructed by taking into account of initial properties of raw material and experimental conditions of present study. At early stages of austenitization, faster C and Cr diffusion was observed in FCC lattice structure due to higher driving force with respect to higher compositional gradient between the carbides and austenite. However, the diffusion rate became slower, since this gradient became smaller with increase of elapsed time of austenitization and/or increase of austenitization temperature. Moreover, an equilibrium state can be reached after a sufficiently long t_γ.

(iii) If sufficiently slow cooling from T_γ to room temperature cannot be provided, these dissolved carbides cannot diffuse from FCC structure to the material matrix. Therefore, they stuck in FCC structure with rapid cooling. This causes distortion in the lattice, and so the formation of BCT lattice structured martensite. A representative micrograph among all the specimens (Figure 4.12, 4.13, 4.14) was given in Figure 4.11 which was obtained from the specimen that austenitized at 900°C for 60 minutes for better observations of remained carbides and martensite matrix. As it can be seen from the micrograph, small quantities of carbides revealed in martensite matrix compared to the as received 100Cr6 specimen.

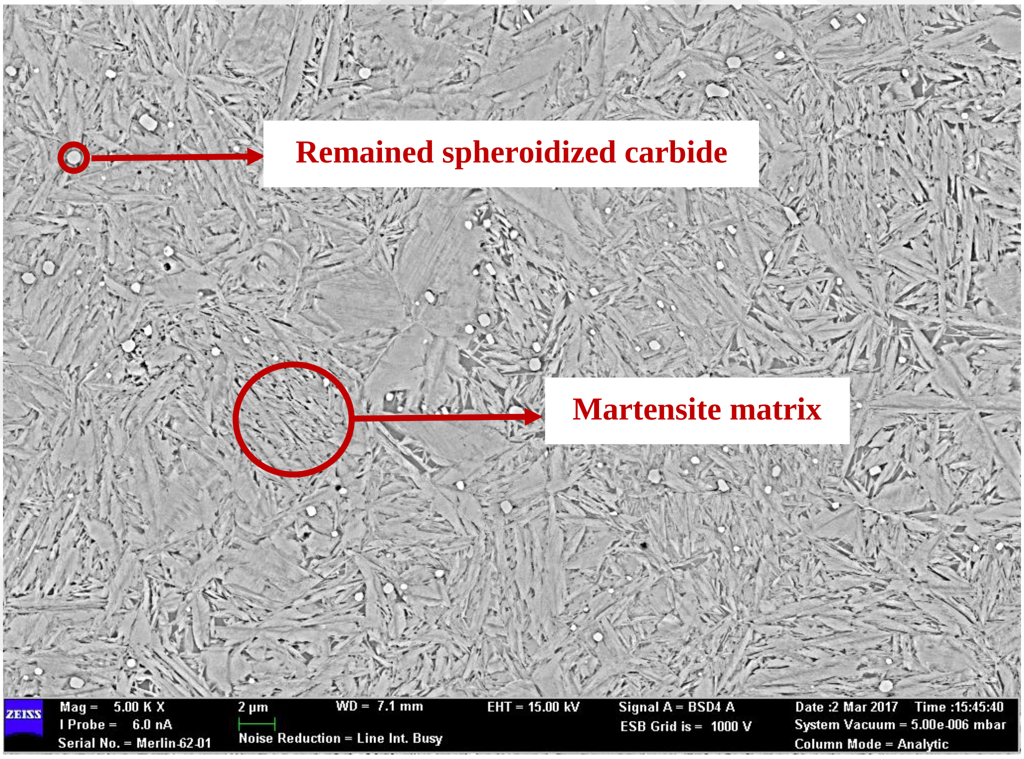

Figure 4. 11 BSD micrograph of 100Cr6 steel specimen that has been austenitized at 900°C for 60 minutes, taken at 5000x magnification

Since carbide dissolution occur during heating and austenitization, calculated carbide fraction values were valid for both of the RT and sub-zero quenched specimens. In other words, specimens that were austenitized at the same austenitization condition had identical carbide fractions. Therefore, the carbide fraction values were classified with respect to austenitization conditions regardless of their cooling conditions.

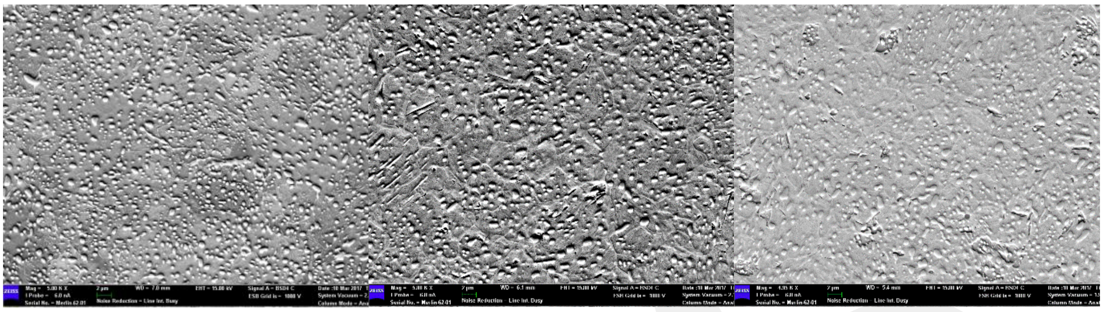

$T\gamma=800^{\circ}C$ $t\gamma=10sec$ $T\gamma=800^{\circ}C$ $t\gamma=2.5min$ $T\gamma=800^{\circ}C$ $t\gamma=5min$

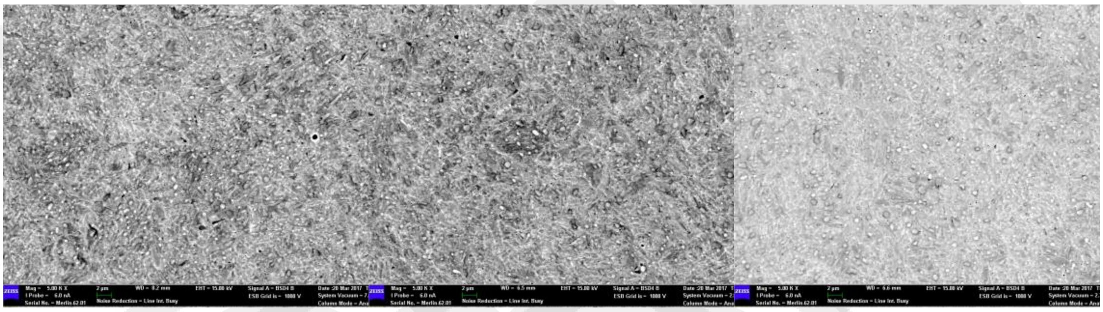

$T\gamma=800^{\circ}C$ $t\gamma=10min$ $T\gamma=800^{\circ}C$ $t\gamma=30min$ $T\gamma=800^{\circ}C$ $t\gamma=60min$

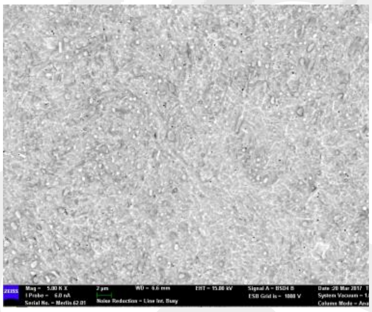

$T\gamma=800^{\circ}C$ $t\gamma=120min$

Figure 4. 12 BSD micrograph of 100Cr6 steel specimens that has been austenitized at 800°C, taken at 5000x magnification. Related heat treatment conditions were specified under each micrograph

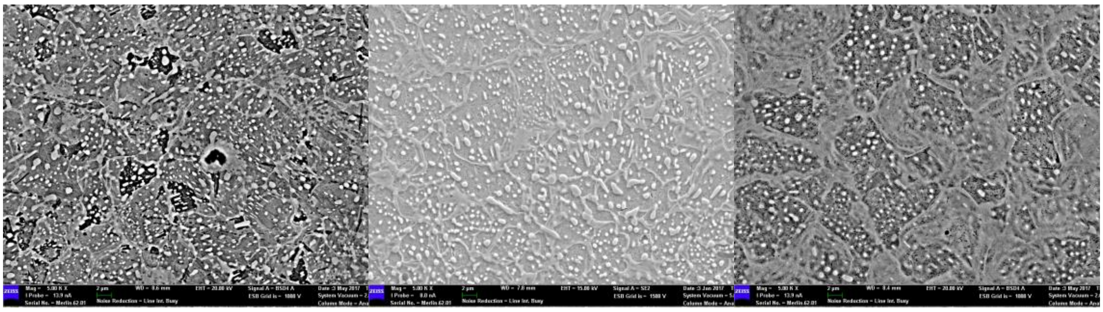

Tγ=850°C tγ=10 sec Tγ=850°C tγ=2.5min Tγ=850°C tγ=5min

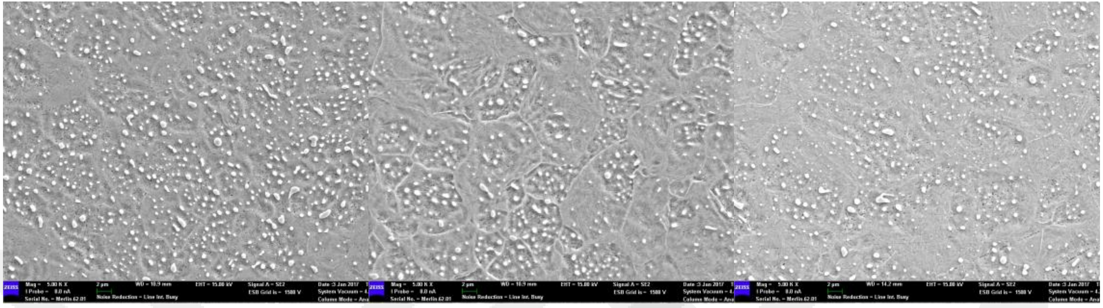

Tγ=850°C tγ=10min Tγ=850°C tγ=30min Tγ=850°C tγ=60min

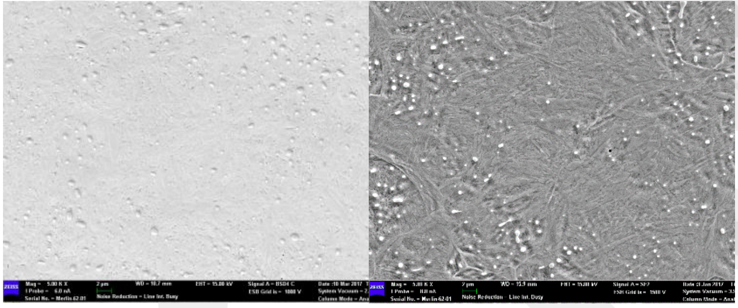

Tγ=850°C tγ=90min Tγ=800°C tγ=120min

Figure 4. 13 BSD micrograph of 100Cr6 steel specimens that has been austenitized at 850°C, taken at 5000x magnification. Related heat treatment conditions were specified under each micrograph

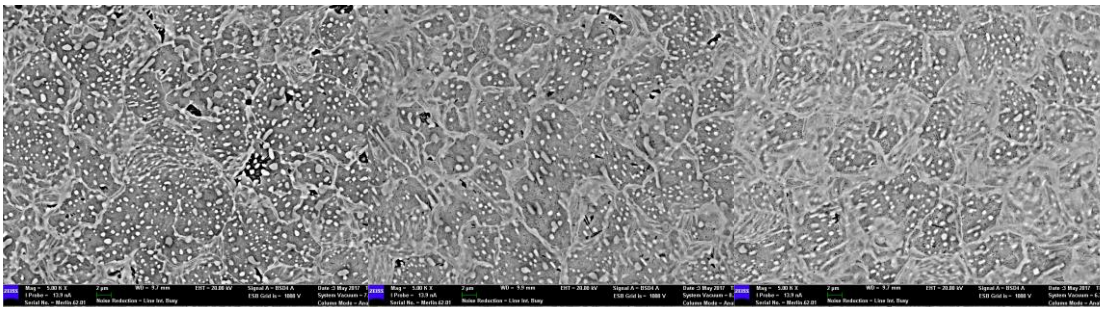

Tγ=900°C tγ=10sec Tγ=900°C tγ=30sec Tγ=900°C tγ=1min

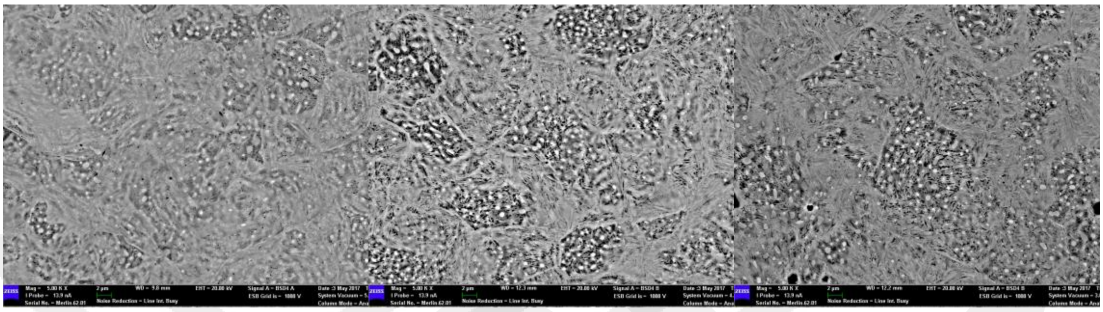

Tγ=900°C tγ=2min Tγ=900°C tγ=4min Tγ=900°C tγ=8min

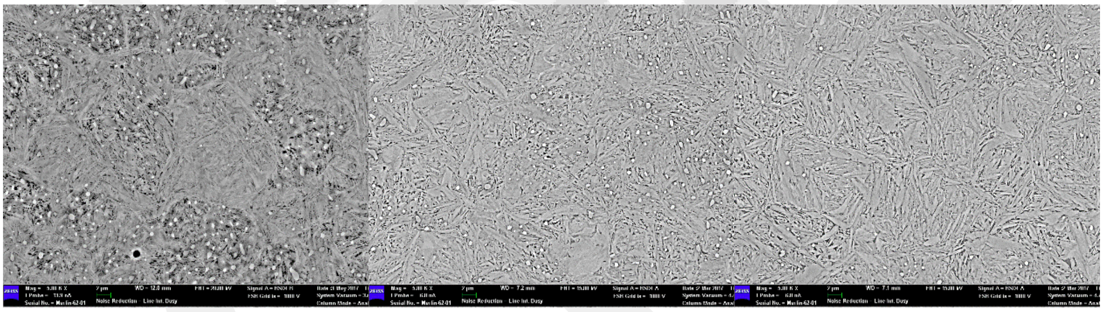

Tγ=900°C tγ=16min Tγ=900°C tγ=30min Tγ=900°C tγ=60min

Figure 4. 14 BSD micrograph of 100Cr6 steel specimens that has been austenitized at 900°C, taken at 5000x magnification. Related heat treatment conditions were specified under each micrograph

The average area fraction of carbides for each set of experiment were given in Table 4.4 and their distributions represented in Figure 4.15-a. In addition, distributions of average number of carbides per mm^2 were illustrated in Figure 4.15-b. As it was expected, carbide amount in the final microstructure of the specimens decreased with increasing austenitization temperature and/or time based on carbide dissolution kinetics. Comparison of Figures 4.15-a, and b showed that each set of experimental curve followed approximately the same asymptotic trend. It was seen in both figures that; carbide dissolution rate became slower after five minutes of austenitization at 800°C and 850°C, whereas it became slower after two minutes of austenitization at 900°C due to faster saturation of austenite by carbon and chromium. Although carbide dissolution was much faster at austenitization temperature of 900°C, 60 minutes of austenitization was not sufficient to dissolve all the carbides, so the final microstructure of these specimens contained 1% of carbides. The simulation results which were performed by DICTRA software (Appendix B) showed that approximately two hours of soaking was necessary for complete carbide dissolution at austenitization temperature of 900°C.

Table 4. 4 Average area fractions of the specimens for each set of experiments

T_γ (°C)	***800***	***t_γ (min)***	***0.17***	***2.5***	***5***	***10***	***30***	***60***	***120***		
		Carbide Area (%)	12.8	10.4	8.8	8.4	8.5	7.7	7.9		
	850	***t_γ(min)***	***0.17***	***2.5***	***5***	***10***	***30***	***60***	***90***	***120***	
		Carbide Area (%)	11.8	9.4	6.0	5.7	4.6	4.5	2.5	1.7	
	900	***t_γ (min)***	***0.17***	***0.5***	***1***	***2***	***4***	***8***	***16***	***30***	***60***
		Carbide Area (%)	11.9	9.4	6.8	7.0	4.5	3.2	2.8	1.7	1.0

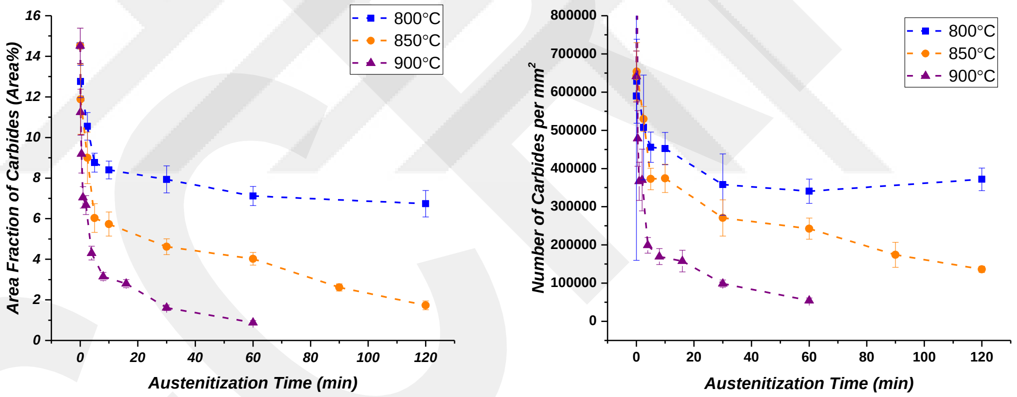

(a) (b)

Figure 4. 15 (a) Area and (b) number fraction distribution of each set of experiment. Markers indicated the average values while error bars indicated the standard deviations of the average value.

Raw Material

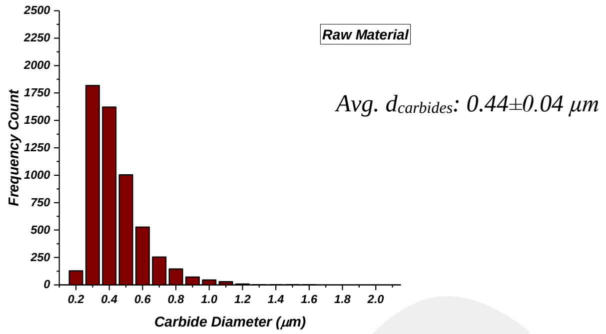

T_A: 800°C- T_A:10 second

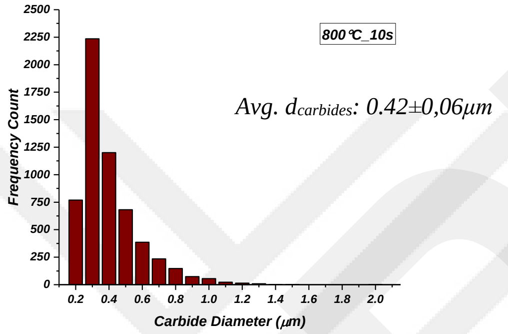

T_A: 800°C- T_A:60 minutes

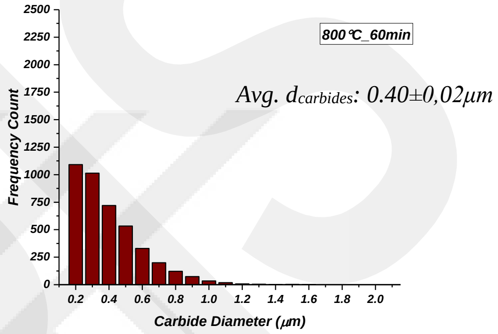

T_A: 850°C- T_A:10 second

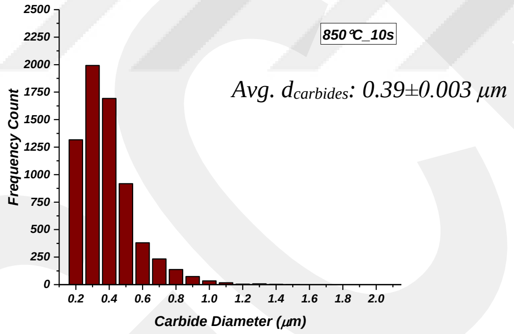

T_A: 850°C- T_A:60 minutes

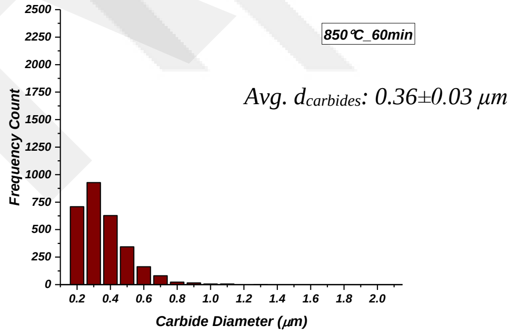

T_A: 900°C- T_A:10 second

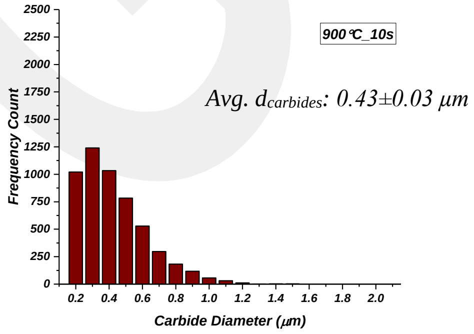

T_A: 900°C- T_A:60 minutes

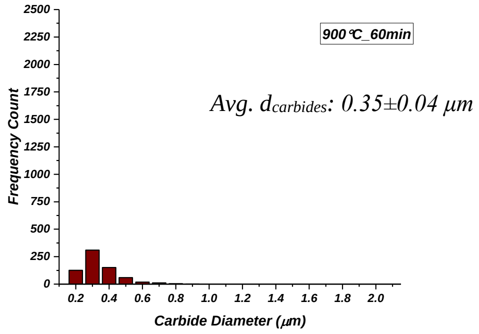

Figure 4. 16 Representative areal frequency count distribution histograms of each set of experiment (carbide diameter range were given in linear scale)

Raw Material

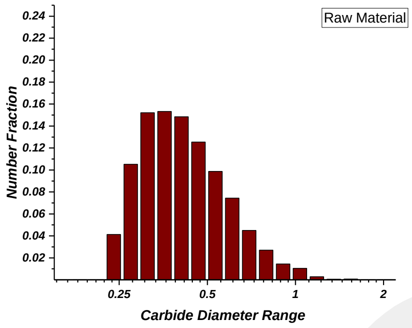

T_A: 800°C- T_A:10 second

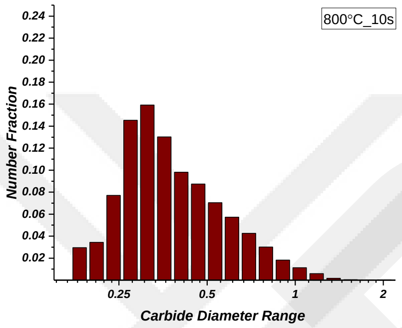

T_A: 800°C- T_A:60 minutes

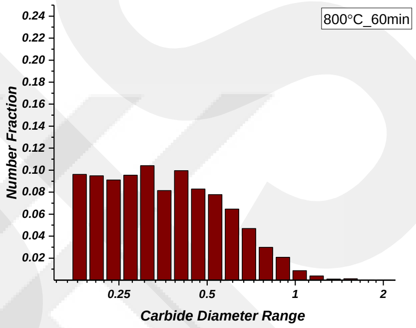

T_A: 850°C- T_A:10 second

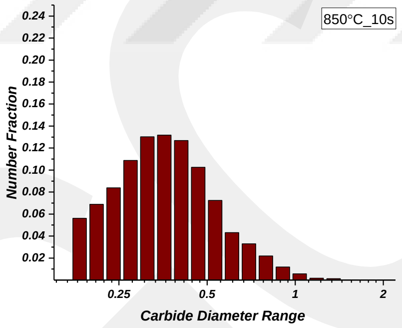

T_A: 850°C- T_A:60 minutes

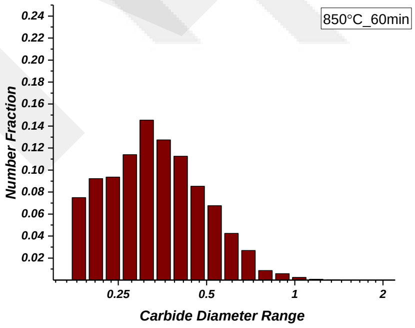

T_A: 900°C- T_A:10 second

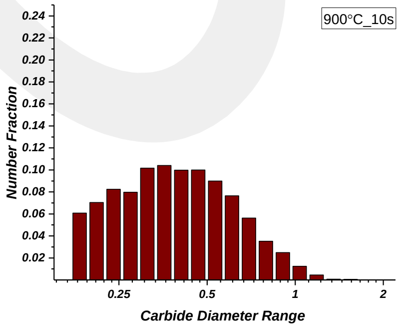

T_A: 900°C- T_A:60 minutes

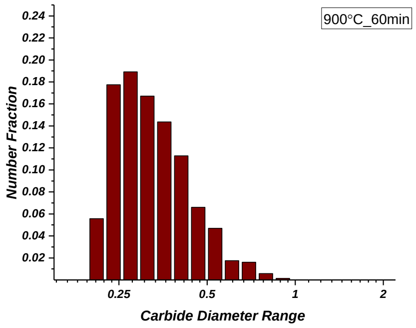

Figure 4. 17 Representative number fraction distribution histograms of each set of experiment (carbide diameter range were given in logarithmic scale)

In addition, more detailed investigations were made by examining the areal and numerical distribution histograms that were obtained by considering each carbide particles that revealed in the micrographs of the specimens. All the histograms and calculated average carbide diameter (Avg. $d_{carbides}$) values of each set of experiment were given in Appendices C and D. Besides, representative areal and numerical histograms were given in Figure 4.16 and 4.17 respectively in order to provide better comparison and so better understanding of these distributions.

Histograms in Figure 4.16 and Figure 4.17 represents number frequencies and number fraction of carbides with respect to carbide diameter. Both figures showed that relatively smaller carbides primarily started to dissolve in the matrix. Therefore, average carbide diameter was higher at early very stage of austenitization due to dominant effect of coarser carbides. However, a reduction was observed for further austenitization steps (higher austenitization duration) due to beginning of dissolution of coarser carbides. Although, standard deviations indicated the positive and negative variation limits of the carbide diameters, general view of the histograms showed that most of the carbides collapsed around average carbide diameter size. Therefore, the calculated average values were representative for overall carbides that has been revealed in the final microstructure of the specimens.

Another microstructural consideration was retained austenite amounts of the heat treated specimens. Sub-zero treated specimens did not contain retained austenite in their final microstructures, due to almost completed martensitic transformations. On the other hand, quenching the specimens from T_{γ} to RT was not sufficient for complete transformation. Therefore, retained austenite measurements were performed in those set of specimens. Detected retained austenite fractions and their distributions were given in Table 4.5 and Figure 4.18, respectively. As it was mentioned in previous subsection, increasing carbide dissolution caused an increase of C amount in FCC austenite which has significant effect on austenite stabilization. Since the austenite was stabilized due to increase of C dissolution, amount of retained austenite increased with increasing austenitization time and/or temperature.

Table 4. 5 Measured retained austenite fractions (%) of each set of experiments

T_γ (°C)	***800***	***t_γ (min)***	***0.17***	***2.5***	***5***	***10***	***30***	***60***	***120***		
		Retained Austenite (%)	1.9	5.4	7.0	6.7	8.0	7.6	8.2		
	850	***t_γ (min)***	***0.17***	***2.5***	***5***	***10***	***30***	***60***	***90***	***120***	
		Retained Austenite (%)	5.9	11.6	14.0	14.9	16.3	15.8	19.2	16.0	
	900	***t_γ (min)***	***0.17***	***0.5***	***1***	***2***	***4***	***8***	***16***	***30***	***60***
		Retained Austenite (%)	10.5	13.7	15.9	18.7	20.7	23.1	24.6	23.4	28.1

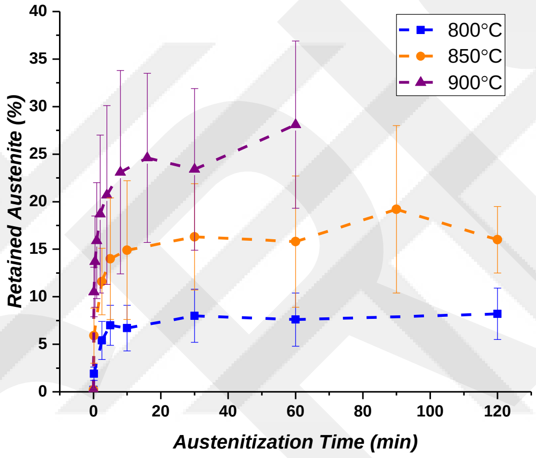

Figure 4. 18 Variation of retained austenite fraction as a function of austenitization time for each specimen. Markers indicated the average values while error bars indicated the standard deviations.

Beside all of these experimental works, the retained austenite fraction can also be estimated as a function of temperature, if martensite fraction is known. Martensite fraction can be calculated by Koistinen-Marburger equation;

$$f_m = 1 - \exp\big(-\Omega(Ms - T)\big) \tag{4.1}$$

where f_m represents the martensite fracture, Ω is a constant for most of the steels and taken as 0.011 regardless of their chemical composition, M_s is the martensite start temperature and T is the temperature that have been reached by quenching [72]. If carbide fractions were neglected, austenite fraction can be calculated as follows;

$$f_\gamma = 1 - f_m \tag{4.2}$$

Using the equations 4.1 and 4.2 retained austenite fractions were also predicted via M_s temperatures, which had been determined from the eight empirical formulas given in Table 4.3. The predicted retained austenite fractions were compared to experimental ones, as shown in in Figure 4.19-a, b, and c.

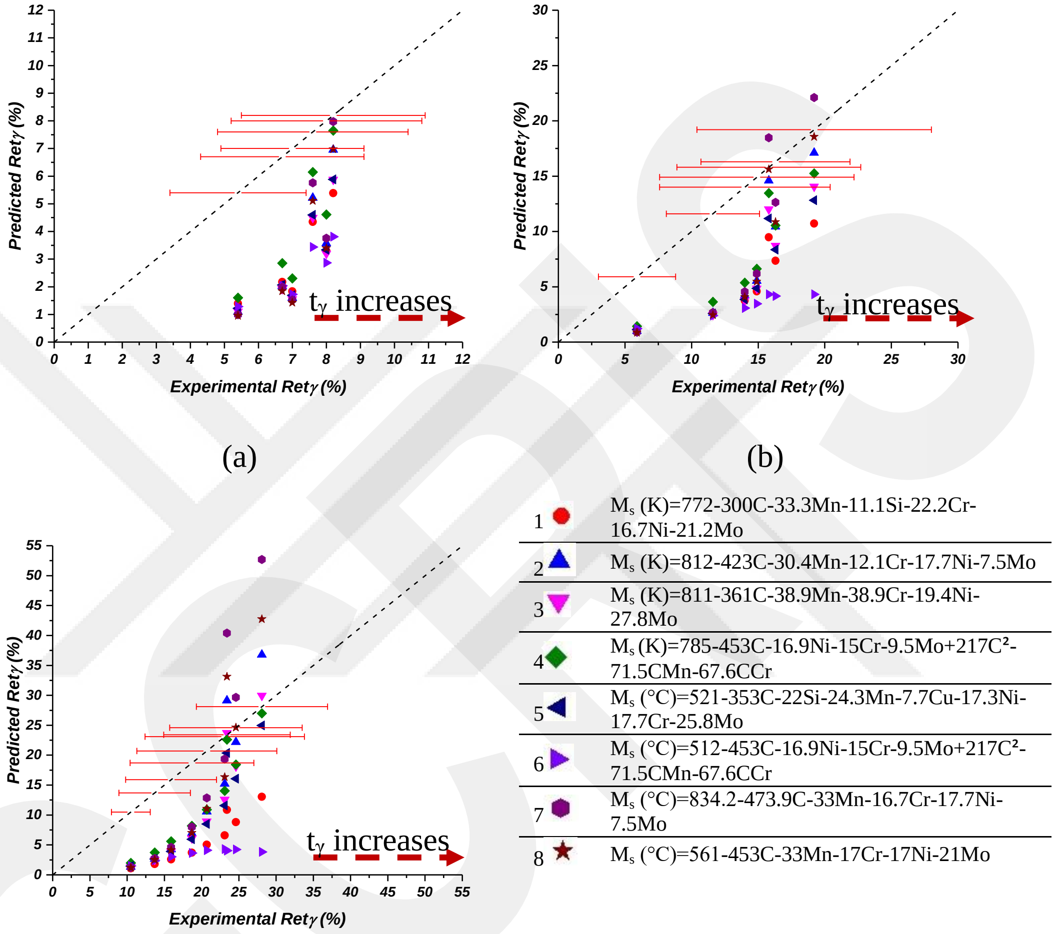

(a) (b)

(c) (d)

Figure 4. 19 Comparison of predicted and experimental retained austenite (Retγ) fractions (%) for austenitization temperatures of (a) 800, (b) 850°C and (c) 900°C. (d) The symbols indicating the emprical formulations used to determine the M_s temperature.

As can be seen from the figures, the predicted retained austenite fractions does not agree well with the experimental results, specifically for the earlier austenitization stages. This behavior can be attributed to the same reasons that were explained for M_s predictions via these empirical formulas. Nevertheless, most of the predicted values were in between the standard deviation ranges, after 30 minutes of austenitization at

800°C, 850°C, and after 4 minutes of austenitization at 900°C. Consequently, these results were promising for estimation of retained austenite fraction as a function of quench temperature by using the equations 4.1, 4.2 and the ones given in 4.19d. It should also be noted that, the accuracy of predicted values of M_s temperature, martensite and retained austenite fractions can be enhanced by developing new and more specific empirical formulas, that consider carbon dissolution kinetics of 100Cr6 steel and also the higher order interactions between the elements.

Another variation that occurred in the final microstructure of the specimens was the matrix hardness values. As it was given in the previous results, specimens that were quenched to RT consist of martensite, carbides and retained austenite; where the sub-zero treated specimens consist of carbides in martensite matrix. Based on this fact, more homogeneous hardness results were expected for the subzero treated specimens. For the specimens that were quenched to RT, on the other hand, the hardness variations were expected to be more, considering the presence of retained austenite in the microstructures. Therefore, only micro hardness measurements were performed on the sub-zero treated specimens in order to specify their matrix hardness; whereas both macro and micro hardness measurements were performed on the specimens that were quenched to RT in order to compare overall and local hardness of the specimens.

The results of the hardness measurements of both set of specimens that were quenched to RT and to -130 °C were given in Figures 4.20-a, b, and Figure 4.21 as a function of both austenitization temperature and time. Moreover, the minimum and maximum hardness values and the standard deviations of each measurement were given in Appendix E. As it was expected, comparison of the micro hardness results of both set of sub-zero treated and RT quenched specimens showed that variations between the specimens' hardness significantly reduced with elimination of the retained austenite. Thus, the hardness values of sub-zero treated specimens asymptotically increased where there was no regular increase observed on the specimens that were quenched to RT due to retained austenite effect.

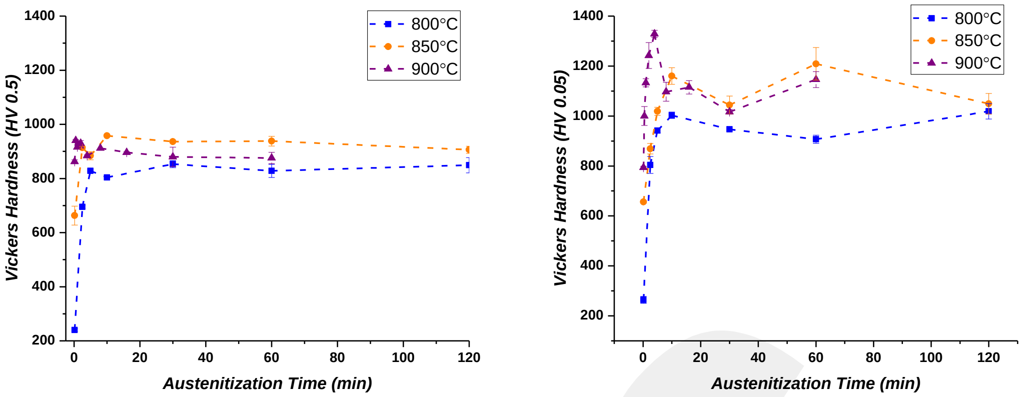

(a) (b)

Figure 4. 20 Variation of (a) macro hardness and (b) micro hardness values of each specimen (quenched to RT), given as a function of austenitization time. Markers indicated the average values while error bars indicated the standard deviations of the average value.

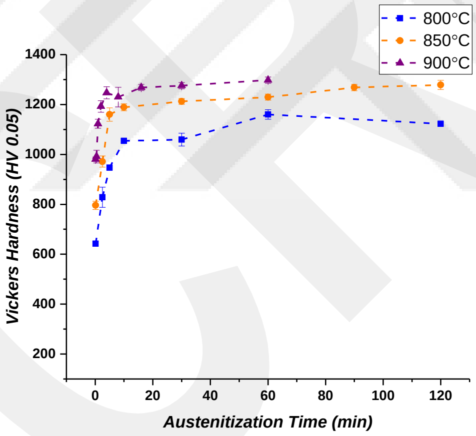

Figure 4. 21 Variation of micro hardness values of each specimen (sub-zero quenched), given as a function of austenitization time. Markers indicated the average values while error bars indicated the standard deviations of the average value.

For this case, there were two main reasons that influenced the hardness of the material; (i) martensite hardness, and (ii) retained austenite.

(i) Martensite hardness was increased by Cr enrichment of FCC lattice structure of austenite due to increase of hardening depth and the tendency for martensitic transformation. Besides, martensite hardness is a function of C amount. Thus, C-enrichment of matrix during austenitization also caused an increase in martensite hardness.

(ii) Increasing fraction of retained austenite caused a decrease in hardness of the specimens that were quenched to RT from austenitization temperature.

In order to clarify this concurrent and nonlinear influence of martensite hardness and retained austenite on matrix hardness, Figure 4.22 represents both hardness and retained austenite variations as a function of carbon content of carburized and oil quenched 4320 steel. Nano hardness values indicate the martensite hardness, and it reaches approximately 70 HRC after 0.80 wt. % of C. Macro hardness measurements (HV500) indicated the hardness values for relatively larger areas which contain both martensite and retained austenite. As carbon content increases, both retained austenite and martensite hardness also increased. Since martensite hardness increases more rapidly than the retained austenite fraction, macro hardness values increases at beginning of carbon dissolution (up to 0.50 wt. %). For further C dissolution steps, retained austenite amount increases asymptotically, and so its effect on hardness also increased. Thus a reduction was observed on macro hardness values based on concurrent effect of martensite hardness and retained austenite [73].

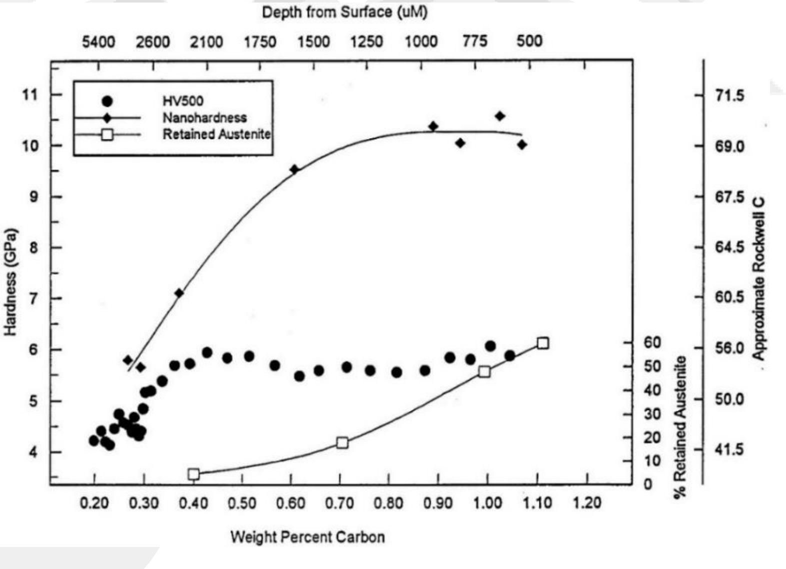

Figure 4. 22 Hardness and retained austenite variation based on carbon content of carburized and oil quenched 4320 steel [73]

Since matrix hardness mainly affected by these two variable it can be calculated as a function of their fractions and hardness values;

$$H = f(f_m H_m) + f(f_\gamma H_\gamma) \tag{4.3}$$

$$H = f(f_m H_m) + f(1 - f_m H_\gamma) \tag{4.4}$$

f_m and f_γ, represented fractions, where H_m and H_γ, represented hardness values of martensite and austenite respectively.

Inferences that have been made from Koistinen-Marburger equation 4.1 showed that nonlinear and concurrent effect of retained austenite and martensite presents on matrix hardness.

For the present case, increasing austenitization time and/or temperature caused an obvious increase of both martensite hardness and retained austenite amount at the same time. Based on these concurrent formations in the specimens that were quenched to RT; hardness of the specimens increased by C and Cr enrichment of the matrix, while reduced by increase of retained austenite amount. Besides, it was seen in the Figure 4.20, that the macro hardness variations were more stable than micro hardness variations. Because the hardness values of overall of the specimens were represented by the macro hardness values due to larger indentation size. However, local hardness values were represented by micro hardness values due to relatively smaller indentation size (Figure 4.23).

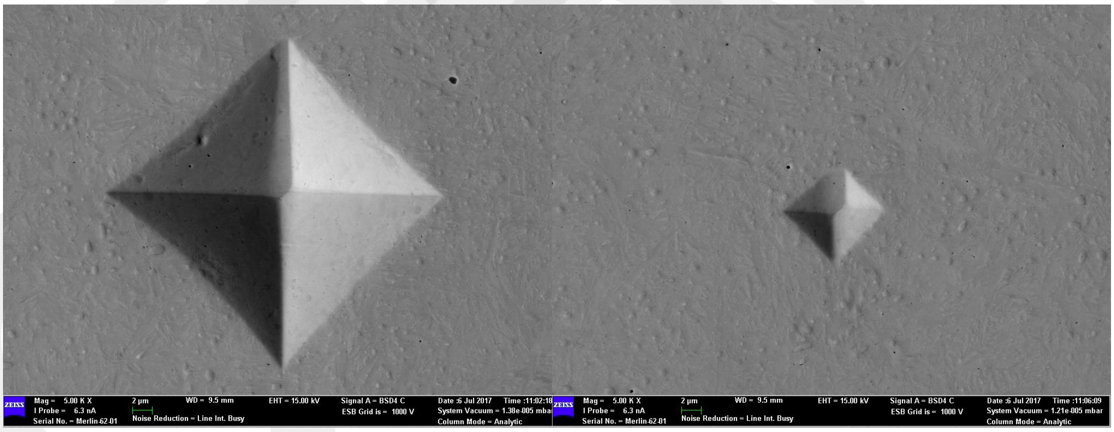

(a) (b)

Figure 4. 23 Comparison of (a) macro (HV 0.5) and (b) micro (HV 0.05) indentation size

Detailed comparison of macro and micro hardness values of each set of experiment of RT quenching (Figure 4.24) showed that, generally micro hardness values were greater than the macro hardness values based on dominant influence of martensite matrix on hardness. As indentation size increased, retained austenite influence on hardness was also increased which caused a reduction of hardness values.

In addition, biggest difference was found between macro and micro hardness at austenitization temperature of 900°C. Since it was the highest austenitization temperature of the present study, variations occurred faster in the microstructures of those specimens. Therefore, it also caused a greater difference between relatively local and overall hardness values.

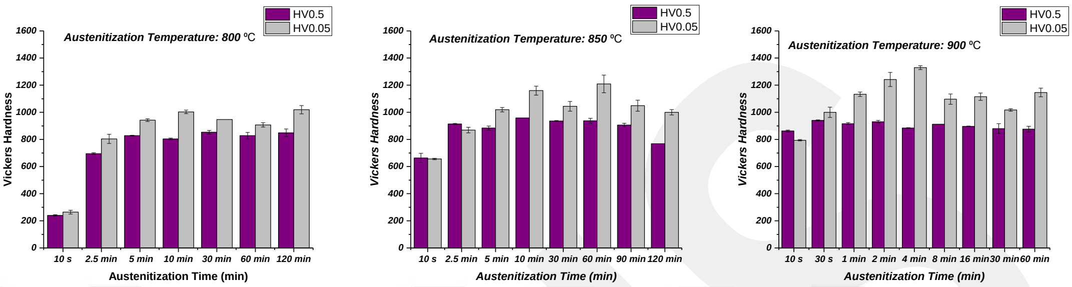

(a) (b) (c)

Figure 4. 24 Comparison of macro and micro hardness values of specimens that were austenitized at (a) 800°C, (b) 850°C and (c) 900°C. Markers indicated the average values while error bars indicated the standard deviations of the average value.

4.3. Magnetic Barkhausen Noise Measurements

Aim of this present study was determining the possibility of nondestructive microstructural characterization of heat treated 100Cr6 steels via MBN technique. This final main subsection of the 4th Chapter will cover all the results and discussions about MBN response and its correlation with the microstructure.

In order to determine the feasibility of this technique on nondestructive microstructural characterization of 100Cr6 steels; MBN response of the specimens were examined individually and then related to their microstructural properties. This relation was identified by correlating MBN response with retained austenite, hardness and carbide fraction of the specimens individually. These correlations were analyzed by simple linear regression method, and goodness of fit was determined by coefficient of determination (R^2 value). Besides, a parameter optimization work was done in order to perform high quality measurements. Thus, totally 320 MBN measurements were performed on each set of specimens by varying of magnetizing voltage between 1V to 16 V in steps of 1V and magnetizing frequency between 50 Hz to 1000 Hz by a step of 50 Hz in order to determine the optimum combinations of MBN measurement parameters. A successful parameter optimization work will be explained in following subsection by summarizing another study which involves samples showing a greater range of hardness values.

The present 100Cr6 steel specimens show very little variation in hardness values. In order to investigate, importance of measurement parameter optimization on collected signals on quenched and tempered SAE 4140 steels were used. Following subsection will cover that optimization work and comparison of its results with present case.

4.3.1. Parameter Optimization for Detecting Hardness Differences

5 mm thick, 22mm diameter specimens were extracted from raw SAE 4140 steel bar, and austenitized at 860°C for 45 minutes, then quenched in water. While a specimen was left as-quenched, the others were tempered at between 200°C and 600°C for 60 minutes. Finally, typical martensitic and tempered structures were obtained after application of heat treatment procedures. Changing the tempering temperatures caused formation of variations in the final microstructures. As-quenched specimen had high dislocation density due to high interstitial carbon content in solid solution of BCT martensite. However, tempering application caused a formation of low carbon martensite at 200°C. Further to this, cementite started to nucleate, and so the dislocation density reduced at higher tempering temperature applications up to 400°C. Moreover, ferrite began to recrystallize and cementite precipitates started to spheroidize and became coarser above 400°C of tempering temperature. General view of these heat treatment procedures showed that martensite softens with increase of tempering temperatures, and so dislocation density reduced significantly.

As it was mentioned in 2nd Chapter, domain wall motions are influenced by the microstructural features in the same manner of dislocation movement. Therefore, as tempering temperature decreased higher interstitial carbon content of BCT martensite remained and so the number of pinning sites increased. Since, domain walls pinned by these small martensite needles, MBN signals of the specimens reduced with decrease of tempering temperature.

Another important consideration for performing reliable, sensitive and valid MBN measurements was parameter (magnetizing voltage and magnetizing frequency) optimization. Therefore, magnetizing voltage varied between 1V and 16 V in steps of 1V and magnetizing frequency between 50 Hz and 1000 Hz in steps of 50 Hz, and so totally 320 MBN measurements were performed on each specimen in order to select correct combination of parameters for good measurement.

✓ *Reliability*

Reliability was defined as goodness of fit (R^2) of the correlations between MBN and hardness variations. Since linear relation was found between the hardness and MBN response, goodness of fit was determined by linear regression method.

The highest R^2 value was calculated as 0.9856 from the MBN measurement that obtained by combination of 50 Hz of magnetizing frequency and 6 V of magnetizing voltage. Since this showed that very good linear correlation was found between the hardness and MBN response of quenched and tempred SAE 4140 steels, hardness can be predict by MBN measurement after optimization. This correlation was shown in Figure 4.25, where distributions of calculated all 320 R^2 values for different parameter combinations given in Figure 4.26. As can be seen from this distribution, the highest values (R^2>0.9) were calculated for combination of magnetizing frequency of 50 Hz with magnetizing voltage between 4-11 V, and magnetizing frequency of 100 Hz with magnetizing voltage between 4-6 V.

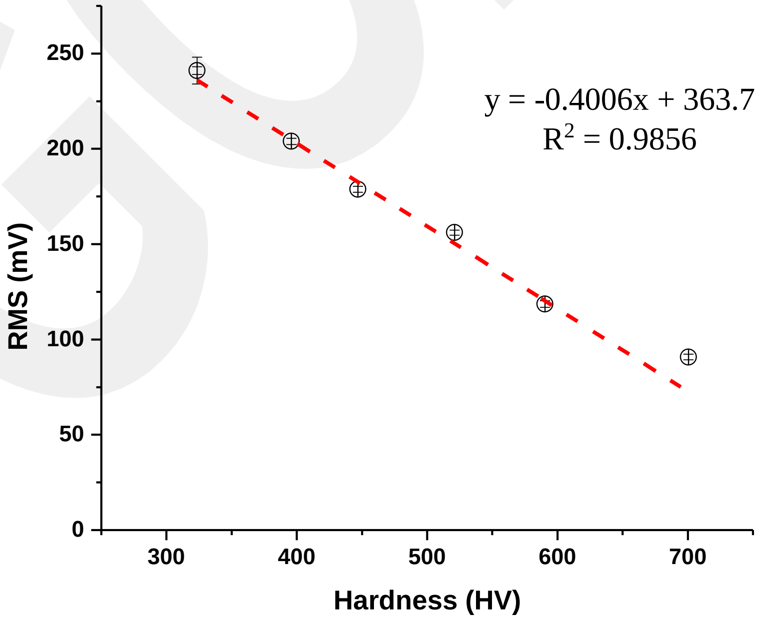

Figure 4. 25 Hardness correlation of 4140 steel specimens which obtained by selected combination of parameters (6V and 50 Hz) [49]

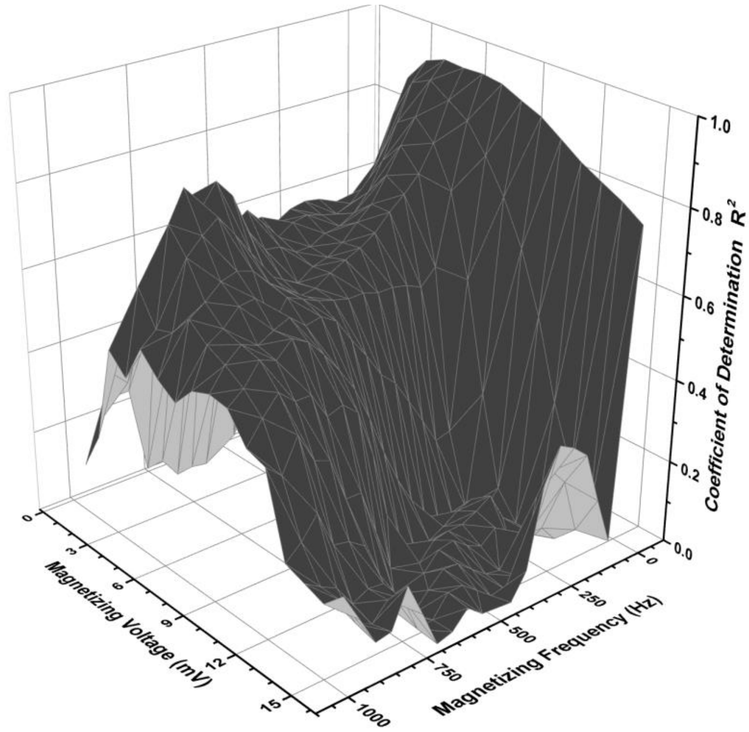

Figure 4. 26 Distribution of all R2 values that calculated for 320 different combinations of magnetizing voltage and frequency [49]

✓ *Sensitivity*

Moreover, sensitivity was considered as difference between the best (the hardest – as quenched) and the worst (the softest – tempered at 600°C) materials, and so it was calculated by using following equation;

$$SI = 100 \times \frac{(RMS_{T600} - RMS_{As-Q})}{RMS_{As-Q}} \tag{4.5}$$

SI represented the sensitivity index of MBN measurement, RMS_{T600} and $RMS_{As\text{-}Q}$ represented the RMS values of the specimens that were tempered at 600°C (the softest), and left as quenched (the hardest) respectively.

Figure 4.27 showed the distribution of calculated SI values for 320 individual MBN measurements. Since good MBN measurements supposed to be sensitive to even slightest variation in the structure, the MBN measurements which gave the highest sensitivity index values were considered as good measurements. The highest sensitivity index values were calculated for combinations of magnetizing voltage between 3-6 V of magnetizing voltage with magnetizing frequency between 50-450 Hz.

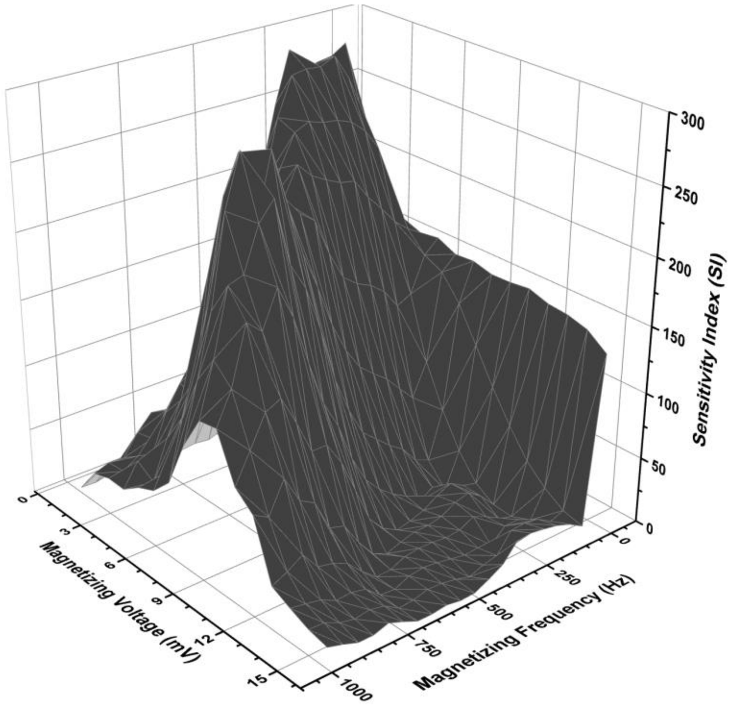

Figure 4. 27 Distribution of all SI values that calculated for 320 different combinations of magnetizing voltage and frequency [49]

- ✓ *Validity*

Further to these, inherent symmetry of the magnetic hysteresis was considered as validity of the measurements. This symmetry of hysteresis was characterized by determining validity index (VI) by considering the collected noise signal data during increasing ($RMS_{positive}$), decreasing ($RMS_{negative}$) applied field and during complete ($RMS_{average}$) hysteresis cycle;

$$VI = 100 \times \frac{|RMS_{positive} - RMS_{negative}|}{RMS_{average}} \tag{4.6}$$

Distributions of calculated VI values were given in Figure 4.28. Regarding to MBN phenomenon, collected data during increase and decrease of applied field supposed to be identical for a valid MBN measurement. Therefore, difference between noise signal data during increasing and decreasing applied field supposed to be zero. Based on this phenomenon, the MBN measurements which gave the lowest VI values considered as good measurements. The lowest VI values were calculated for the combinations of magnetizing frequency between 50-200 Hz with magnetizing voltage between 1-4 V.

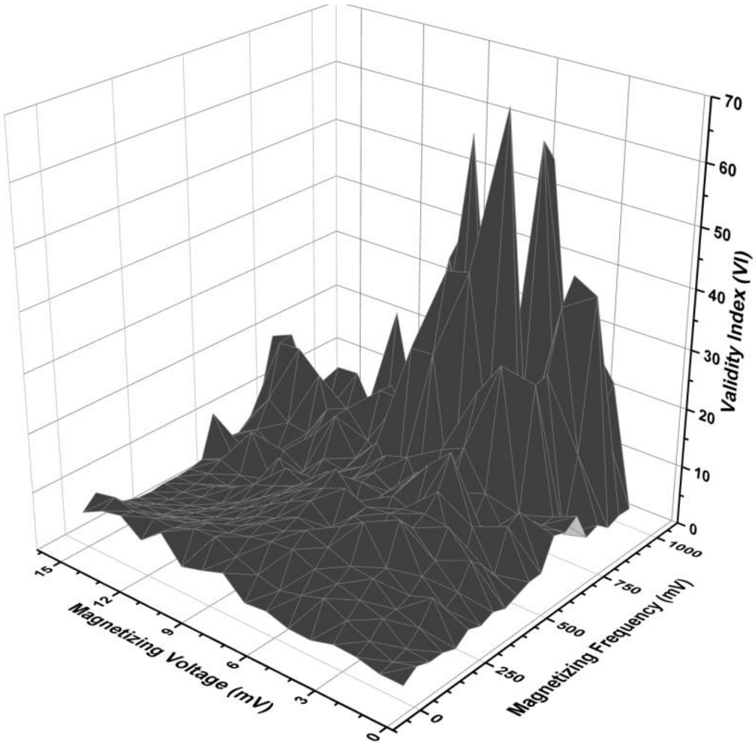

Figure 4. 28 Distribution of all SI values that calculated for 320 different combinations of magnetizing voltage and frequency [49]

Although all of these three indicators; reliability, sensitivity and validity, maximized individually, a single set of parameter was not sufficient to maximize three of them at the same time. Therefore, a new voting formula (given below) was proposed to find a good set of parameters for obtaining reliable, sensitive and valid MBN measurements at the same time.

$$Score = 100 \times \frac{aR^2 + b\left(\frac{SI}{SI_{max}}\right) + c\left(\frac{VI_{max} - VI}{VI_{max}}\right)}{a+b+c} \tag{4.7}$$

Where a, b and c were weighting coefficients, R^2 was the coefficient of determination, SI was sensitivity index values, SI_{max} was calculated maximum sensitivity index value, VI was validity index vales and VI_{max} was calculated maximum validity index value. Weighting coefficients of a, b, and c was selected as 2.5, 1.5, and 1 respectively based on priority of these indicators due to requirements of the present case. This voting formula provided to specify very good MBN measurement parameters regardless of individual consideration of these three indicators. Distribution of calculated score values out of 100 were given in the Figure 4.29.

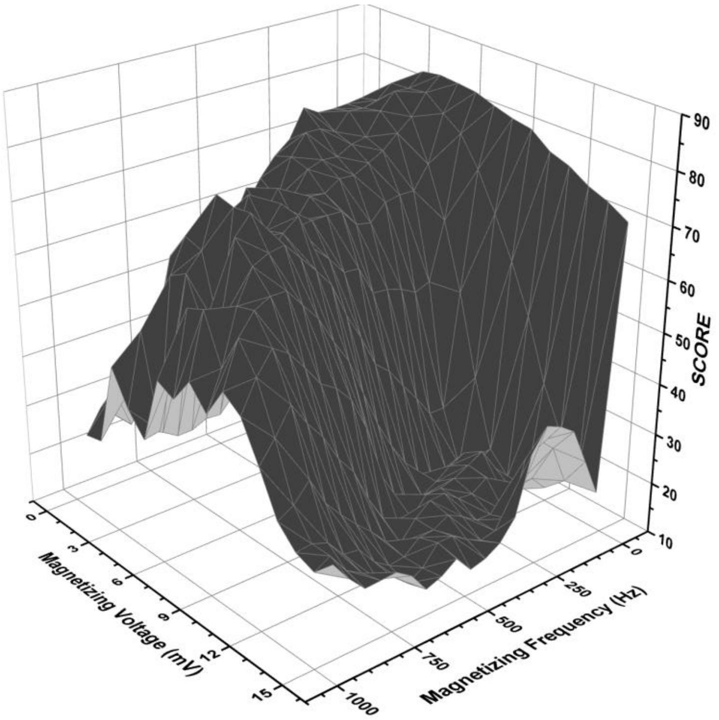

Figure 4. 29 Distribution of all score values that calculated for 320 different combinations of magnetizing voltage and frequency [49]

Based on this optimization work and application of the new voting formula, combination of 50 Hz of magnetizing voltage and 6 V of magnetizing frequency was selected in order to perform reliable, sensitive and valid MBN measurements on quenched and tempered SAE 4140 steels.

MBN profiles that obtained by good and bad measurement parameter combinations were illustrated in Figure 4.30. MBN profile that was given in Figure 4.30-a obtained by combination of very low magnetizing voltage and frequency (1V-50Hz). Thus, MBN signals could not be distinguished from the background noise signal. Besides, MBN profiles that were given in Figure 4.30-b obtained by combination of very high magnetizing voltage and low magnetizing frequency. Thus, magnetization exceeded to saturation level due to application of very high magnetizing voltage. However, proper MBN measurements and so the profiles could be obtained by selected very good combinations of measurement parameters (Figure 4.30-c).

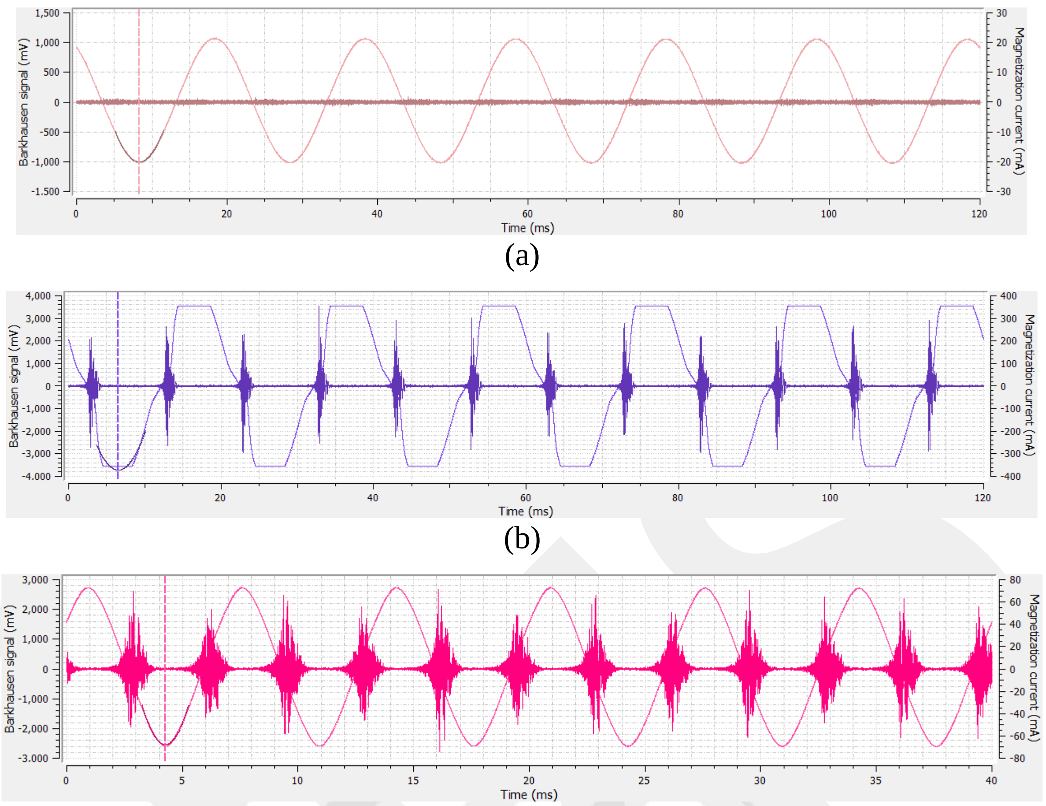

(a)

(b)

(c)

Figure 4. 30 MBN profiles that obtained by applying (a) too low magnetic field (1V & 50Hz) (b) too high magnetic field (16V & 50Hz), and (c) proper magnetic field (6V & 50Hz)

In brief, MBN signals were mainly affected from the matrix hardness and measurement parameters. Therefore, very good correlation was obtained between hardness and MBN response of the specimens, due to occurrence of significant differences on the matrix hardness, and parameter optimization by proposed voting formula [49].

Comparison of the present case of heat treated 100Cr6 steels with quenched-tempered SAE 4140 steels showed that: Relatively simpler microstructural variations obtained in SAE 4140 steels compared to heat treated 100Cr6 steels. Because, identical martensitic microstructures obtained in SAE 4140 steels after quenching due to application of the same austenitization and quenching processes. Their microstructural variations obtained by varying the tempering temperatures. Increase of the temperature cause a reduction of dislocation density and also hardness of the specimens due to carbon release of supersaturated martensite. So, main differences between the specimens originated from this variations (lower and higher interstitial carbon content) on martensitic structures. Based on this fact, MBN measurement mainly influenced by matrix hardness of SAE 4140 steel specimens, where it influenced by concurrent and nonlinear effect of matrix hardness, amount of retained austenite and residual carbides of 100Cr6 steel specimens. In addition, the microstructural differences of 100Cr6 steel specimens were not significantly distinguishable as the matrix hardness difference of SAE 4140 steel specimens.

Since MBN was concurrently influenced by martensite hardness, retained austenite and carbide fractions, it can be considered as a function of these three microstructural features, and so;

$$MBN = k_m f(f_m RMS_m) + k_c f(f_c RMS_c) - k_\gamma f\left(f_\gamma\right) \tag{4.8}$$

MBN is also equal to following formula by merging it with Koistinen-Marburger equation:

$$MBN = k_m f((1 - \exp(-\Omega(M_s - T))\, RMS_m) + k_c f(f_c RMS_c) - k_\gamma f(1 - f_m) \tag{4.9}$$

Moreover, 4140 steel specimens’ geometries were more suitable for general purpose probe of MBN system. Therefore, stronger signals were collected on the 4140 specimens, while weaker signals were detected on the 100Cr6 specimens.

In the present study, as it was specified above, MBN signals of the specimens were influenced by three main microstructural properties: (i) martensite hardness, (ii) retained austenite amount, and (iii) remaining carbide amount.

Following subsections will cover individual MBN correlations of these three properties for the specimens that were austenitized at 800°C, 850°C and 900°C then quenched to room temperature and sub-zero temperature. The correlations of the specimens that were sub-zero treated and the ones that were quenched to RT will be given separately due to generation of mainly different microstructural properties. In addition, the common and uncommon trends observed in the correlations will be discussed. Finally, general view of concurrent influence of microstructural properties will be discussed.

4.3.2. MBN Correlations of the Specimens Quenched to Room Temperature

The microstructural variations in the set of specimens that were austenitized at 800°C, 850°C and 900°C, and then quenched to room temperature were as discussed in the previous subsection 4.2 “Microstructural Characterization”. As it was mentioned, martensite hardness, retained austenite amount and carbide fractions were varied by varying the austenitization conditions. All of these three microstructural parameters have different magnetic properties. Austenite is paramagnetic and it becomes antiferromagnetic below its Neel temperature (-233°C). Besides, martensite and cementite are hard magnetic phases which cannot be magnetized and demagnetized easily. Since increase of mechanical strength cause an increase on magnetic hardness, increase of both martensite and cementite amount presents similar behavior [74]–[77].

Although these interdependent microstructural variations in 100Cr6 steel specimens had dynamic equilibrium, they had concurrent nonlinear effects on MBN response due to the carbide dissolution kinetics. Since all of these three properties influenced the MBN response at the same time, they could not be distinguished individually by MBN measurements. Increase of martensite hardness, retained austenite amount and carbide fraction caused a reduction of MBN response. However, these three properties did not maximize or minimize at the same time. For example, decrease of carbide fraction caused an increase of martensite hardness and retained austenite amount by increase of austenitization temperature and/or time. Individual MBN correlations with matrix hardness, retained austenite amount and carbide fraction of the specimens were given in Figure 4.32, 4.33, and 4.34 respectively. MBN response of the specimens was represented by RMS value of the collected signal. Increase of matrix hardness was supposed to cause a reduction of RMS value. However, there were no linear increase on the matrix hardness values, since it was raised by martensite hardness and also reduced by increase of retained austenite amount and dissolution of carbides at the same time. Apart from this, very weak MBN signals were detected on the specimens that contained;

(i) higher interstitial carbon content in martensite, which had finer martensite needles, due to increase on number of pinning obstacles.

(ii) higher amount of austenite due to its inherent non-magnetic property.

Moreover, the signals also lowered by the reason of improper accordance between the specimens and measurement probe. Therefore, parameter optimization was not sufficient for obtaining proper signals and good correlations due to all of these shortcomings of the measurement system and the concurrent influences of microstructural properties. A set of measurement parameters (magnetizing voltage and frequency), which resulted relatively stronger signals was selected individually for the specimens that were austenitized at 800°C, 850°C, and 900°C among 320 MBN measurements. This optimization improved the results together with a band-pass filtering of the raw data between 50-1000 kHz. Consequently, 500 Hz of magnetizing frequency and 6 V of magnetizing voltage were selected for the measurements of the specimens that were austenitized at 800°C where 600 Hz of magnetizing frequency and 6 V of magnetizing voltage were selected for the measurements of the specimens that were both austenitized at 850°C and 900°C. Representative MBN profiles that (for the specimens that were austenitized at 800°C, 850°C, and 900°C) obtained by the combinations of optimized measurement parameters were given in Figure 4.31. Each MBN profile showed that even after optimization work, noise signal was quite weak. Thus, differentiation of the signals from the background noise signal was also very difficult. Due to this low signal detection, MBN correlations of all set of the specimens were adversely affected.

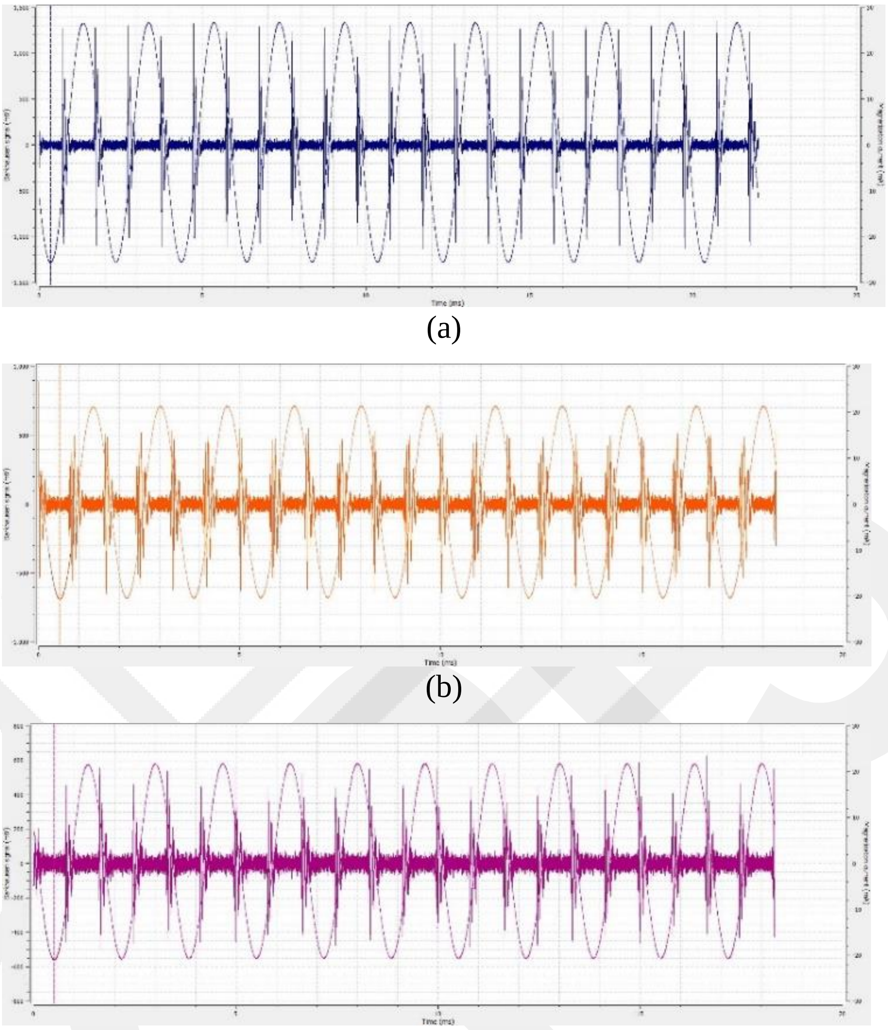

(a)

(b)

(c)

Figure 4. 31 MBN profiles obtained by optimized combination of measurement parameters for the specimens austenitized 30 minutes at (a) 800°C (6V & 500Hz), (b) 850°C (6V & 600Hz), and (c) 900°C (6V & 600Hz)

4.3.2.1. Hardness Correlation (RT Quenching)

As can be seen from the Figure 4.32, correlations between matrix hardness and RMS of the signals were very weak, especially for the set of measurements of the specimens that were austenitized at 850°C then quenched to RT. This might be caused by observation of very weak signal and also very little difference between the MBN responses of the specimens due to small differentiation of their hardness values. Since these small differences of hardness increased, calculated R^2 values also increased for the set of experiment of both T_γ of 800°C and 900°C. Although this improvement of R^2 values, the correlations were still far from ideal.

Besides, only the hardness correlations of the specimens that were austenitized at 800°C followed the expected trend (RMS of measurement decreased with increase of matrix hardness), where the specimens that were austenitized at 900°C followed the opposite trend (RMS of measurement increased with decrease of matrix hardness) to the expected one. This opposite behavior might be attributed to another microstructural parameter (i.e. retained austenite, or carbide fraction), that might have more significant influence on MBN response for those set of specimens.

Moreover, confidence and prediction bands were indicated for each correlation in the Figure 4.32. The prediction bands shows the possible standard deviation range of a data point and they were implied that the data was 95% accurately predictable, while the confidence bands implied that the data was 95% confidently lied within the confidence interval. Thus, it also specified the limits of possible y (hardness) values with respect to x (RMS) values. Besides, the widths of the confidence bands became smaller with reduction of standard error of predicted y (hardness) data. In order to compare these confidence intervals; corresponding upper, lower and middle hardness values were indicated from the narrowest width of each correlation in the figures.

Obviously, the widths of confidence intervals were wider for the hardness and RMS correlations of the specimens that were austenitized at 800°C and 850°C while it became narrower for the specimens that were austenitized at 900°C. It might be explained by comparison of the standard deviation of the y values (hardness values) for the specimens that were austenitized at 900°C (±152 HV), 800°C (±264 HV), and 850°C (±174 HV). Thus, the narrowest intervals might be observed in the Figure 4.32-c compared to the others, since the smallest standard deviation of hardness value observed from the set of specimens that were austenitized at 900°C. In addition, most of the data points lied within these confidence bands, and none of them lied outside of the limits of prediction bands. However, the confidence intervals were very broad especially for the specimens that were austenitized at 800°C and 850°C, which means that; the range of 95% confidence limits was not sensitive for prediction of corresponding hardness values based on RMS response of the specimens. Consequently, these MBN measurements were not sufficient for direct determination of the matrix hardness.

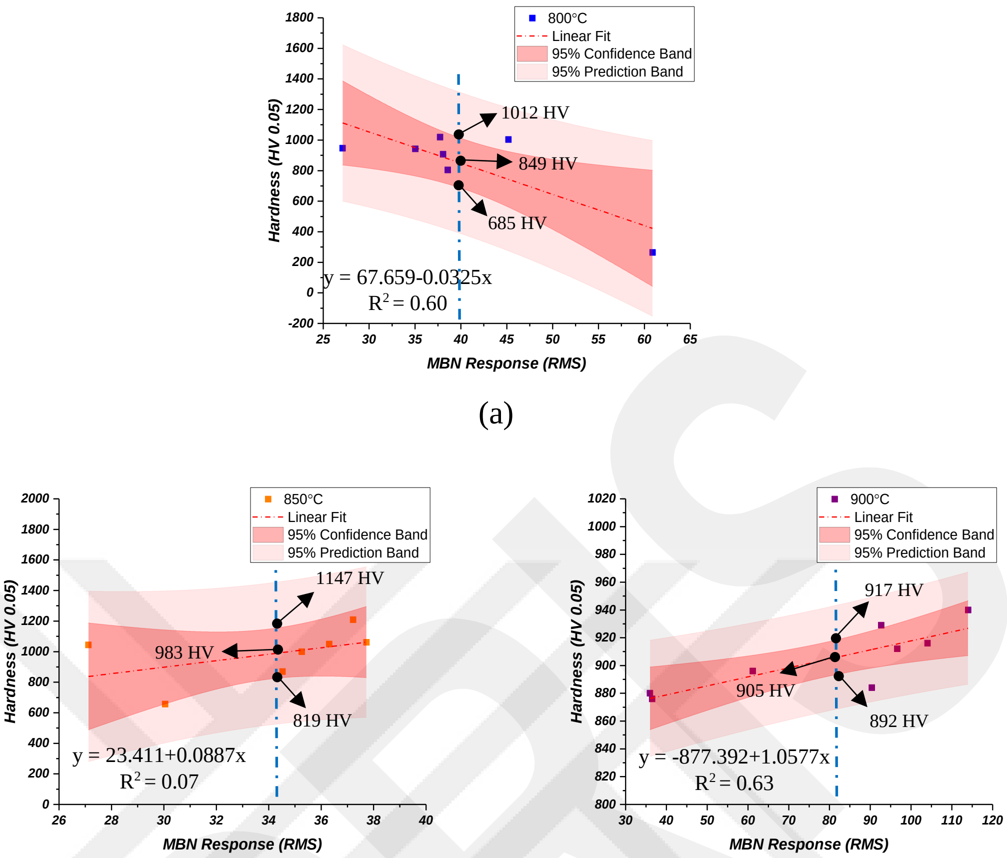

(a)

(b) (c)

Figure 4. 32 Correlations between matrix hardness and MBN response of the specimens that were austenitized at (a) 800°C (b) 850°C and (c)900°C quenched to RT

4.3.2.2. Retained Austenite Correlation (RT Quenching)

Retained austenite correlations of each set of experiment of 800°C, 850°C and 900°C were indicated in Figure 4.33- a, b and c respectively. As can be seen from the figures, the worst correlation was observed from set of the specimens that were austenitized at 850°C due to the weakest differentiation of MBN responses. However, better ones were observed for the specimens that were austenitized at 800°C and 900°C comparing to especially their hardness correlations. Based on inherent nonmagnetic property of austenite, MBN responses of specimens were expected to be decreased with increase of retained austenite amount. Therefore, the slopes of the linear fits were expected to be negative. It was clearly seen that, the correlations of the specimens that were both austenitized at 800°C and 900°C were followed expected trend.

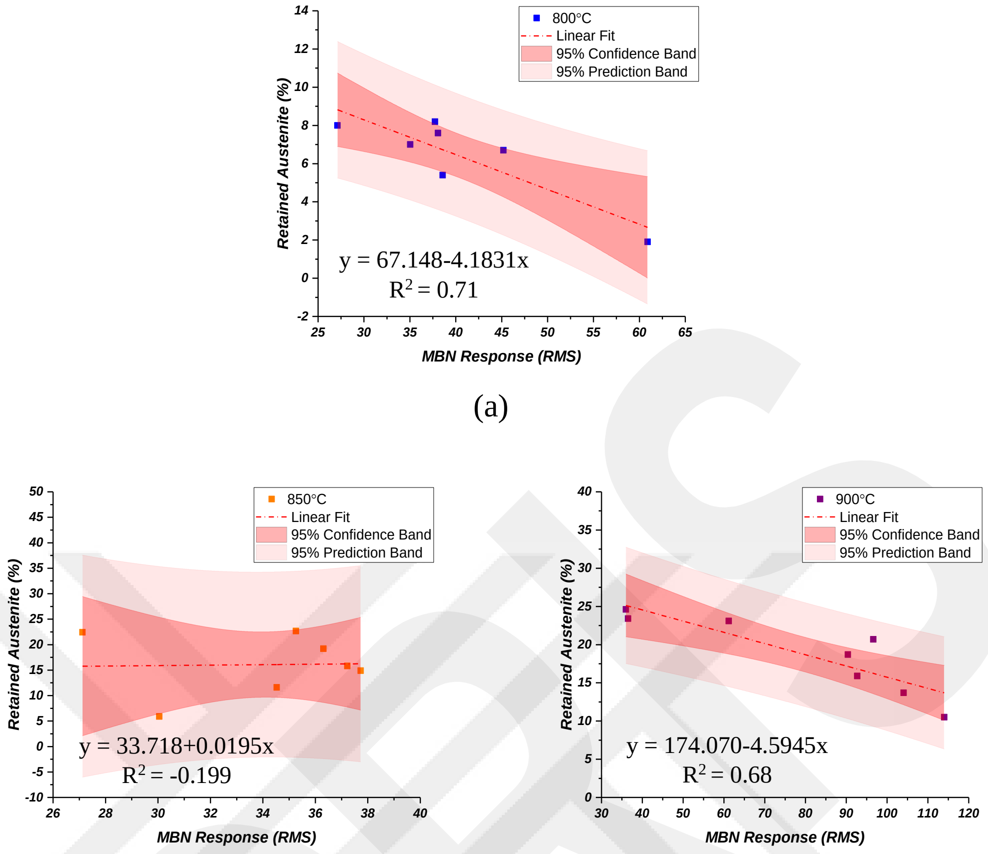

(a)

(b)

(c)

Figure 4. 33 Correlations between retained austenite and MBN response of the specimens austenitized at (a) 800°C (b) 850°C and (c)900°C and quenched

Moreover, similar (to the cases of hardness correlations) situations were observed for the confidence and prediction bands of the correlations between the retained austenite and MBN response. While most of the data points were lied within the 95% confidence intervals, these ranges of the limits were very large for sensitive prediction of corresponding retained austenite values based on MBN response of the specimens especially for the specimens that were austenitized at 800°C and 850°C then quenched to room temperature.

4.3.2.3. Carbide Fraction Correlation (RT Quenching)

Finally, correlations between MBN responses of the specimens with their carbide fractions were given in Figure 4.34- a, b, c for the specimens that were austenitized at 800°C, 850°C and 900°C respectively. Carbide fraction influence on MBN response does not directly depend on number or area fractions of the specimens, but it influences hardness and retained austenite amount due to carbide dissolution kinetics.

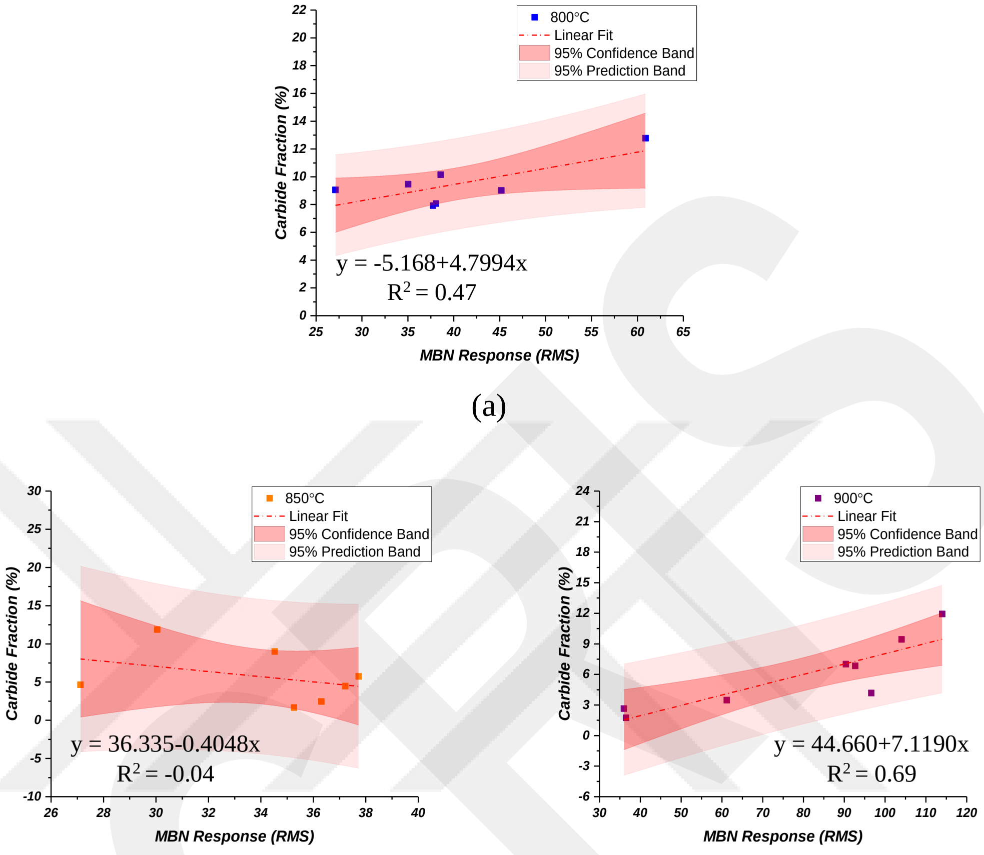

(a)

(b)

(c)

Figure 4. 34 Correlations between carbide fraction (area%) and MBN response of the specimens austenitized at (a) 800°C (b) 850°C and (c)900°C and quenched

The carbide fraction correlation of the specimens that were austenitized at 850°C was also very low due to same reason of its hardness and retained austenite correlations. However, carbide fraction correlation of the specimens that were austenitized at both 800°C and 900°C followed the same trend as carbide fraction increased, RMS of the measurements also increased. This behavior of MBN might be associated with carbide dissolution influence on retained austenite amount; since more carbide dissolution in austenite structure causes an increase of amount of austenite that remained in the final microstructure. Since it is nonmagnetic, it caused a reduction on MBN signals of the measurements for the specimens that contained higher amount of retained austenite. Apart from the low R^2 values which implied the goodness of correlations, very wide range of confidence limits were observed. Thus, MBN responses of specimens were not sufficient for sensitive characterization of their carbide fractions as well.

All of these correlations (Figure 4.32, 4.33, and 4.34) showed that although MBN would be a new promising technique for microstructural characterization of 100Cr6 steels quenched to RT after austenitization, it was not sufficient under these capabilities of the measurement system and with these individual simple linear relations. All of these concurrent changes in the microstructures are needed to be distinguished. Moreover, their interdependent relation and influence on MBN has to be analyzed by a new nonlinear correlation formula that considers retained austenite, C in martensite and carbide fraction of the structure based on carbide dissolution kinetics and their combined effect on MBN response of the 100Cr6 steel specimens. Apart from this, another measurement probe which will be compatible with the dilatometer specimens, and will be able to collect even stronger signals has to be designed. If these improvements are provided in future works, MBN technique may have a great importance among the other microstructural characterization techniques due to its nondestructive nature, fastness and compatible system for automation.

4.3.2. MBN Correlations of the Specimens Quenched to Subzero Temperature

Totally 320 MBN measurements were also performed on each set of specimen by varying the magnetizing voltage in step of 1 V between 1 V to 16 V and varying the magnetizing frequency in step of 50 Hz between 50 Hz to 1000 Hz. In order to qualify the collected raw signal data, it was filtered between 10-1000 kHz, and then optimization works have been also done for present case;

- 50 Hz of magnetizing frequency and 11 V of magnetizing voltage was selected for the measurements of the specimens that were austenitized at 800°C and quenched to -130°C
- 150 Hz of magnetizing frequency and 4 V of magnetizing voltage was selected for the measurements of the specimens that were austenitized at 850°C and quenched to -130°C

- 50 Hz of magnetizing frequency and 3 V of magnetizing voltage was selected for the measurements of the specimens that were austenitized at 900°C then quenched to -130°C

Representative MBN profiles which were obtained by combination of optimized measurement parameters (for the specimens that were austenitized at 800°C, 850°C, and 900°C) were given in Figure 4.35- a, b, and c (respectively).

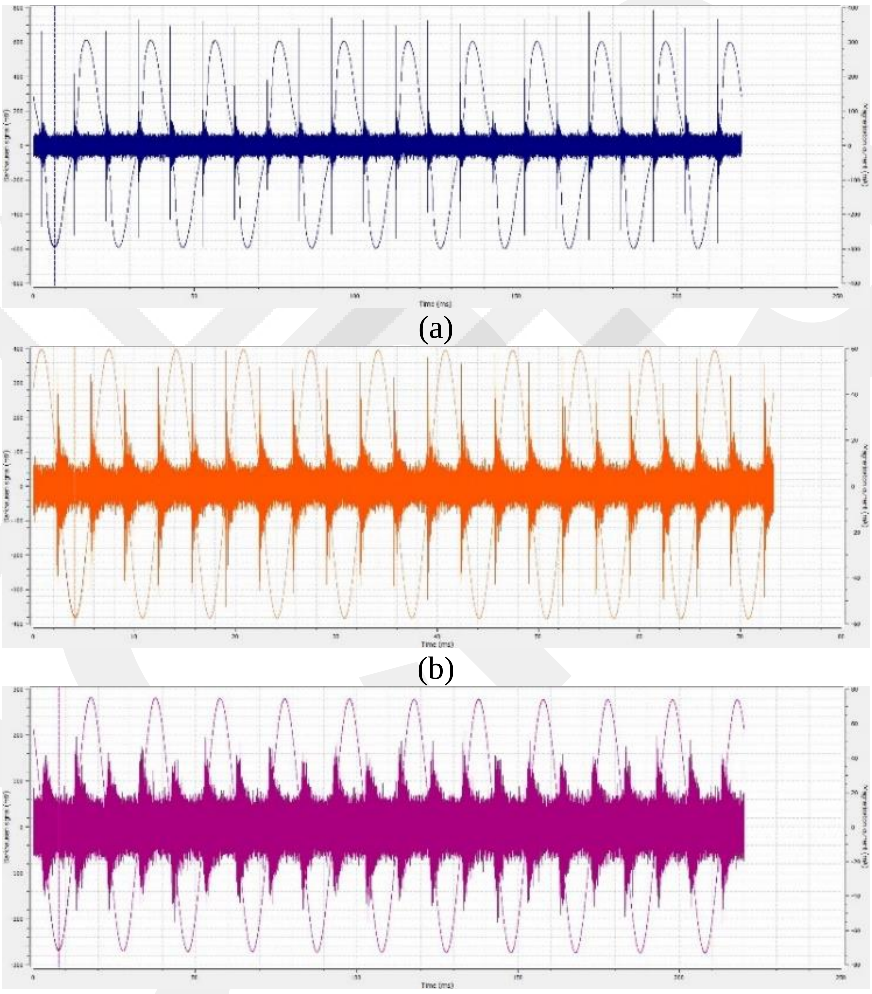

(a)

(b)

(c)

Figure 4. 35 MBN profiles obtained by optimized combination of measurement parameters for the specimens austenitized 30 minutes at (a) 800°C (11V & 50Hz), (b) 850°C (4V & 150Hz), and (c) 900°C (3V & 50Hz)

MBN profiles of each experiment showed that noise signal was also quite weak for the sub-zero treated specimens. However, relatively better MBN measurements were obtained with combination of selected parameters for each set of experiment compared to other 319 combinations. Therefore, hardness and carbide fraction correlations with

RMS of the measurements were characterized under these selected measurement parameters. In addition to this optimization work, since fully martensitic transformation obtained in the sub-zero treated specimens, retained austenite did not influence the results. For this case of the present study, MBN correlations were expected to be improved due to elimination of retained austenite effect on the signals. Thus, only the martensite hardness and carbide fraction correlations were considered.

4.3.2.1. Hardness Correlation (Sub-zero Quenching)

The relations between the matrix hardness and the MBN response of the specimens that were austenitized at 800°C, 850°C and 900°C then quenched to -130°C were given in Figure 4.36-a, b, and c respectively. As it was seen from the figures, hardness correlations of each set of experiment improved compared to the correlations of the RT quenched specimens. This improvement is due to the fact that matrix hardness became the main factor on MBN response by elimination of retained austenite. Especially, significant improvement was observed on the hardness correlations of the sub-zero treated specimens that were austenitized at 850°C.

In addition, all of the hardness correlations followed the expected trend (RMS of measurement decreased with increase of matrix hardness) except the set of specimen that austenitized at 900°C. This might be explained by occurrence of relatively higher hardness values in these specimens, especially after a certain austenitization time. Since increase of interstitial C content of martensite lowers the MBN signals, weaker RMS values were calculated from this set of specimen. Therefore, it could not be significantly distinguished by MBN measurement based on this fact. Obviously, the carbon content of martensite of the specimens raised with increase of T_γ, and so the lowest RMS values were calculated from the specimens that were austenitized at 900°C, where the highest ones calculated from the specimens that were austenitized at 800°C. Comparison of calculated R^2 values showed that, an improvement on the strength of the collected noise signal caused an increase of goodness of fit of the correlations.

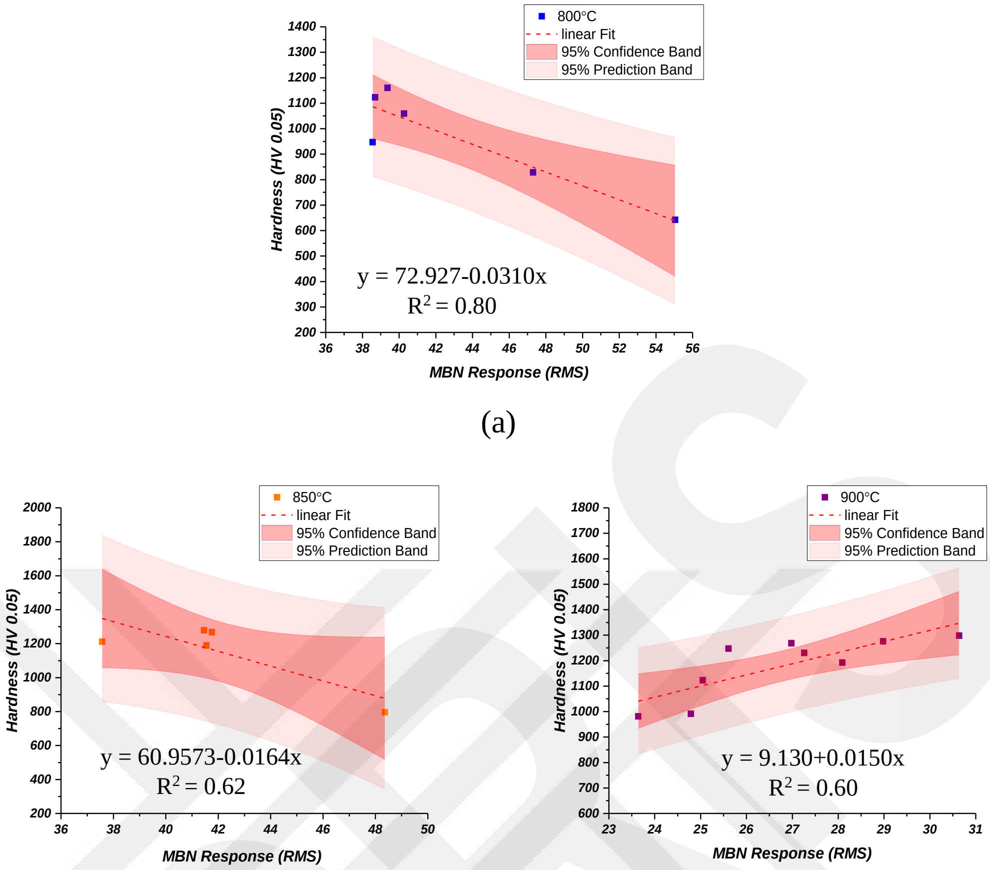

(a)

(b) (c)

Figure 4. 36 Correlations between matrix hardness and MBN response of the specimens that were austenitized at (a) 800°C (b) 850°C and (c) 900°C and subzero quenched

In addition to all of these considerations on influences of revealed microstructural properties on MBN signals, it was also lowered due to incompatible geometrical properties of the dilatometer specimens for the measurement probe. Nevertheless, elimination of retained austenite influence on MBN response caused significant improvements on correlations of the specimens that were austenitized at 800°C and 850°C compared to the correlations of the RT quenched specimens. Although these improvements on goodness of fit, it was resulted as, MBN measurements did not provide sufficiently sensitive determination of hardness values from its MBN response (RMS value), based on their wide confidence intervals.

4.3.2.2. Carbide Fraction Correlation (Sub-zero Quenching)

Another microstructural property that had an influence on MBN response of the specimens was the remaining carbides in the final microstructure of sub-zero treated

100Cr6 steel specimens. Therefore, MBN correlations with carbide fractions were examined for each set of experiment of 800°C, 850°C and 900°C and given in Figure 4.37-a, b, and c respectively.

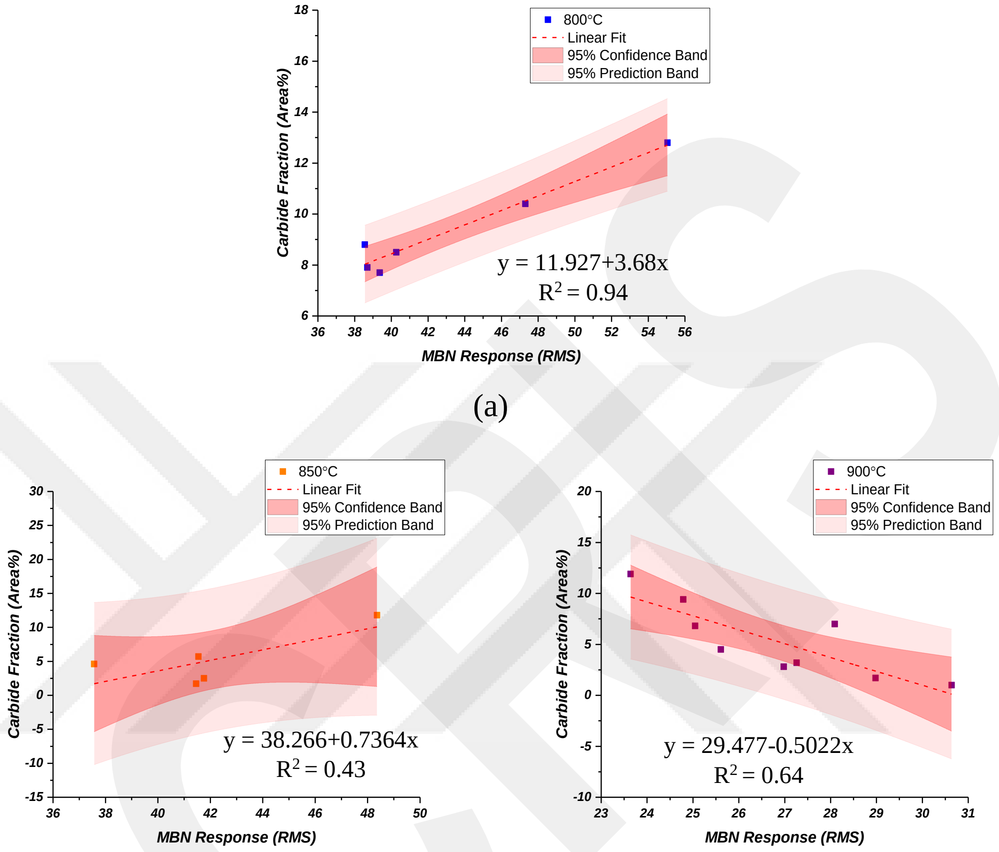

(a)

(b) (c)

Figure 4. 37 Correlations between carbide fraction (area%) and MBN response of the specimens that were austenitized at (a) 800°C (b) 850°C and (c)900°C and subzero quenched

Since the carbides pinned the domain wall motion, RMS values of the measurements were expected to be reduced due to decrease of its amount with increase of austenitization time and/or temperature. This trend was observed only on the set of experiments involve austenitization at 900°C. However, other set of experiments followed an opposite trend. This opposite behavior may be explained based on carbide dissolution effect on matrix hardness. Although reduction of carbide fraction in the structure caused a decrease of number of pinning obstacles, its dissolution caused an increase on carbon content of the martensite which caused formation of finer martensite needles. Since domain wall motions pinned by smaller martensite needles/laths MBN response of specimens reduced based on this fact. Thus, RMS values of the specimens austenitized at 800°C and 850°C decreased with reduction of carbide amount due to increase of martensite hardness of the structure.

Among all of these set of experiments, the best correlation was found for the set of specimens that were austenitized at 800°C, which gave the highest MBN response compared to the others. Moreover, its confidence interval was narrower, so carbide fraction might be determined 95% accurately from its MBN response. On the other hand, considering the correlations of the specimens that were austenitized at 850°C and 900°C, it was possible to predict negative carbide fraction values within 95% confidence band due to their wider confidence intervals. Thus, these indicated upper and lower confidence limits showed that MBN measurements of these set of specimens were not sufficient for accurate determination of carbide fractions directly from their MBN response.

Finally, outlook and conclusion of this present study will be given in following 5th Chapter.

CHAPTER 5

OUTLOOK AND CONCLUSION

In this study, the effects of austenitization temperature and time on microstructural variations of 100Cr6 steels were investigated through a series of experiments composed of two main cases. Those are, (i) austenitization temperature varied while austenitization time kept constant, (ii) austenitization time varied while keeping the austenitization temperature constant. After austenitization experiments, the specimens were characterized by metallographic (optical and scanning electron microscopy), analytical (OES, XRD), mechanical (macro/micro hardness) and micro-magnetic (MBN) characterization techniques. The results are supported by theory (thermodynamics, kinetics, diffusion, and electromagnetism) and numerical simulations. The conclusions of the study can be summarized as follows:

1- Hardness of the specimens that were quenched to RT after austenitization mainly affected by two parameters; (i) martensite hardness, and (ii) retained austenite. On the other hand, the hardness was mainly determined from only (i) martensite hardness for the sub-zero treated specimens. Although these two parameters have dynamic equilibrium, their concurrent effect on hardness was not linear. Therefore, at early stages of austenitization, both macro and micro hardness raised due to dominant influence of martensite hardness, where; this regular increase changed into regular decreases and increases for further stages of austenitization based on concurrent effects of martensite hardness ad retained austenite on hardness.

2- The M_S temperature and Ret_γ fraction of heat treated 100Cr6 steels can be estimated via empirical relations. The accuracy of those relations rely on the estimation of carbide dissolutions. Current reported relations agree well for the case of 900°C austenitized specimens; in which carbides dissolve almost completely.

3- Microstructural parameters of heat treated 100Cr6 steels (i.e. retained austenite, martensite hardness, and carbide fraction) influenced the MBN response of the specimens, based on carbide dissolution kinetics. Therefore considering only the individual simple linear relations between the microstructural properties and MBN responses of the specimens were not sufficient for direct characterization of individual property with respect to its MBN response.

4- Magnetic Barkhausen noise technique is found to be sensitive to microstructure and the related hardness variations in quenched and tempered steel microstructures, in which the hardness variation is above 300 HV. The sensitivity, validity and reliability of the MBN technique strongly depends on the selection of measurement parameters. A new procedure is proposed, that considers the sensitivity, reliability and inherent symmetry of the magnetic hysteresis, for selecting the optimum measurement parameters.

5- MBN technique correlates with the microstructure variations in 100Cr6 steel specimens. However, it should be noted that the prediction bands are quite wide, indicating insufficient sensitivity. The narrow hardness variations in 100Cr6 also limits the use of MBN technique in its current form to differentiate 100Cr6 steel samples austenitized at different temperature and time combinations.

Consequently, despite all of the inabilities of the MBN measurement system and indistinguishable concurrent formations in the microstructure, the results of each set of specimen that both quenched to RT and sub-zero treated were promising for the nondestructive characterization of heat treated 100Cr6 steels by MBN technique. If the measurements were performed with a probe more compatible to the dilatometer specimens, and stronger external magnetization is utilized, stronger raw signals would be collected, which in turn increase the measurement sensitivity. Most probably, the correlations would significantly get better with improvement of the quality of signals.

Apart from the capabilities of the measurement system, some of the correlations were considerable ($R^2>0.60$) for the specimens, and showed with '+' sign in following Table 5.1 and the rests were represented with '-' sign.

Table 5. 1 Assesment of MBN correlations for each condition

		Hardness	Carbide Fraction	Retained austenite
RT Quenching	800°C	+	-	+
	850°C	-	-	-
	900°C	+	+	+
Sub-zero Treated	800°C	+	+	
	850°C	+	-	
	900°C	+	+	

Although individual simple linear relations were not sufficient for direct characterization of microstructural features of 100Cr6 steel specimens via MBN technique due to their broad confidence and prediction intervals, the results were promising since all of the data points were lied within these intervals for all conditions. Therefore, it is concluded that; analyzing the nonlinear and concurrent effects of retained austenite, martensite hardness and carbide fraction on MBN response of the specimens may significantly improve the correlations. This means, a new non-linear model has to be defined based on carbide dissolution kinetics, nonlinear formation of presented phases and their influences on MBN signals.

As a future work, a new measurement probe which will be able to apply external magnetization is recommended. This would increase the strength of the applied field, and so would provide higher quality MBN measurements on 100Cr6 dilatometer specimens. Besides, other signal processing methods can be used in order to differentiate the meaningful signals from the background noise signals. Moreover, a new non-linear model can be proposed based on carbide dissolution kinetics of 100Cr6 steel by analyzing the interactions of all of the parameters (i.e. C in austenite, retained austenite amount, remained carbide fractions and distributions) that affect the hardness of the specimens and their individual influences on MBN response.

REFERENCES

[1] NTN Bearing Corporation, “An Introduction to Ball Bearings,” pp. 1–24, 1994.

[2] E. V Zaretsky, “Selection Rolling Element Bearing Steels for Long-Life Application,” Ohio, USA, 1986.

[3] E. Persson, “Austenite Grain Growth in Bearing Steels,” Stockholm, 2013.

[4] ASTM International, *ASTM E3-01, Standard Guide for Preparation of Metallographic Specimens*. West Conshohocken, USA, 2001.

[5] ASTM International, *ASTM E975-13, Standard Practice for X-Ray Determination of Retained Austenite in Steel with Near Random Crystallographic Orientation*. 2003.

[6] M. Blaow, J. T. Evans, and B. a. Shaw, “Magnetic Barkhausen Noise: The Influence of Microstructure and Deformation in Bending,” *Acta Mater.*, vol. 53, no. 2, pp. 279–287, 2005.

[7] M. M. Blaow and M. A. Ballem, “Magnetic Barkhausen Noise : Aspects of Generation and Modeling,” *Int. J. Eng. Inf. Technol.*, vol. 1, no. 2, pp. 36–40, 2015.

[8] K. Davut, “Characterization of Steel Microstructures by Magnetic Barkhausen Noise Technique,” Middle Eats Technical University, 2006.

[9] L. Mierczak, D. C. Jiles, and G. Fantoni, “A New Method for Evaluation of Mechanical Stress Using the Reciprocal Amplitude of Magnetic Barkhausen Noise,” *IEEE Transctions Magn.*, vol. 47, no. 2, pp. 459–465, 2013.

[10] M. Woydt and R. Wäsche, “The History of the Stibeck curve and ball bearing steels: the role of Adolf Martens.,” *Wear*, vol. 268–1542, no. 6, 2010.

[11] H. K. D. H. Bhadeshia, “Progress in Materials Science Steels for Bearings,” *Prog. Mater. Sci.*, vol. 57, no. 2, pp. 268–435, 2012.

[12] D. Dowson and B. J. Hamrock, “History of Ball Bearings,” Cleveland, OH, United States, 1981.

[13] F. C. Kahlbaugh, “Heat Treatment of SAE 52100 Steel,” California, 1960.

[14] J. M. Beswick, *Bearing Steel Technologies*, 8th ed. West Conshohocken, USA, 2014.

[15] G. Krauss, *ASM International, Steels; Processing, Structure, and Performance,* 2nd ed. 2015.

[16] G. F. Vander Voort, *ASM International, Atlas of Time-Temperature Diagrams for Irons and Steels*. USA, 1991.

[17] A.S.M. Handook, “Volume 4:Heat Treating,” in *ASM Handbook*, USA, 1991.

[18] J. Trzaska, “Calculation of Critical Temperatures by Empirical Formulae,” *Arch. Metall. Mater.*, vol. 61, no. 2, pp. 981–986, 2016.

[19] M. Peet, “Prediction of Martensite Start Temperature,” *Mater. Sci. Technol.*, vol. 31, no. 11, pp. 1370–1375, 2014.

[20] S. van der Z. Wang, Jiajun, Pieter J. van der Wolk, “Determination of Martensite Start Temperature in Engineering Steels Part I. Empirical Relations Describing the Effect of Steel Chemistry,” *Mater. Trans.*, pp. 761–768, 2000.

[21] A. Garcia Junceda, C. Capdevilla, F. G. Caballero, and C. Garcia de Andres, “Dependence of Martensite Start Temperature on Fine Austenite Grain Size,” *Scr. Mater.*, vol. 58, pp. 134–137, 2008.

[22] S.-J. Lee and K. Park, “Prediction of Martensite Start Temperature in Alloy Steels with Different Grain Sizes,” *Met. Mater. Trans.*, vol. 44, no. August, pp. 3423–3427, 2013.

[23] H. Yang and H. K. D. H. Bhadeshia, “Austenite grain size and the martensite-start temperature,” *Scr. Mater.*, vol. 60, no. 7, pp. 493–495, 2009.

[24] J. Epp, H. Surm, O. Kessler, and T. Hirsch, “In situ X-ray Phase Analysis and Computer Simulation of Carbide Dissolution of Ball Bearing Steel at Different Austenitizing Temperatures,” *Acta Mater.*, vol. 55, pp. 5959–5967, 2007.

[25] W. Song, P. C. Gerhard, I. Ulrich, P. Dierk, and R. Wolfgang, “On the Spheroidized Carbide Dissolution and Elemental Partitioning in a High Carbon Bearing Steel 100Cr6,” *Metall. Mater. Trans.*, pp. 595–606, 2014.

[26] B. Uluğ, “Sıfıaltı Kreojenik Isıl İşlemin 100Cr6 ve 8620 Kalite Çeliklerin Özellikleri Üzerine Etkisi,” İstanbul Teknik University, 2006.

[27] D. Das, K. K. Ray, and A. K. Dutta, “Influence of Temperature of Sub-Zero Treatments on the Wear Behaviour of Die Steel,” *Wear*, vol. 267, pp. 1361–1370, 2009.

[28] D. Das, R. Sarkar, A. Kishore, and K. Kumar, “Influence of Sub-Zero Treatments on Fracture Toughness of AISI D2 Steel,” *Mater. Sci. Eng. A*, vol. 528, pp. 589–603, 2010.

[29] M. Perez, C. Sidoroff, A. Vincent, and C. Esnouf, “Microstructural Evolution of Martensitic 100Cr6 Bearing Steel during Tempering : from Thermoelectric Power Measurements to the Prediction of Dimensional Changes,” *Acta Mater.*, vol. 57, no. 11, pp. 3170–3181, 2009.

[30] J. Chakraborty, D. Bhattacharjee, and I. Manna, “Development of Ultrafine Bainite + Martensite Duplex Microstructure in SAE 52100 Bearing Steel by Prior Cold Deformation,” *Scr. Mater.*, vol. 61, no. 6, pp. 604–607, 2009.

[31] J. Chakraborty, D. Bhattacharjee, and I. Manna, “Austempering of Bearing Steel for Improved Mechanical Properties,” *Scr. Mater.*, vol. 59, pp. 247–250, 2008.

[32] C. M. Amey and H. Huang, “Distortion in 100Cr6 and Nanostructured Bainite,” *Mater. Des.*, vol. 35, pp. 66–71, 2012.

[33] N. Luzginova, L. Zhao, and J. Sietsma, “Evolution and Thermal Stability of Retained Austenite in SAE 52100 Bainitic Steel,” *Mater. Sci. Eng. A*, vol. 448, pp. 104–110, 2007.

[34] B. Hallstedt, W. Bleck, and J. F. Lo, “On the Microstructure and Properties of 100Cr6 Steel Processed in the Semi-Solid State,” *Acta Mater.*, vol. 55, pp. 6553–6560, 2007.

[35] C. A. Stickels, “Carbide Refining Heat Treatments for 52100 Bearing Steel,” *Metall. Trans.*, vol. 5, pp. 864–874, 1974.

[36] I. V Rivero and C. O. Ruud, “Deviation of Residual Stress Patterns in 52100

Bearing Bteel due to Inherent Microstructural Transformations after Rolling Contact," vol. 53, pp. 381–393, 2004.

[37] C. A. Stickels and A. M. Janotik, "Controlling Residual Stresses in 52100 Bearing Steel by Heat Treatment," *Metall. Trans.*, pp. 467–473, 1980.

[38] C.-G. Stefanita, *From Bulk to Nano: the Many Sides of Magnetism*. Springer Science & Bussiness Media, 2008.

[39] J. M. D. Coey, *Magnetism and Magnetic Materials*. Edinburg, UK, 2010.

[40] "https://www.doitpoms.ac.uk/tlplib/ferromagnetic/types.php." 2017.

[41] K. H. J. Buschow and F. R. De Boer, *Physics of Magnetism and Magnetic Materials*. New York, 2003.

[42] S. Chikazumi, *Physics of Ferromagnetism*. New York, 1197.

[43] B. D. Cullity and C. D. Graham, *Introduction to Magnetic Materials*, 2nd ed. USA, 2009.

[44] R. Hull, C. Jagadish, R. M. Osgood, and Z. M. Wang, *Springer Series in Materials Science, The Physics of Ferromagnetism*, vol. 158. 2012.

[45] "https://earthref.org/MagIC/books/Tauxe/Essentials/WebBook3ch4.html." 2017.

[46] L. H. Diez, "Magnetization Reversal Dynamics in Ferromagnetic Semiconductors," Suisse, 2011.

[47] Http://www.ndt.net/article/v11n06/wong/wong.htm, "httpwww." 2017.

[48] M. M. Blaow and B. A. Shaw, "Magnetic Barkhausen Noise Profile Analysis : Effect of Excitation Field Strength and Detection Coil Sensitivity in Case Carburized Steel," 2014.

[49] E. Arslan, K. Davut, and C. Şimşir, "Optimization of Sensitivity and Reliability of Magnetic Barkhausen Technique for Detecting Hardness Differences on Quenched and Tempered AISI 4140 Steels," in *ICBM-11*, 2015.

[50] V. Moorthy, B. a. Shaw, and P. Hopkins, "Surface and Subsurface Stress Evaluation in Case-Carburised Steel Using High and Low Frequency Magnetic

Barkhausen Emission Measurements," *J. Magn. Magn. Mater.*, vol. 299, no. 2, pp. 362–375, 2006.

[51] V. Moorthy, S. Vaidyanathan, K. Laha, T. Jayakumar, K. B. S. Rao, and B. Raj, "Evaluation of Microstructures in 2 . 25Cr-1Mo and 9Cr-1Mo Steel Weldments Using Magnetic Barkhausen Noise," vol. 231, pp. 98–104, 1997.

[52] K. Davut and C. H. Gür, "Monitoring the Microstructural Evolution in Spheroidized Steels by Magnetic Barkhausen Noise Measurements," *J. Nondestruct. Eval.*, vol. 29, pp. 241–247, 2010.

[53] M. Rocío, N. Astudillo, M. Núñez, J. Ruzzante, P. Gómez, G. Claudio, L. Rodrigues, and M. Isabel, "Correlation between Martensitic Phase Transformation and Magnetic Barkhausen Noise of AISI 304 Steel," *Procedia Mater. Sci.*, vol. 9, pp. 435–443, 2015.

[54] M. Erdogan, M. Kaplan, and C. H. Gür, "Characterization of Dual-Phase Steels Using Magnetic Barkhausen Noise Technique," *J. Nondestruct. Eval.*, vol. 26, no. 2, pp. 79–87, 2007.

[55] S. Kahrobaee, M. Kashefi, S. Kahrobaee, M. Kashefi, M. Engineering, and E. Faculty, "Assessment of Retained Austenite in AISI D2 Tool Steel Using Magnetic Hysteresis and Barkhausen Noise Parameters," vol. 24, no. March, pp. 1192–1198, 2015.

[56] C. Gatelier-Rothea, J. Chicois, and R. Fougeres, "Characterization of Pure Iron and (130 P . P . M .) Carbon ± Iron Binary Alloy by Barkhausen Noise Measurements : Study of Tthe Influence of Stress and Microstructure," *Acta Mater.*, vol. 46, no. 14, pp. 4873–4882, 1998.

[57] X. Luo, Y. Wang, L. Wang, J. Xie, and Y. Zhang, "Non-Destructive Hardness Measurement of Hot-Stamped High Strength Steel Sheets based on Magnetic Barkhausen Noise," *Procedia Eng.*, vol. 81, no. October, pp. 1768–1773, 2014.

[58] M. Lindgren and T. Lepist, "Utilization of Barkhausen Noise Magnetizing Sweeps for Case-Depth Detection from Hardened Steel," *NDT E Int.*, vol. 52, pp. 95–102, 2012.

[59] F. A. Franco, M. F. R. Gonzalez, and M. F. de Campos, "Relation Between

Magnetic Barkhausen Noise and Hardness for Jominy Quench Tests in SAE 4140 and 6150 Steels," *J. Nondestruct. Eval.*, vol. 32, pp. 93–103, 2013.

[60] A. Ktena, E. Hristoforou, G. J. L. Gerhardt, F. P. Missell, F. J. G. Landgraf, D. L. Rodrigues, and M. Alberteris-campos, "Barkhausen Noise as a Microstructure Characterization Tool," *Phys. B Phys. Condens. Matter*, vol. 435, pp. 109–112, 2014.

[61] N. Chukwuchekwa, A. Moses, and P. Anderson, "Barkhausen Noise in Grain Oriented 3 % Si-Fe at 50 Hz," *J. Electr. Eng.*, vol. 61, no. 7, pp. 69–72, 2010.

[62] L. R. Padovese, "Magnetic Barkhausen Noise and Hysteresis Loop in Commercial Carbon steel : Influence of Applied Tensile Stress and Grain Size," *J. Magn. Magn. Mater.*, vol. 231, no. 2, pp. 299–306, 2001.

[63] D. Blazek, M. Neslušan, M. Mic, and D. Blaz, "Extraction of Barkhausen Noise from the Measured Raw Signal in High-Frequency Regimes," vol. 94, pp. 456–463, 2016.

[64] S. Desvaux, M. Duquennoy, J. Gualandri, and M. Ourak, "The Evaluation of Surface Residual Stress in Aeronautic Bearings Using the Barkhausen Noise Effect," *NDT E Int.*, vol. 37, pp. 9–17, 2004.

[65] A. Mi, J. Pi, Z. Durstová, and M. Neslu, "Concept of Damage Monitoring after Grinding for Components of Variable Hardness," *Procedia Mater. Sci.*, vol. 12, pp. 60–65, 2016.

[66] M. Neslusan, J. Cizek, K. Kolarik, and M. Chillikove, "Journal of Materials Processing Technology Monitoring of Grinding Burn via Barkhausen Noise Emission in Case-Hardened Steel in Large-Bearing Production," *Mater. Process. Technol.*, vol. 240, pp. 104–117, 201AD.

[67] B. T. G. 2010, "Manual of BÄHR Dilatometer Dil805," 2010.

[68] C. A. Schneider, W. S. Rasband, and K. W. Eliceiri, "NIH Image to ImageJ: 25 Years of Image Analysis," *Nat. Methods*, vol. 9, no. 7, pp. 671–675, 2012.

[69] T. Sourmail and C. Mateo-Garcia, "Critical assessment of models for predicting the Ms temperature of steels," Madrid, Spain.

[70] T. Sourmail, “Critical assessment of models for predicting the M s temperature of steels,” vol. 34, pp. 323–334, 2005.

[71] “https://www.phase-trans.msm.cam.ac.uk/map/steel/programs/ms-empirical2014.html.” 2017.

[72] D. Koistinen and R. Marburger, “A General Equation Prescribing the Extent of the Austenite-Martensite Transformation in Pure Iron-Carbon Alloys and Plain Carbon Steels,” *Acta Metall.*, vol. 7, no. 59, 1959.

[73] G. Krauss and G. Krauss, “Martensite in steel : strength and structure,” 1999.

[74] A. Das, “Magnetic Properties of Cyclically Deformed Austenite,” *J. Magn. Magn. Mater.*, vol. 361, no. June 2014, pp. 232–242, 2014.

[75] U. Gonser, C. J. Meechan, A. H. Muir, and H. Wiedersich, “Determination of Néel Temperatures in FCC Iron,” *J. Appl. Phys.*, vol. 34, no. 8, pp. 2373–2378, 1963.

[76] A. I. Ul’yanov, E. P. Elsukov, A. A. Chulkina, A. V. Zagainov, N. B. Arsent’eva, G. N. Konygin, V. F. Novikov, and V. V. Isakov, “The Role of Cementite in the Formation of Magnetic Hysteresis Properties of Plastically Deformed High-Carbon Steels: I. Magnetic Properties and Structural State of Cementite,” *Russ. J. Nondestruct. Test.*, vol. 42, no. 7, pp. 452–459, 2006.

[77] J. Ding, H. Huang, P. G. McCormick, and R. Street, “Magnetic Properties of Martensite-Austenite Mixtures in Mechanically Milled 304 Stainless Steel,” *J. Magn. Magn. Mater.*, vol. 139, no. 1–2, pp. 109–114, 1995.

APPENDICES

APPENDIX A

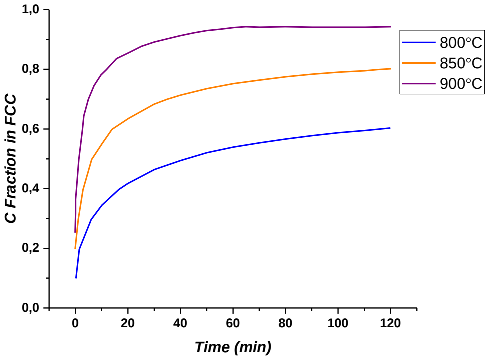

(a) C dissolution in FCC austenite structure of 100Cr6 steel during austenitization

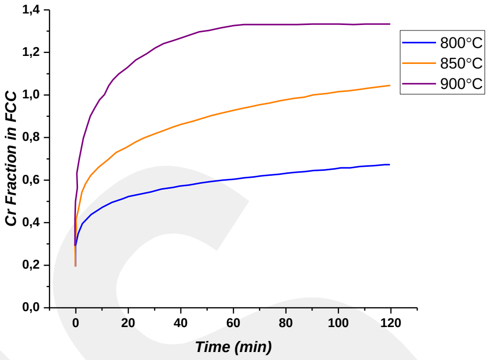

(b) Cr dissolution in FCC austenite structure of 100Cr6 steel during austenitization

APPENDIX B

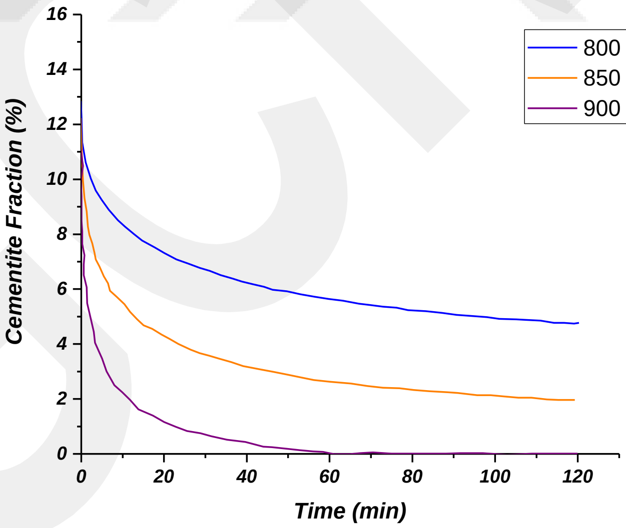

Cementite dissolution in FCC austenite structure of 100Cr6 steel during austenitization at 800 °C, 850°C and 900°C

APPENDIX C

The histograms that were drawn as frequency counts of carbides versus their diameters for each specimen.

**Related heat treatment conditions and average carbide diameter values were given in the right sides of each histogram.

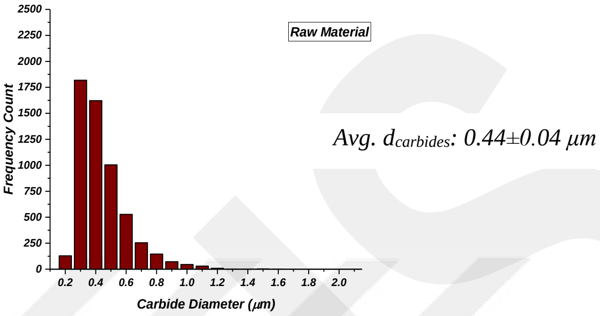

Avg. $d_{carbides}$*: 0.44±0.04 μm*

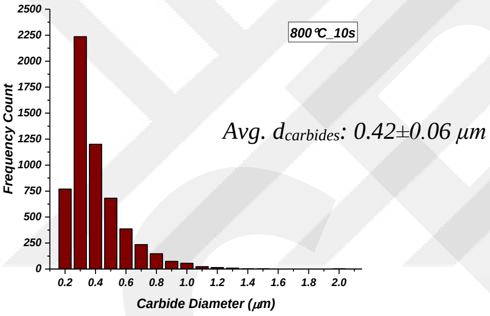

Avg. $d_{carbides}$*: 0.42±0.06 μm*

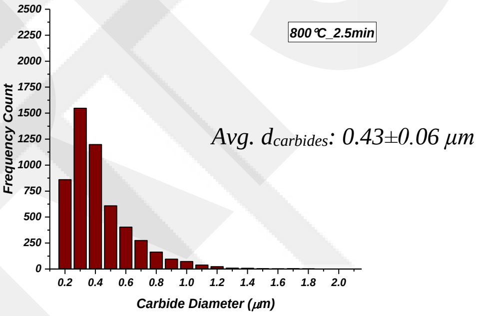

Avg. $d_{carbides}$*: 0.43±0.06 μm*

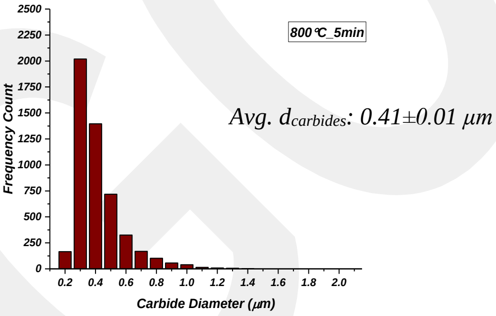

Avg. $d_{carbides}$*: 0.41±0.01 μm*

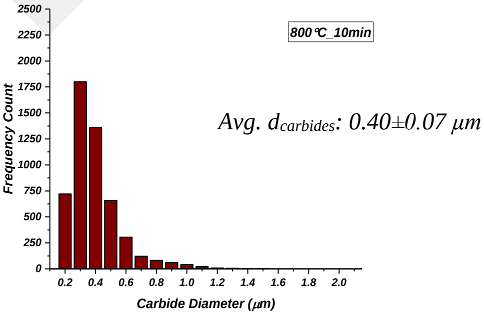

Avg. $d_{carbides}$*: 0.40±0.07 μm*

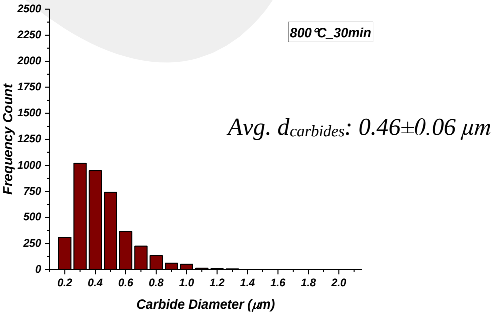

Avg. $d_{carbides}$*: 0.46±0.06 μm*

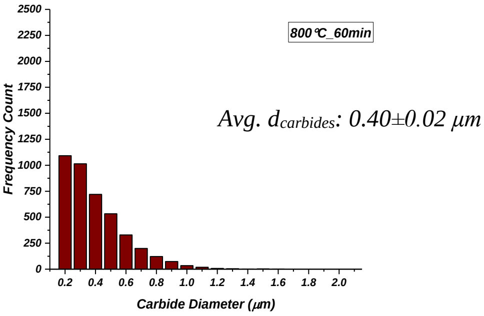

Avg. $d_{carbides}$*: 0.40±0.02 μm*

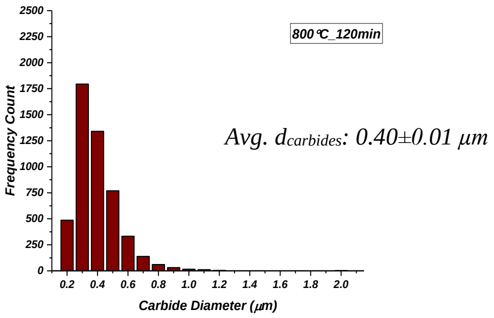
800℃_120min
Avg. $d_{carbides}$: 0.40±0.01 µm
Frequency Count
0
250
500
750
1000
1250
1500
1750
2000
2250
2500
0.2
0.4
0.6
0.8
1.0
1.2
1.4
1.6
1.8
2.0
Carbide Diameter (µm)

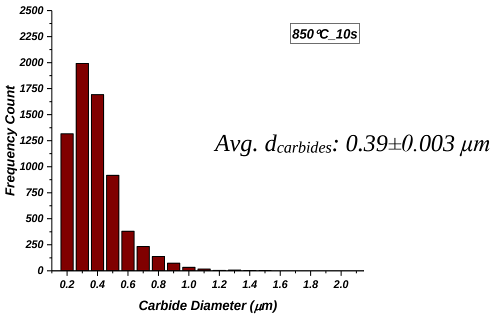
850℃_10s
Avg. $d_{carbides}$: 0.39±0.003 µm
Frequency Count
0
250
500
750
1000
1250
1500
1750
2000
2250
2500
0.2
0.4
0.6
0.8
1.0
1.2
1.4
1.6
1.8
2.0
Carbide Diameter (µm)

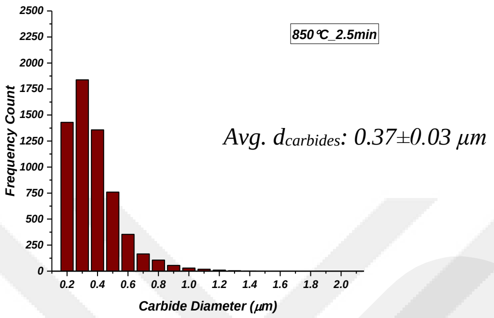
850℃_2.5min
Avg. $d_{carbides}$: 0.37±0.03 µm
Frequency Count
0
250
500
750
1000
1250
1500
1750
2000
2250
2500
0.2
0.4
0.6
0.8
1.0
1.2
1.4
1.6
1.8
2.0
Carbide Diameter (µm)

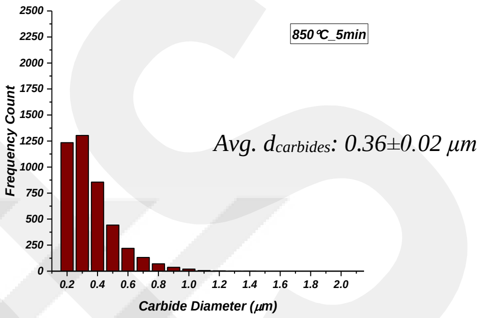
850℃_5min
Avg. $d_{carbides}$: 0.36±0.02 µm
Frequency Count
0
250
500
750
1000
1250
1500
1750
2000
2250
2500
0.2
0.4
0.6
0.8
1.0
1.2
1.4
1.6
1.8
2.0
Carbide Diameter (µm)

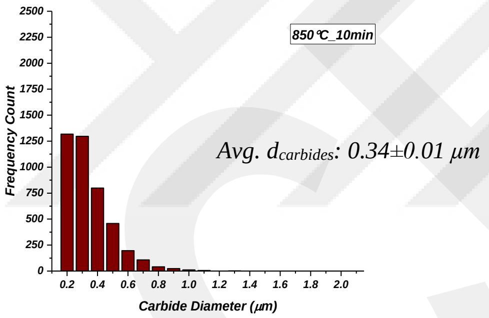
850℃_10min
Avg. $d_{carbides}$: 0.34±0.01 µm
Frequency Count
0
250
500
750
1000
1250
1500
1750
2000
2250
2500
0.2
0.4
0.6
0.8
1.0
1.2
1.4
1.6
1.8
2.0
Carbide Diameter (µm)

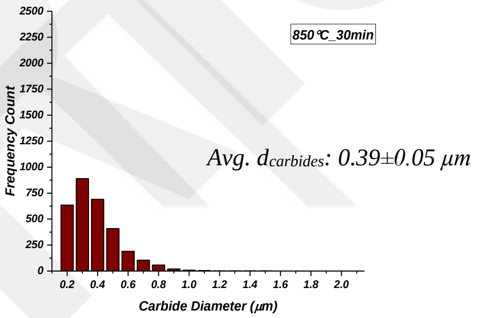
850℃_30min
Avg. $d_{carbides}$: 0.39±0.05 µm
Frequency Count
0
250
500
750
1000
1250
1500
1750
2000
2250
2500
0.2
0.4
0.6
0.8
1.0
1.2
1.4
1.6
1.8
2.0
Carbide Diameter (µm)

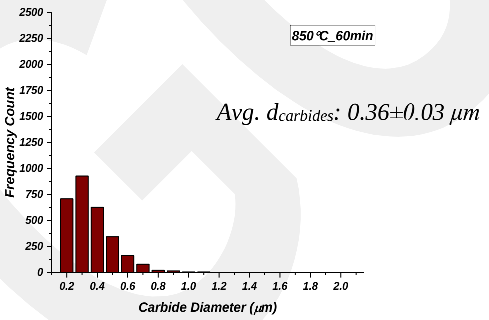
850℃_60min
Avg. $d_{carbides}$: 0.36±0.03 µm
Frequency Count
0
250
500
750
1000
1250
1500
1750
2000
2250
2500
0.2
0.4
0.6
0.8
1.0
1.2
1.4
1.6
1.8
2.0
Carbide Diameter (µm)

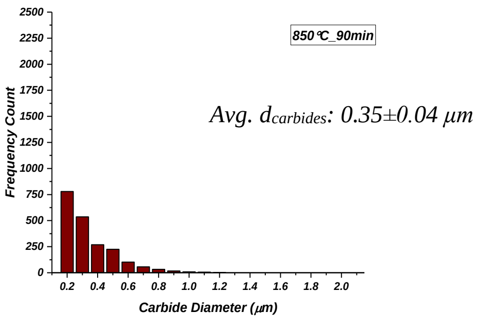
850℃_90min
Avg. $d_{carbides}$: 0.35±0.04 µm
Frequency Count
0
250
500
750
1000
1250
1500
1750
2000
2250
2500
0.2
0.4
0.6
0.8
1.0
1.2
1.4
1.6
1.8
2.0
Carbide Diameter (µm)

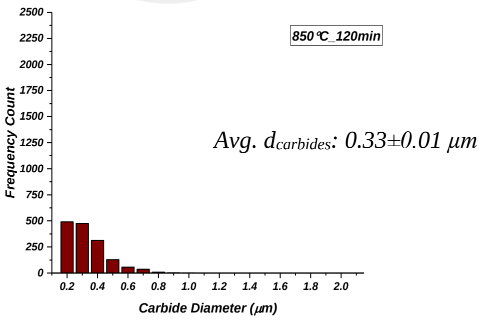
850℃_120min
Avg. $d_{carbides}$: 0.33±0.01 µm
Frequency Count
0
250
500
750
1000
1250
1500
1750
2000
2250
2500
0.2
0.4
0.6
0.8
1.0
1.2
1.4
1.6
1.8
2.0
Carbide Diameter (µm)

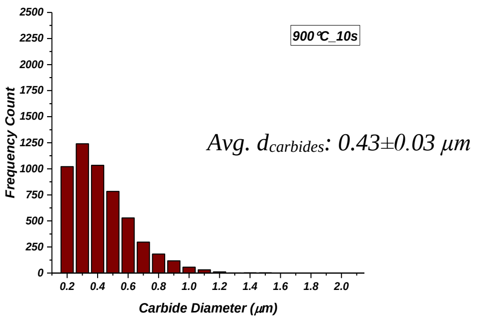
900℃_10s
Avg. $d_{carbides}$: 0.43±0.03 µm
Frequency Count
0
250
500
750
1000
1250
1500
1750
2000
2250
2500
0.2
0.4
0.6
0.8
1.0
1.2
1.4
1.6
1.8
2.0
Carbide Diameter (µm)

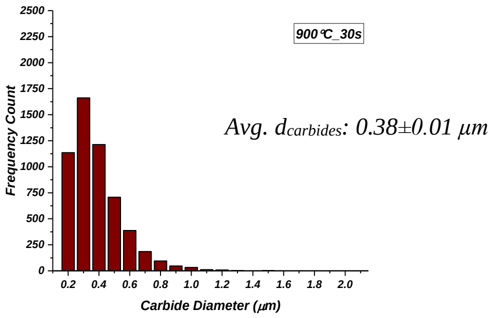
900℃_30s
Avg. $d_{carbides}$: 0.38±0.01 μm
Frequency Count
Carbide Diameter (μm)
0
250
500
750
1000
1250
1500
1750
2000
2250
2500
0.2
0.4
0.6
0.8
1.0
1.2
1.4
1.6
1.8
2.0

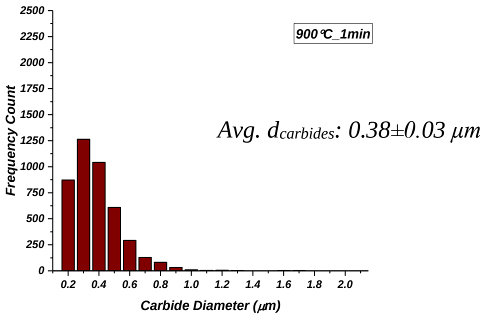
900℃_1min
Avg. $d_{carbides}$: 0.38±0.03 μm
Frequency Count
Carbide Diameter (μm)

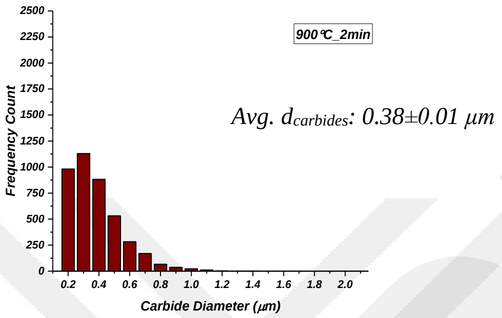
900℃_2min
Avg. $d_{carbides}$: 0.38±0.01 μm
Frequency Count
Carbide Diameter (μm)

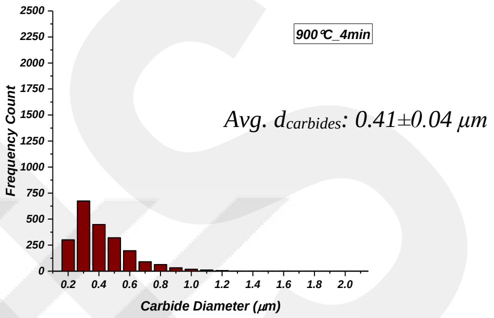
900℃_4min
Avg. $d_{carbides}$: 0.41±0.04 μm
Frequency Count
Carbide Diameter (μm)

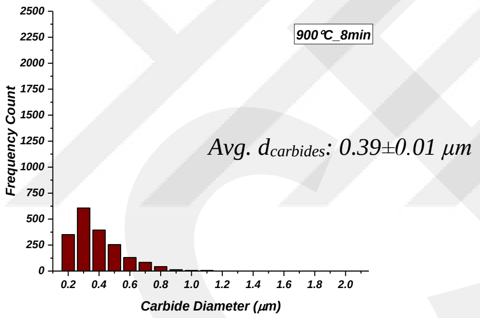
900℃_8min
Avg. $d_{carbides}$: 0.39±0.01 μm
Frequency Count
Carbide Diameter (μm)

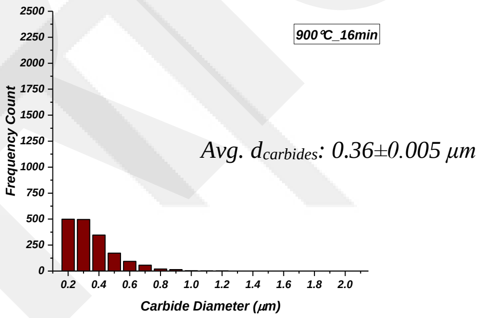
900℃_16min
Avg. $d_{carbides}$: 0.36±0.005 μm
Frequency Count
Carbide Diameter (μm)

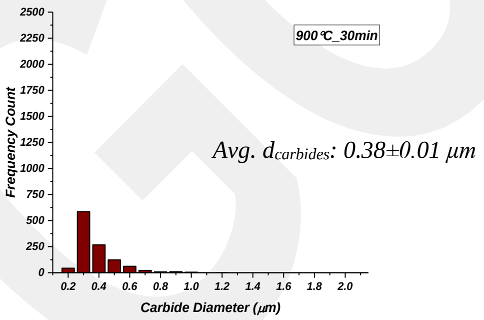
900℃_30min
Avg. $d_{carbides}$: 0.38±0.01 μm
Frequency Count
Carbide Diameter (μm)

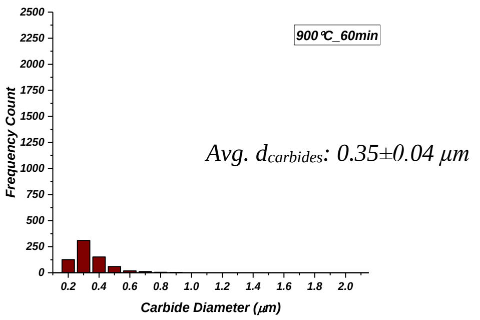
900℃_60min
Avg. $d_{carbides}$: 0.35±0.04 μm
Frequency Count
Carbide Diameter (μm)

APPENDIX D

The histograms that were drawn as number fractions of carbides versus their diameters for each specimen.

**Related heat treatment conditions were given in the right sides of each histogram.

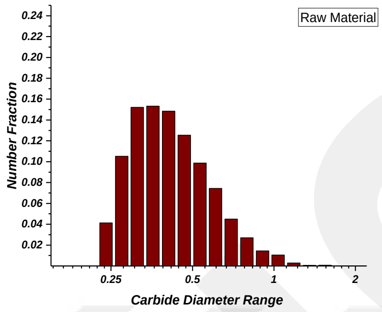

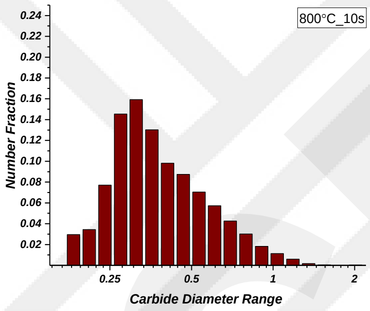

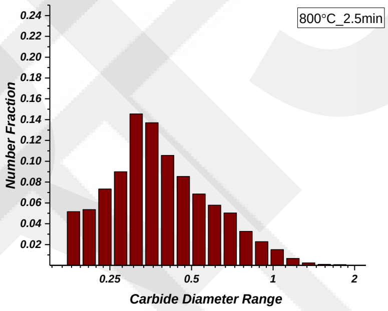

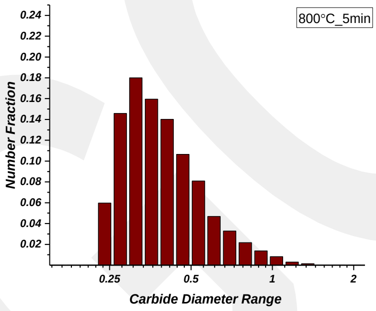

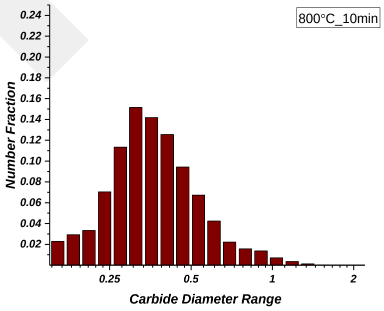

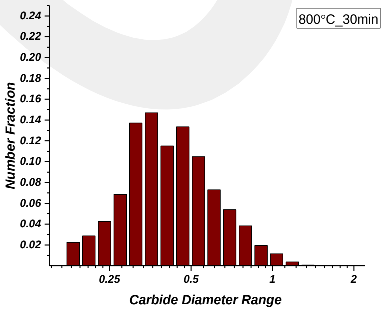

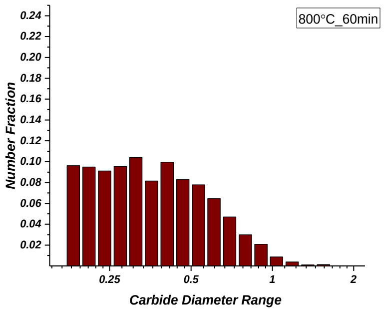

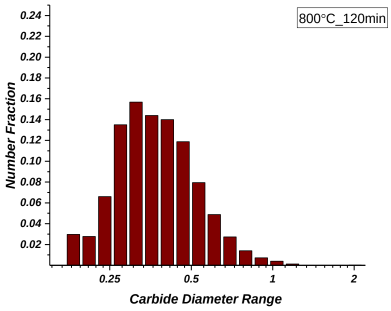
800°C_120min
Number Fraction
0.24
0.22
0.20
0.18
0.16
0.14
0.12
0.10
0.08
0.06
0.04
0.02
0.25
0.5
1
2
Carbide Diameter Range

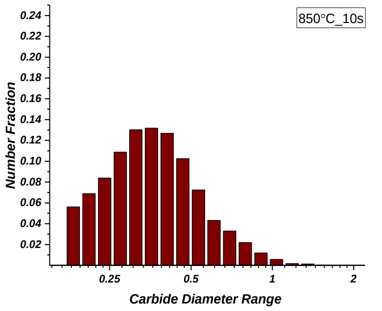
850°C_10s
Number Fraction
0.24
0.22
0.20
0.18
0.16
0.14
0.12
0.10
0.08
0.06
0.04
0.02
0.25
0.5
1
2
Carbide Diameter Range

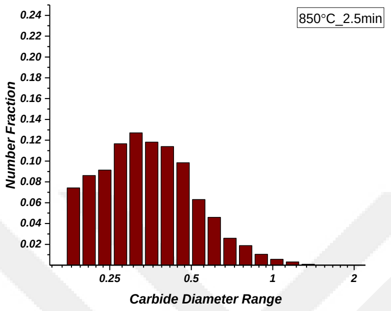
850°C_2.5min
Number Fraction
0.24
0.22
0.20
0.18
0.16
0.14
0.12
0.10
0.08
0.06
0.04
0.02
0.25
0.5
1
2
Carbide Diameter Range

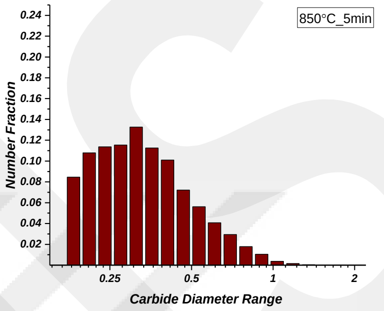
850°C_5min
Number Fraction
0.24
0.22
0.20
0.18
0.16
0.14
0.12
0.10
0.08
0.06
0.04
0.02
0.25
0.5
1
2
Carbide Diameter Range

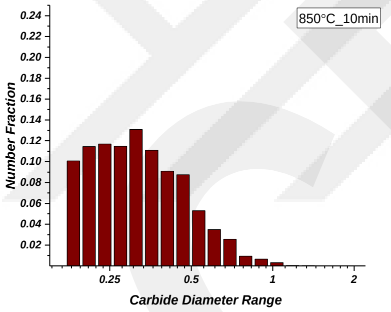
850°C_10min
Number Fraction
0.24
0.22
0.20
0.18
0.16
0.14
0.12
0.10
0.08
0.06
0.04
0.02
0.25
0.5
1
2
Carbide Diameter Range

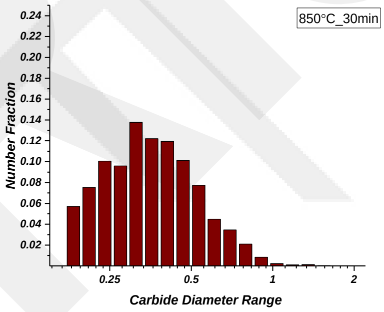
850°C_30min
Number Fraction
0.24
0.22
0.20
0.18
0.16
0.14
0.12
0.10
0.08
0.06
0.04
0.02
0.25
0.5
1
2
Carbide Diameter Range

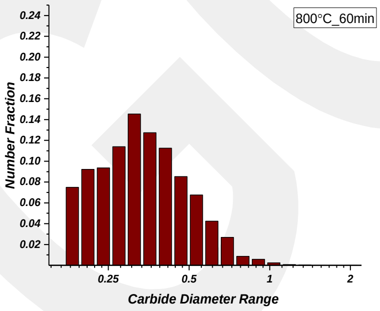
800°C_60min
Number Fraction
0.24
0.22
0.20
0.18
0.16
0.14
0.12
0.10
0.08
0.06
0.04
0.02
0.25
0.5
1
2
Carbide Diameter Range

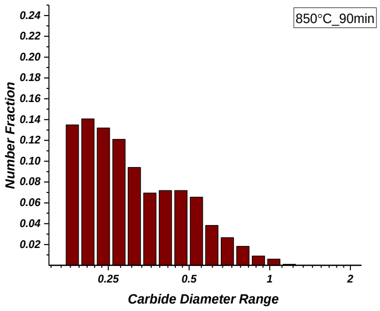
850°C_90min
Number Fraction
0.24
0.22
0.20
0.18
0.16
0.14
0.12
0.10
0.08
0.06
0.04
0.02
0.25
0.5
1
2
Carbide Diameter Range

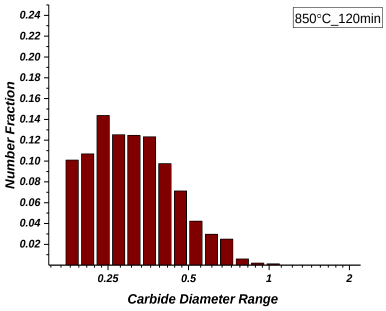
850°C_120min
Number Fraction
0.24
0.22
0.20
0.18
0.16
0.14
0.12
0.10
0.08
0.06
0.04
0.02
0.25
0.5
1
2
Carbide Diameter Range

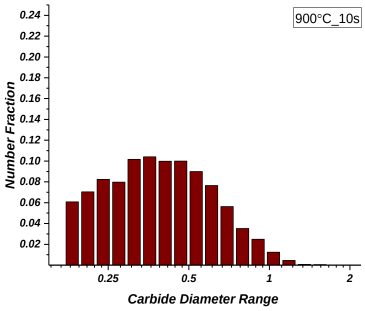
900°C_10s
Number Fraction
0.24
0.22
0.20
0.18
0.16
0.14
0.12
0.10
0.08
0.06
0.04
0.02
0.25
0.5
1
2
Carbide Diameter Range

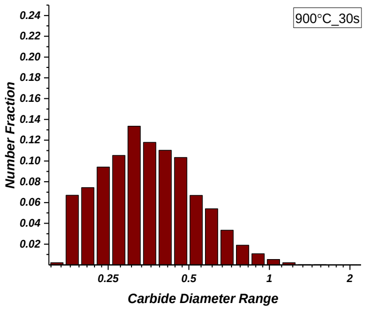
900°C_30s
Number Fraction
0.24
0.22
0.20
0.18
0.16
0.14
0.12
0.10
0.08
0.06
0.04
0.02
0.25
0.5
1
2
Carbide Diameter Range

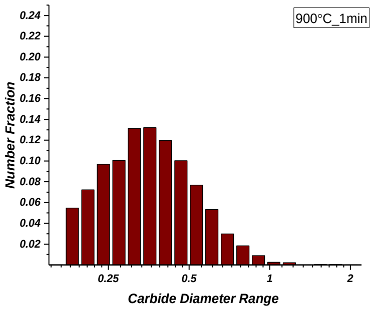
900°C_1min
Number Fraction
0.24
0.22
0.20
0.18
0.16
0.14
0.12
0.10
0.08
0.06
0.04
0.02
0.25
0.5
1
2
Carbide Diameter Range

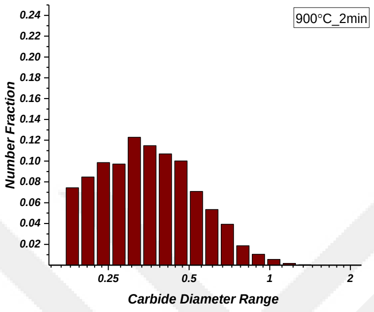
900°C_2min
Number Fraction
0.24
0.22
0.20
0.18
0.16
0.14
0.12
0.10
0.08
0.06
0.04
0.02
0.25
0.5
1
2
Carbide Diameter Range

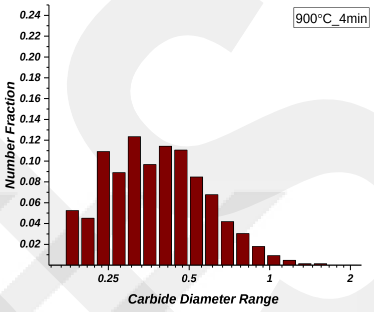
900°C_4min
Number Fraction
0.24
0.22
0.20
0.18
0.16
0.14
0.12
0.10
0.08
0.06
0.04
0.02
0.25
0.5
1
2
Carbide Diameter Range

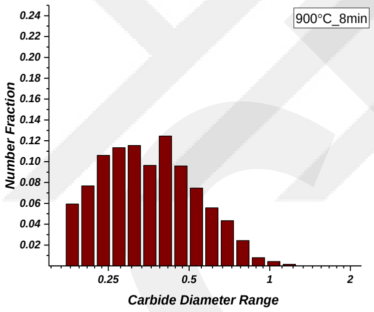
900°C_8min
Number Fraction
0.24
0.22
0.20
0.18
0.16
0.14
0.12
0.10
0.08
0.06
0.04
0.02
0.25
0.5
1
2
Carbide Diameter Range

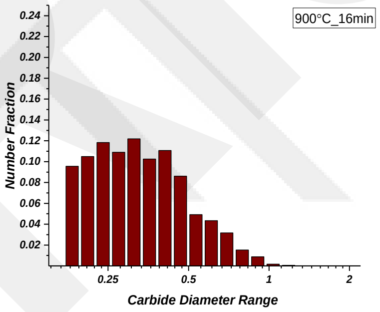
900°C_16min
Number Fraction
0.24
0.22
0.20
0.18
0.16
0.14
0.12
0.10
0.08
0.06
0.04
0.02
0.25
0.5
1
2
Carbide Diameter Range

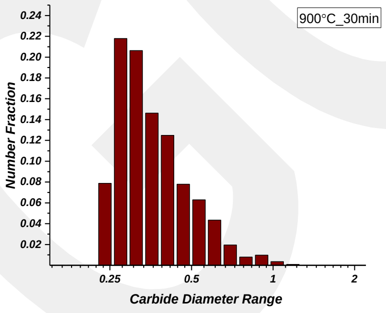
900°C_30min
Number Fraction
0.24
0.22
0.20
0.18
0.16
0.14
0.12
0.10
0.08
0.06
0.04
0.02
0.25
0.5
1
2
Carbide Diameter Range

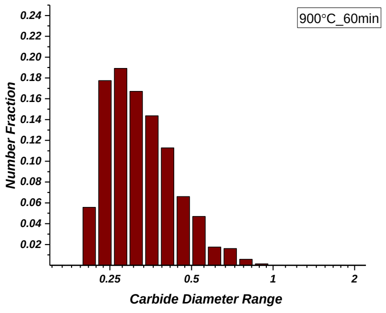
900°C_60min
Number Fraction
0.24
0.22
0.20
0.18
0.16
0.14
0.12
0.10
0.08
0.06
0.04
0.02
0.25
0.5
1
2
Carbide Diameter Range

APPENDIX E

Maximum, minimum and standard deviation values of macro (HV 0.5) and micro (HV0.05) hardness values of each RT quenched specimens

HV 0.5				
T_γ	**t_γ**	**Min Value**	**Max Value**	**St. Dev.**
800ºC	**10 s**	242	244	5
	2.5min	688	700	6
	5 min	825	830	3
	10 min	798	809	6
	30 min	841	864	13
	60 min	798	864	24
	120 min	809	876	28

HV 0.5				
T_γ	**t_γ**	**Min Value**	**Max Value**	**St. Dev.**
850ºC	**10 s**	668	696	35
	2.5min	912	919	4
	5 min	870	900	15
	10 min	958	958	0
	30 min	932	938	3
	60 min	951	912	18
	90 min	894	919	13
	120 min	768	768	0

HV 0.5				
T_γ	**t_γ**	**Min Value**	**Max Value**	**St. Dev.**
900ºC	**10 s**	858	870	7
	30 s	945	938	4
	1 min	912	925	8
	2 min	919	938	10
	4 min	882	888	3
	8 min	912	912	0
	16 min	894	900	3
	30 min	841	912	36
	60 min	853	894	21

HV 0.05				
T_γ	**t_γ**	**Min Value**	**Max Value**	**St. Dev.**
800ºC	**10 s**	272	248	14
	2.5min	767	833	34
	5 min	927	947	10
	10 min	991	1014	13
	30 min	947	947	0
	60 min	887	927	16
	120 min	991	1062	31

HV 0.05				
T_γ	**t_γ**	**Min Value**	**Max Value**	**St. Dev.**
850ºC	**10 s**	646	658	5
	2.5min	850	887	13
	5 min	1014	1037	13
	10 min	1141	1219	40
	30 min	1062	1062	0
	60 min	1114	1261	65
	90 min	1006	1087	41
	120 min	969	1014	20

HV 0.05				
T_γ	**t_γ**	**Min Value**	**Max Value**	**St. Dev.**
900ºC	**10 s**	783	799	9
	30 s	907	1062	76
	1 min	1114	1170	32
	2 min	1087	1294	104
	4 min	1294	1364	28
	8 min	1014	1199	76
	16 min	1062	1170	54
	30 min	1006	1022	9
	60 min	1105	1179	32